FACULDADE DE ENGENHARIA DA UNIVERSIDADE DO PORTO

Design of an atmospheric chamber for in-situ mechanical testing in H_2-rich environment

Francisco José Picão Vieira



Mechanical Engineering Master's Degree

Supervisor at FEUP: Professor Pedro Sousa

Supervisors at INEGI: Daniel Braga and Tiago Domingues

Porto, 2023

Design of an atmospheric chamber for in-situ mechanical testing in H_2-rich environment

Francisco José Picão Vieira

Mechanical Engineering Master's Degree

Porto, 2023

Abstract

This dissertation was carried out in a business environment, in the *Instituto de Ciência e Inovação em Engenharia Mecânica e Engenharia Industrial* (INEGI), in the *Unidade de Monitorização Avançada e Integridade Estrutural* (UMAI).

The dissertation's objective is to design an atmospheric chamber for in-situ mechanical testing in H_2-rich environment.

Hydrogen is considered a promising solution for achieving a low-carbon economy due to its abundance, lightweight nature, and interesting properties. Although, hydrogen embrittlement, the deterioration of material's mechanical properties caused by hydrogen, poses a significant obstacle to the advancement of hydrogen solutions.

However, the understanding of this phenomenon is still limited, and comprehensive research on the consequences of embrittlement in different materials is lacking. Therefore, conducting various tests is crucial to enhance our understanding of the challenges associated with hydrogen gas (H_2).

To address this, a mechanical test chamber was developed for application on two machines in the INEGI laboratory: the High-Speed Machine and the Portable Test Machine v2. This solution enables hydrogen embrittlement tests with axial forces up to 20 kN, both in tension and compression.

The design process began with a literature review, which identified key safety considerations for hydrogen gas use, hydrogen embrittlement-resistant materials, and other relevant features, from where is possible to better design the intended solution.

The complete design of the mechanical chamber incorporates dynamic requirements, with careful consideration of important parts and hydrogen safety specifications. These specifications include O-rings, various valves, and sensors to monitor the chamber atmosphere.

Hydrogen generation during the tests will be achieved through the use of alkaline electrolysis of salt water. This method was chosen for its simplicity and applicability to this solution.

To ensure the safety of the chamber, a structural analysis was conducted, resulting in necessary design changes and validating the final structure. The chamber is capable of safely performing tests with axial forces up to 20 kN and an internal pressure of up to 5 MPa.

Given the significance of hydrogen safety, strict control measures must be implemented to mitigate the associated risks of H_2 in all system applications, as emphasized in this study.

The dissertation concludes with the presentation of findings and suggests further development projects aimed at advancing our understanding of hydrogen and facilitating technological progress in this field.

Keywords: Hydrogen Embrittlement Testing, H_2 rich environment, Atmospherical Chamber, In-situ Hydrogen Testing, Mechanical Design

Resumo

Esta dissertação foi realizada em ambiente empresarial, no Instituto de Ciência e Inovação em Engenharia Mecânica e Engenharia Industrial (INEGI), na Unidade de Monitorização Avançada e Integridade Estrutural (UMAI).

O objetivo do present trabalho é o projeto de uma câmara atmosférica para ensaios mecânicos in-situ em ambientes ricos em H_2.

O hidrogénio, devido à sua abundância, leveza e propriedades distintas, é considerado uma solução promissora para alcançar uma economia de baixo carbono. No entanto, a fragilização por hidrogénio, deterioração das propriedades mecânicas do material por este gás, representa um obstáculo significativo ao avanço das soluções de hidrogénio.

Contudo, a compreensão deste fenómeno é ainda limitada, faltando uma investigação abrangente sobre as consequências da fragilização em diferentes materiais. Assim, a realização de vários testes é crucial para melhorar a compreensão dos desafios associados ao gás hidrogénio (H_2).

Para tal, foi desenvolvida uma câmara de ensaios mecânicos para aplicação em duas máquinas do laboratório do INEGI: a *High-Speed Machine* e a *Portable Test Machine* v2. Esta solução permite a realização de ensaios de fragilização por hidrogénio com forças axiais até 20 kN, tanto em tração como em compressão.

O processo de conceção iniciou-se com uma revisão bibliográfica, onde se identificou as principais considerações de segurança para a utilização do gás hidrogénio, os materiais resistentes à fragilização por hidrogénio e outras características relevantes, a partir das quais é possível conceber melhor a solução pretendida.

O design completo da câmara mecânica incorpora requisitos dinâmicos, tendo uma consideração cuidadosa de peças importantes e especificações de segurança do hidrogénio. Estas especificações incluem O-rings, várias válvulas e sensores para monitorizar a atmosfera da câmara.

A produção de hidrogénio durante os testes será conseguida através da utilização da eletrólise alcalina da água salgada. Este método foi escolhido pela sua simplicidade e aplicabilidade a esta solução.

Para garantir a segurança da câmara, foi efetuada uma análise estrutural que resultou nas alterações necessárias ao projeto e na validação da estrutura final. A câmara tem capacidade para efetuar ensaios em segurança com forças axiais até 20 kN e uma pressão interna até 5 MPa.

Dada a importância da segurança do hidrogénio, devem ser implementadas medidas de controlo rigorosas para mitigar os riscos associados ao H_2 em todas as aplicações do sistema, tal como enfatizado neste estudo.

A dissertação termina com a apresentação dos resultados e sugere novos projetos de desenvolvimento destinados a melhorar a nossa compreensão do hidrogénio e a facilitar o progresso tecnológico destas soluções.

Palavras-chave: Ensaios de fragilização por hidrogénio, Ambientes ricos em H_2, Câmara atmosférica, Ensios de hidrogénio in-situ, Projeto Mecânico

Acknowledgments

The completion of this dissertation and my academic journey would not have been possible without the support and availability of the individuals who have been involved throughout the years. Their contributions have made this challenging path much more manageable, and I am deeply grateful to each and every one of them.

First and foremost, I would like to express my heartfelt appreciation to my supervisors, Pedro Sousa, Daniel Braga, and Tiago Domingues. Their guidance, encouragement, and valuable suggestions have played a significant role in the development of this work. Their unwavering support and willingness to help have been instrumental in achieving the objectives of this dissertation.

To INEGI, a renowned technological innovation center, for providing me with the opportunity to carry out this dissertation in a corporate setting. I am grateful for the working conditions and the privilege of being part of such an esteemed institution. I would also like to extend my gratitude to the collaborators at INEGI who welcomed me and provided assistance whenever needed.

I would like to express my deep gratitude to my parents for their unwavering support throughout my life. Their guidance and sacrifices have shaped me into the person I am today, and I am forever grateful. To them, to my grandparents, to my cousins and to my aunt Lídia I am vert grateful for the opportunities they have provided, which have allowed me to pursue my education at this esteemed institution.

To my friends, I am incredibly grateful for the wonderful times we have shared and for the unwavering support they have provided. I would like to extend a special thank you to the friends I have made in academic traditions, with whom I have shared knowledge, frustrations, and victories that have made this path feasible.

Finally, I would like to express my sincere appreciation to all the teachers who have been a part of my academic journey. Their expertise and dedication have provided me with invaluable learning experiences. Without their commitment to education, none of this would have been possible.

Your support and contributions have been invaluable, and I am truly grateful for the role each of you has played in my master's thesis and academic journey.

To all those mentioned above, my heartfelt thanks.

"Nobody said it was easy,
No one ever said it would be this hard,
Oh, take me back to the start."

Coldplay, The Scientist

Contents

1 Introduction **1**
- 1.1 Objectives, Scope and Motivation . . . 1
- 1.2 Dissertation Methodology . . . 2
- 1.3 Dissertation Structure . . . 3

2 State of the Art **5**
- 2.1 Hydrogen: definition and properties . . . 5
- 2.2 Hydrogen: sources and energy applications . . . 6
  - 2.2.1 Hydrogen Classification . . . 7
  - 2.2.2 Hydrogen as energy source . . . 8
- 2.3 Hydrogen Generation . . . 9
- 2.4 Hydrogen Embrittlement . . . 10
- 2.5 Hydrogen Embrittlement Testing . . . 12
  - 2.5.1 Specimen as chamber solutions . . . 13
  - 2.5.2 External to the specimen chamber solutions . . . 15
  - 2.5.3 Apparatus summary . . . 22

3 Chamber Design **25**
- 3.1 System Requirements . . . 26
  - 3.1.1 Hydrogen Gas Use Requirements . . . 27
  - 3.1.2 Material Safety Requirements . . . 27
  - 3.1.3 Present System Requirements . . . 28
- 3.2 Subsystems and Functional Diagram . . . 30
  - 3.2.1 Hydrogen Source . . . 31
  - 3.2.2 Sensors . . . 40
  - 3.2.3 Valve Sealing . . . 43
  - 3.2.4 Chamber Atmosphere Release . . . 44
  - 3.2.5 Inert Gas Flush . . . 44
  - 3.2.6 Fuctional Diagram . . . 44
- 3.3 Conceptual Design . . . 45
- 3.4 Final Design . . . 46
- 3.5 Chamber Tube Design (1) . . . 48
  - 3.5.1 Chamber Walls Material . . . 49
  - 3.5.2 Chamber Format . . . 49
  - 3.5.3 Chamber Dimensions . . . 50
- 3.6 End Caps design (3 and 4) . . . 52
- 3.7 Fixation Solution (5, 6 and 7) . . . 53
  - 3.7.1 Fixation part of the through hole end cap design (5) . . . 54

3.7.2 Fixation part of the load cell connected end cap design (6) 55
3.7.3 Fixation Rods design (7) 56
3.8 O-rings Flanges design (2) 57
3.9 Dynamic Sealing design (8 and 9) 58
3.10 O-rings sizing 60
3.10.1 O-ring between End Cap (3) and Fixation part (5) 62
3.10.2 O-ring between fixation part (5) and bushing (9) 63
3.10.3 O-rings applied in the flanges (2) 63
3.10.4 O-ring dynamic between dynamic rod (8) and bushing (9) 64
3.10.5 O-ring between end cap (4) and fixation part (6) 67
3.10.6 Hoses O-rings sizing 67
3.11 Sensors Placement 69
3.12 Valve sealing and hoses 71
3.13 Screws, Nuts and Washers 73
3.14 Design for Manufacturing 75
3.15 Chapter Summary 76

4 Structural Validation **77**
4.1 Modeling Assumptions 77
4.2 Critical Sections 79
4.3 Modeling Strategy 80
4.3.1 Fused Quartz tube analysis 81
4.3.2 Load Cell connected section analysis 83
4.3.3 Dynamic Sealing Rod analysis 88
4.4 Simulations Results Discussion 90
4.4.1 Quartz Tube Results Analysis 90
4.4.2 Load Cell Connected Section Results Discussion 91
4.4.3 Dynamic Sealing Rod Results Discussion 93
4.5 Compressive force simulation 96
4.6 Structural Validation summary 97

5 Conclusion **99**
5.1 Final Conclusions 99
5.2 Future Works 101

References **103**

A Mechanical Drawing of the solution **111**

B O-ring flanges (2) technical drawings **113**

C End Cap through (3) technical drawing **117**

D End Cap Load Cell connected (4) technical drawing **119**

E Fixation Part Through (5) technical drawing **121**

F Fixation Part Load Cell connected (6) technical drawing **123**

G Fixation rod (7) technical drawing **125**

H Dynamic Sealing Rod (8) technical drawing **127**

I Dynamic Sealing Bushing (9) technical drawing **129**

J Sensor Placement technical drawing **131**

K Bill of Materials **133**

L BlueRobotics Wet Link Penetrator M14 **137**

M SPIR STAR 6mm Hose **139**

N Habonim H24 Valve **143**

O Redfluid Check Valve **147**

P Gotze Armaturen pressure relief valve **149**

Q Assembly and User Guide **153**

List of Figures

2.1 Schematic representation of three hydrogen embrittlement mechanisms [6] 5
2.2 Hydrogen Properties [7] 6
2.3 Global hydrogen consumption by industry [9] 7
2.4 Hydrogen Colors from its source [10] 7
2.5 Steam Methane Reforming Process [13] 9
2.6 Gasification Process Schematics [14] 10
2.7 Schematic diagram of hydrogen embrittlement mechanism [5] 11
2.8 Apparatus presented in Ogata, 2008 [20] 14
2.9 Technical drawing of the sample geometry used in Boot et al., 2021 15
2.10 **(a)** Picture of the specimen and adapters in the tensile tester. **(b)** Section of the test area, displaying the bottom adapter and the connection with the specimen [21] . . 15
2.11 Apparatus presented by ZwickRoell **(a)** where pressure vessel is lowered and **(b)** with thick walls metal cylinder chamber [22] 16
2.12 Schematics of the apparatus presented by Shimadzu and the used specimen [23] . 17
2.13 Apparatus presented by Ghent University [25] 18
2.14 Apparatus presented in Hajilou et al., 2018 [26] 18
2.15 Apparatus presented in Yokogawa et al., 2008 [27] 20
2.16 Schematics of the apparatus presented in Alvine et al., 2014 with an **(a)** operational schematic of the *in-situ* tensile tester with sample and **(b)** a schematic of a typical "dog-bone" sample. [28] 21
2.17 Apparatus used by Alvine et al., 2014 with the **(a)** side view of the *in-situ* tensile tester and the key parts, **(b)** the *in-situ* tester resting inside the high-pressure hydrogen autoclave prior to sealing and **(c)** the top of the high-pressure hydrogen autoclave after sealing [28] 22

3.1 PTM2 machine existent in INEGI laboratory 25
3.2 HSM machine existent in INEGI laboratory 26
3.3 Subsystems and applicable components 31
3.4 Schematic of electrolysis of saltwater [33] 34
3.5 Ossila Electrolysis H-Type Tank, Diaphragm and Lids [43] 38
3.6 Ossila Electrolysis H-Type Tank Schematics [43] 38
3.7 Schematics of the Electrode from Ossila [38] 39
3.8 DC adjustable power supply [45] 39
3.9 Pressure and Temperature Sensor, H_2 Resistant [46] 41
3.10 Hydrogen Gas Module 0-1000 ppm [49] 42
3.11 Sensor placement part 42
3.12 General use of each valve type [52] 43
3.13 Functional Diagram Schematics 45

3.14 BlueRobotics Watertight Enclosure for ROV/AUV (6" Series) product view [53] . 46
3.15 BlueRobotics Watertight Enclosure for ROV/AUV (6" Series) 2D technical drawing [53] . . . 46
3.16 Exploded view of the final solution, with labeled parts . . . 47
3.17 Final Solution Design . . . 47
3.18 3D CAD of the chamber walls . . . 51
3.19 3D CAD of the end cap connected to the load cell . . . 53
3.20 3D CAD of the end cap with a through-hole . . . 53
3.21 Fixation System assembled . . . 54
3.22 3D CAD of the fixation part of the through hole end cap - top view . . . 55
3.23 3D CAD of the fixation part of the through hole end cap - down view . . . 55
3.24 3D CAD of the fixation part of the load cell connected end cap - top view . . . 56
3.25 3D CAD of the fixation part of the load cell connected end cap - down view . . . 56
3.26 3D CAD of the threaded rods . . . 57
3.27 3D CAD of the O-ring flanges . . . 58
3.28 Dynamic Reciprocating Seal Schematics . . . 60
3.29 **(a)** Partial view and **(b)** isometric view of the 3D CAD of the Dynamic Sealing metal components . . . 60
3.30 Exposure Rating Guide of Chemical Compatibility [62] . . . 61
3.31 Hydrogen Gas compatible materials [62] . . . 61
3.32 O-ring materials compatible with H_2 [63] . . . 62
3.33 BLueRobotics M14 penetrator for the power cables [66] . . . 70
3.34 Hose Type-6mm SPIR STAR [67] . . . 71
3.35 H24 Habonim valve [68] . . . 72
3.36 Redfluid check valve and components materials [69] . . . 72
3.37 Gotze Armaturen series 420 pressure relief valve [70] . . . 73
3.38 Exploded detail view of the screws, nut and washers allocation . . . 74

4.1 Preload table of some metric screw sizes [72] . . . 79
4.2 Relation of units system to Abaqus [73] . . . 81
4.3 Fused Quartz properties inserted in Abaqus software . . . 82
4.4 Quartz Tube mesh . . . 82
4.5 Quartz Tube applied internal pressure . . . 82
4.6 Chamber wall resulting stresses in MPa . . . 83
4.7 Chamber wall resulting displacements in mm . . . 83
4.8 Example of the coupling constrain application . . . 84
4.9 Connector Section properties defined in Abaqus to simulate the screws . . . 85
4.10 Contact propertied applied between surfaces . . . 86
4.11 Interactions and mesh of the load cell connected section . . . 86
4.12 Introduction of M3 preload in Abaqus . . . 87
4.13 Axial maximum force applied in Abaqus simulation . . . 87
4.14 Load Cell connected section stresses in MPa . . . 88
4.15 Cut views of the Load Cell connected section stresses in MPa, in different planes 88
4.16 Boundary Condition and Force applied to the Rod . . . 89
4.17 Stresses applied in dynamic rod, in MPa . . . 89
4.18 Dynamic Rod resulting displacements in mm . . . 90
4.19 Load Cell connected section stresses in MPa, MP35N . . . 92
4.20 Cut views of the Load Cell connected section stresses in MPa, MP35N . . . 92
4.21 AISI 316LVM properties depending of the cold worked percentage [74] . . . 94

4.22 Stresses applied in dynamic rod in MPa, AISI 316LVM 95
4.23 Dynamic Rod resulting displacements in mm, AISI 316 LVM 95
4.24 Load Cell connected section stresses in MPa, compression 96
4.25 Cut views of the Load Cell connected section stresses in MPa, compression . . . 96

List of Tables

3.1 Functional and Safety Requirements 30
3.2 Comparison between Electrolysis Solutions, extracted from Vincent et al., 2018 [17] 32
3.3 Advantages and Disadvantages of the electrolysis processes, extracted from Vincent et al., 2018 [17] 33
3.4 Bill of Materials 48

4.1 Proprieties of AISI 316L and Fused Quartz 78
4.2 Quartz Tube stress values obtained in Abaqus and the material property 90
4.3 Load Cell connected stress values obtained in Abaqus and the material property . 91
4.4 Proprieties of MP35N and AISI 316L 92
4.5 Load Cell connected section maximum stress value obtained in Abaqus and the MP35N property 93
4.6 Dynamic Sealing Rod stress values obtained in Abaqus and the material property 93
4.7 Proprieties of AISI 316LVM cold worked and AISI 316L 94
4.8 Dynamic Sealing Rod stress values obtained in Abaqus and the AISI 316LVM property 96
4.9 Load Cell connected section maximum stress value obtained in Abaqus with compressive force and the MP35N property 97

Abbreviations

AEM	Anion Exchange Membrane
AIDE	Adsorption Induced Dislocation Emission
ASTM	American Society for Testing and Materials
BOM	Bill of Materials
CAD	Computer-Aided Design
CAE	Computer-Aided Engineering
CCS	Carbon Capture and Storage
CS	Cross section
CT	Compact tension
FEUP	*Faculdade de Engenharia da Universidade do Porto*
FKM	Fluorocarbon
H	Hydrogen
H_2	Hydrogen Gas
HE	Hydrogen Embrittlement
HELP	Hydrogen-Enhanced Localized Plasticity
HEDE	Hydrogen-Enhanced Decohesion
HSM	High-Speed Machine
ID	Inside Diameter
INEGI	*Instituto de Ciência e Inovação em Engenharia Mêcanica e Engenharia Industrial*
ISO	International Organization for Standardization
NBR	Buna-N (Nitrilic Butadiene Rubber)
PEM	Proton Exchange Membrane
PTM2	Portable Test Machine v2
SSRT	Slow Strain Rate Testing
SMR	Steam Methane Reforming
SOE	Solid Oxide Electrolyser
UMAI	*Unidade de Monitotização Avançada e Integridade Estrutural*

Chapter 1

Introduction

The use of hydrogen as a clean and sustainable energy carrier has gained significant attention in recent years because of its ability to solve environmental concerns while decreasing our reliance on fossil fuels [1]. As hydrogen continues to emerge as a viable alternative, it is crucial to ensure the safety and reliability of hydrogen infrastructure, particularly in applications such as hydrogen pipelines [2]. Conducting accurate and representative testing of materials, components, and systems in hydrogen-rich environments is one of the major challenges in this regard.

1.1 Objectives, Scope and Motivation

Globally, the effects of introducing hydrogen in pipelines, blended with fossil fuel, such as natural gas, has been a matter of investigation. The low knowledge about the hydrogen effects in materials is a problem to this innovation, because hydrogen has low ignition energy, is the smallest element in the universe and it weakens the properties of some steels, which increases the leakage risks [3].

Particularly, hydrogen pipelines are essential for the effective movement and distribution of hydrogen. These pipelines do, however, face particular difficulties like hydrogen embrittlement, leaks, and material deterioration [2].

The lack of information on hydrogen has hindered the advancement of innovative solutions. The issue of hydrogen embrittlement has generated global interest, resulting in a substantial increase in studies conducted by institutions worldwide. These studies aim to develop guidelines for durable and reliable hydrogen infrastructure materials, systems, and components, ensuring their safe and effective operation.

Hydrogen embrittlement is a phenomenon that refers to the deterioration of material properties caused by the presence of gaseous hydrogen, H_2. Extensive studies have been conducted to explore the mechanisms underlying this embrittlement, resulting in the identification of three main embrittlement mechanisms: hydrogen-enhanced decohesion (HEDE), hydrogen-enhanced localized plasticity (HELP), and adsorption induced dislocation emission (AIDE) [4].

The limited knowledge regarding the impact of hydrogen, particularly on materials degradation, has spurred the development of innovative solutions aimed at studying its effects on a wide range of materials under varying conditions and through diverse approaches. This endeavour represents a significant advancement in environmental research and presents a promising new market to explore. Despite the extensive research conducted in this field over the years, the availability of commercially produced hydrogen embrittlement chambers has been limited, with the majority being tailored for internal use rather than widespread commercialization. Therefore, there remains a pressing need for increased accessibility to hydrogen embrittlement chambers to facilitate comprehensive research and analysis in this area.

Better understanding of the effects of hydrogen in the materials would be a massive step in moving to a low-carbon economy, and the required investigations about the investment results and economic viability could be carried out.

This dissertation was carried out in a business environment, in the *Instituto de Ciência e Inovação em Engenharia Mecânica e Engenharia Industrical* (INEGI), based in Porto. The curricular internship had, as main objective, the design of an atmospheric chamber for in-situ mechanical testing in H_2 rich environments. The motivation for the author results from the interest and taste for mechanical design and experimental mechanics.

Specifically, this dissertation's objective is to design a test chamber to be implemented in already existing tension-compression machines, having as primarily objective the use with H_2 rich environments. The chamber's hydrogen resistance also makes it adaptable for testing under various gaseous environments, enabling a wide range of tests to be conducted.

This work incorporates a comprehensive literature review of existing chamber designs, extracting essential requirements that guided the development process. Subsequently. with the acquired information, a conceptual design and component selection were carried out, followed by the creation of a 3D design using Computer Aided Design (CAD) software.

A crucial step in every design process is structural validation. This validation ensures the design's stability and its safety usage in the intended conditions. The structural integrity of the designs is usually tested with Finite Element Method (FEM) analysis.

To design the H_2 environmental chamber it was necessary to resort to software such as Solidworks for CAD and Abaqus for FEM simulations. These tools played a vital role in creating and validating the chamber design to ensure its optimal performance.

The development of the proposed solution in this dissertation took into consideration and adhered to the specific standards for conducting hydrogen embrittlement tests. Following these standards, the solution ensures the accurate and reliable assessment of hydrogen embrittlement effects, further enhancing the credibility and applicability of the research findings.

1.2 Dissertation Methodology

To develop this dissertation the following methodology was followed:

1. Research about hydrogen properties, production and relevant aspects to consider when dealing with this element;
2. Literature review of the already existing solutions to hydrogen embrittlement testing and relevant standards to apply in this work;
3. Development of the chamber design and manufacturing designs of its components;
4. Structural validation of the designed solution.

1.3 Dissertation Structure

The present dissertation is composed of five chapters, beginning with the current chapter 1, which provided an introduction, describing the main objectives, the followed methodology, the contextual framework, and the relevant literature basis and existing technologies interest that have motivated the production of this dissertation.

In chapter 2, an introduction about hydrogen properties is made, presenting its categories and applications, for example, the economic interest in the energy sector. Hydrogen sources are also mentioned, establishing different hydrogen generation processes and its low-carbon economic interest.

Furthermore, a brief overview regarding the challenges associated with hydrogen embrittlement and its detrimental effects in materials is presented. The interest and dangers of hydrogen embrittlement testing are also explained. Commonly employed tests are then presented, along with eight existing apparatuses that served as inspiration and guidance for the design process.

In chapter 3, are stated the primary machines in which the chamber solution is intended to be applied, along with the present system requirements, to ensure hydrogen safety and support machine loads and environmental pressure. Subsequently, the chapter explores the subsystems that constitute this solution, providing a comprehensive description of each, accompanied by an analysis of the system's functional diagram.

Furthermore, based on the determined requirements and associated subsystems, the dissertation progresses forward to the detailed design phase, displaying the design options and their reasoning. This section addresses the dimensioning of the parts and other necessary components, such as O-rings and valves. Towards the end of the chapter, the focus shifts to the manufacturing processes and designs, as the intention is to manufacture certain parts of the chamber.

In chapter 4, a structural analysis of the critical section is presented, from which it is possible to draw conclusions. In response to the identified challenges, the dissertation presents the proposed solutions and necessary project changes. These solutions effectively address the noted problems and are designed to improve the overall performance and functionality of the project. Therefore, the material properties of the composing materials are here compared to obtained simulation results, finalizing with the project structural validation.

Finally, in the last chapter, chapter 5, conclusions about the developed solutions and future development suggestions are presented.

Chapter 2

State of the Art

The use of hydrogen in commercial and industrial applications, such as, in fuel cells and industrial processes (ammonia production, oil refining, methanol production, etc.), has led to an increased awareness of the detrimental effects of hydrogen on the mechanical properties of materials. Several materials, including steels, titanium alloys, and aluminium alloys, can be subjected to hydrogen embrittlement. The complex mechanisms of hydrogen embrittlement can include hydrogen diffusion and trapping, as well as interactions between hydrogen and material dislocations [5]. A schematic of some hydrogen embrittlement mechanisms is represented in figure 2.1.

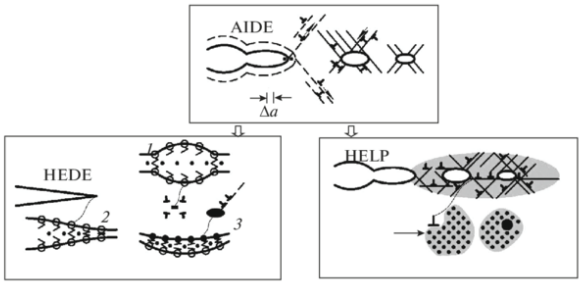


Figure 2.1: Schematic representation of three hydrogen embrittlement mechanisms [6]

2.1 Hydrogen: definition and properties

Hydrogen is a chemical element with the atomic number 1 and its symbol is the letter H. More than 90% of all atoms are hydrogen [5], and it is the lightest and most abundant element in the universe, making up approximately 75% of its elemental mass.

Hydrogen has a melting point of -259.2 °C and a boiling point of -252.8 °C, so, at standard temperature and pressure, it exists as a gas, composed of diatomic molecule, forming H_2. This gas is colourless, odourless, tasteless and highly flammable. Hydrogen is a highly reactive element and it can easily be combined with other elements to form compounds. The several unique properties of this element makes it important in many different fields [7].

This element has a high energy content, and it can be considered a clean-burning fuel source. When hydrogen burns, it reacts with oxygen to produce water vapor and heat, meaning that there are no emissions of harmful content or pollutants [7].

Overall, hydrogen is an abundant, versatile and essential element, with a range of unique properties that make it valuable in a variety of applications. As research and development in this area continue to advance, it is likely that we will continue to discover new and innovative uses for this important substance, unlocking its full potential and contributing to a more sustainable and prosperous future for all. Some chemical property of hydrogen can be observed in figure 2.2.

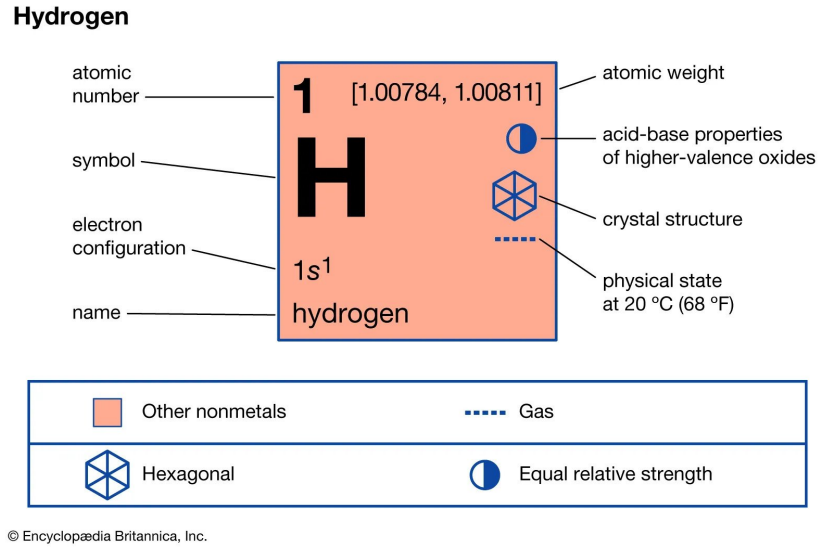


Figure 2.2: Hydrogen Properties [7]

2.2 Hydrogen: sources and energy applications

Hydrogen is the most abundant chemical element in the universe, and when in diatomic gas form, may play a key role in achieving a low-carbon economy. Many ways exist to produce hydrogen gas, as it can be extracted from water, biomass and fossil fuels. It can then be applied in transportation, power generation or storage, various industrial processes, among other applications.

Hydrogen has a high energy density per unit of mass (between 120 and 142 mega-joules per kilogram [MJ/kg]) [8], so many applications will require small masses of it. The hydrogen can be compressed or liquefied for storage, so it may be more easily transported.

This element is becoming globally important as alternative source of energy, however, this alternative energy, represents less than 10% of hydrogen global consumption, as seen in figure 2.3. In 2020, 90% of hydrogen are consumed in ammonia production, petroleum refining and methanol production. The primarily use of hydrogen is the ammonia production, representing 55% of hydrogen consumption, having as main applications the agricultural and chemical industries, being used as an important part of fertilizer production and as an environmental-friendly and affordable

refrigerant. Hydrocracking to petroleum products creation represents 25% of the hydrogen use, and the methanol production use the remaining 10% of hydrogen. This petroleum refining industry represents 35% of global hydrogen use [9].

The remaining 10% of hydrogen use includes its use as alternative energy source and several other industries applications, as food, metalworking, medicine, etc.. Hydrogen energy industry is opening opportunities in transportation and energy industries, applying this element as alternative to fossil fuels. Some areas where the hydrogen interest is growing are space exploration, aviation, public and personal transport, power generation, among others [9].

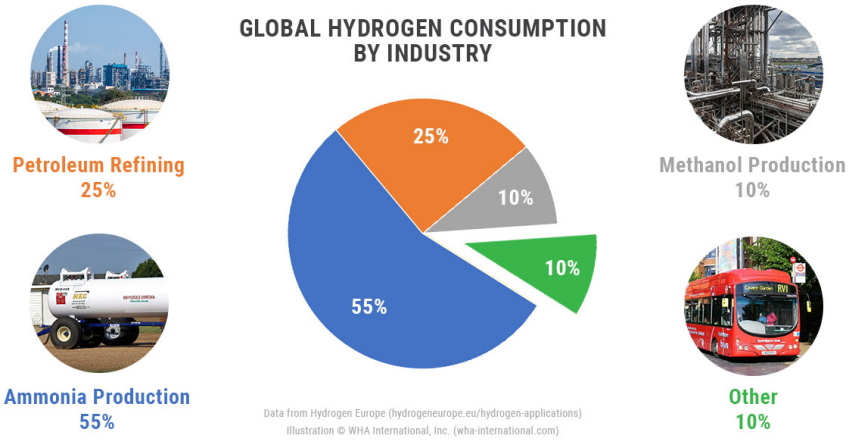


Figure 2.3: Global hydrogen consumption by industry [9]

2.2.1 Hydrogen Classification

Hydrogen is classified into multiple groups according to the way it is generated and any associated environmental effects. Hydrogen comes in a variety of different forms, which are denominated as colours, such as green or blue hydrogen. In figure 2.4 the hydrogen colors and its production process can be observed.

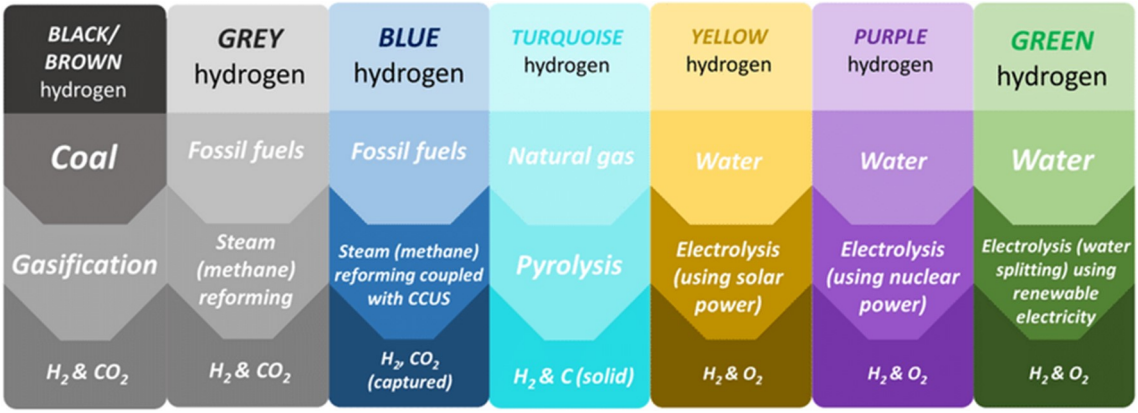


Figure 2.4: Hydrogen Colors from its source [10]

The most prevalent variety of hydrogen is grey hydrogen, which can be generated by steam methane reforming (SMR) from fossil fuels, including natural gas, coal or oil. Grey hydrogen generates a vital part of greenhouse gases, since the carbon dioxide produced during the SMR process is normally discharged into the atmosphere [10].

With a similar generation process, blue hydrogen is produced by SMR but it has a carbon capture and storage (CCS) step. Since it emits fewer greenhouse gases than grey hydrogen, blue hydrogen is a more environmentally friendly choice than grey hydrogen [10].

Black/brown hydrogen is created from gasification of coal produces brown hydrogen. Like grey hydrogen, black hydrogen produces substantial amounts of greenhouse gas emissions [11].

Green hydrogen is created through the electrolysis process of water, splitting the H_2O particles into hydrogen and oxygen while using electricity generated from renewable electricity such as wind or solar. Since there are no greenhouse gas emissions produced during the production of green hydrogen, it is considered as a clean hydrogen source [11].

Turquoise hydrogen is produced from natural gas using a process known as methane pyrolysis. Instead of producing carbon dioxide as a by-product, this procedure produces solid carbon, which reduces greenhouse gas emissions. However, even though this method is cleaner than the other fossil fuels-based methods, it is not yet economically viable [11].

When the electrolysis process is used with nuclear power, purple hydrogen results. The elevated temperatures from the nuclear reactors used to produce purple hydrogen could be used to produce steam to improve other hydrogen production processes. The production of purple hydrogen has lower greenhouse gas emissions [11].

Like green hydrogen, yellow hydrogen is produced through electrolysis by solar power, with photoelectric splitting [11].

The prices of manufacturing, the effects on the environment and the technological difficulties associated with each of these hydrogen forms vary. Whatever type of hydrogen is used relies on several variables, including resource availability, economic viability and environmental impact.

2.2.2 Hydrogen as energy source

Compared to conventional fossil fuels, hydrogen has several environmental benefits, for it does not contribute to the greenhouse effect and it does not pollute the air or contribute to the formation of acid rain. Also, hydrogen can be produced from renewable sources, and the technology for this production is in constant development [12].

Hydrogen may be one of the cleaner energy sources or mean of storage of clean energy. However, there are several challenges that need to overcome to achieve net zero carbon emissions. One of the biggest challenges is the excessive cost of hydrogen production, which is currently more expensive than conventional fossil fuels. Additionally, storage and transportation of hydrogen can be expensive and represent a difficulty because of a lack of infrastructure for hydrogen distribution.

One of the many challenges with transporting hydrogen in pipelines is the potential for hydrogen embrittlement of metals [2]. Also, other challenges are associated with hydrogen transport,

such as leakage, because of the low size of the gas particles, corrosion and compatibility with existing pipeline infrastructure.

As stated previously, hydrogen has an enormous potential to assume a significant role in the transition to a low-carbon economy, but there are still several challenges that need to be surpassed. Nevertheless, considerable progress has been made and this technology will continue to evolve.

2.3 Hydrogen Generation

Hydrogen can be produced from various sources, and the most common methods of hydrogen production are steam reforming, electrolysis and gasification. Steam reforming is the most common method and produces the largest amount of hydrogen.

Steam reforming and gasification have similar procedures, differing in the feedstock: steam reforming produces hydrogen from hydrocarbons, which can be found in natural gas, biomass and petroleum [13], and gasification uses the carbon-containing components of the feedstock to produce synthetic gas and the feedstock can be coal, biomass or waste materials [14]. These processes involve heating the feedstock, mixing it with steam, and utilizing a catalyst bed to produce hydrogen gas and carbon monoxide. Subsequently, the carbon monoxide is further reacted with steam to generate additional hydrogen. However, this is a fossil fuel-based process, so it is not the cleaner method of hydrogen production. Also, both procedures produce carbon dioxide, needing the introduction of a catalyser, a pressure-swing adsorption method or a cryogenic distillation method at a low temperature to assure the highest purity of hydrogen [15]. In figures 2.5 and 2.6 brief schematics of these processes can be seen.

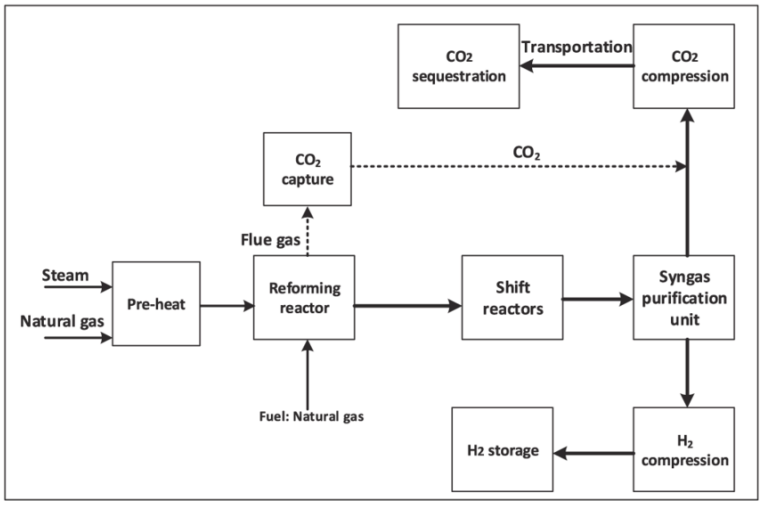


Figure 2.5: Steam Methane Reforming Process [13]

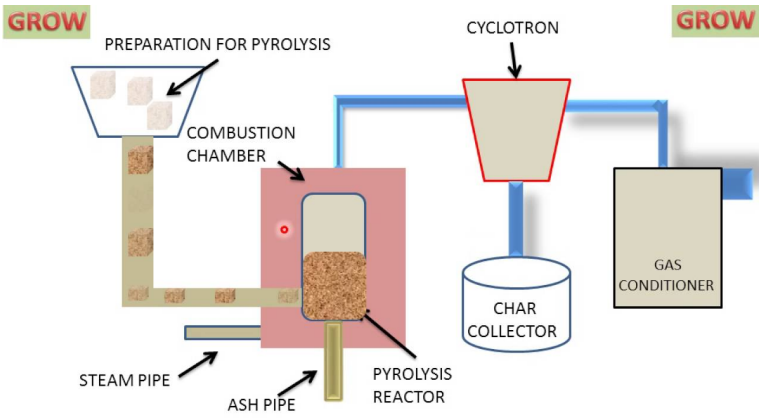


Figure 2.6: Gasification Process Schematics [14]

Electrolysis is one of the environmentally friendly alternatives to produce hydrogen gas because it uses the water as feed-stock. Electrolysis consists of two electrodes, cathode and anode, that with the help of electrical current will create hydrogen gas and another element, for example oxygen or chlorine, which depends on water purity. There are diverse types of electrolysis technologies, and currently there are three leading technologies and one in the development phase.

The most common method is the alkaline electrolysis, where the anode and cathode are separated by a diaphragm preventing the hydrogen from mixing with the other gas again and it does not depend upon a noble metal. In the Proton Exchange Membrane (PEM) electrolysis produces the purest hydrogen, however, the electrolyte is in a solid special form, usually with an Iridium-Gold-Platinum composition, turning the solution expensive. The Solid Oxide Electrolyser (SOE) works in elevated temperatures (700 °C - 800 °C), producing the electrolysis with water vapor, leading to higher efficiencies. The Anion Exchange Membrane (AEM) electrolysis is still in development, and it has a structure similar to PEM and uses the same process as alkaline electrolysis in the electrodes. In AEM the membrane is less expensive than PEM cell because it is a polymeric based membrane, and it produces purest hydrogen than alkaline electrolysis, so it can become the best efficiency vs cost method with the technology development [16, 17].

2.4 Hydrogen Embrittlement

Hydrogen embrittlement is a phenomenon where the mechanical properties of the materials are compromised due to the presence of hydrogen, which diffuses in the materials deteriorating its mechanical properties [5]. Hydrogen embrittlement, generally abbreviated to HE, represents a major challenge to the production, storage and transportation of hydrogen gas, and this hydrogen embrittlement is also known as the producer of hydrogen-induced cracking or hydrogen-induced damage [12]. In comparison to other common gases at equivalent pressures, hydrogen is more likely to leak quickly through some materials, cracks, or weak joints because of its tiny molecule size [5]. This easy penetration of hydrogen atoms through the materials and the high concentration of hydrogen gas in an environment make the prevention of hydrogen embrittlement exceedingly difficult [12].

The interaction of hydrogen atoms with the crystal lattice is a cause of concern in several materials, such as various metals used in the hydrogen storage and other engineering applications, where mechanical properties as tensile strength and fatigue strength are depreciated. The hydrogen embrittlement can lead to catastrophic effects, like fracture, and it often results in destructive cracks. This phenomenon is referred as the introduction of a hydrogen atom that dramatically lower a material's strength, when subjected to a hydrogen environment. The proposed mechanisms that cause hydrogen embrittlement are hydrogen-enhanced decohesion (HEDE), hydrogen-enhanced localized plasticity (HELP), and adsorption induced dislocation emission (AIDE). There are still various researches going about hydrogen embrittlement because the core mechanism responsible for hydrogen embrittlement is still unsatisfactory [4, 5]. In figure 2.7 is seen a schematic of hydrogen embrittlement mechanism.

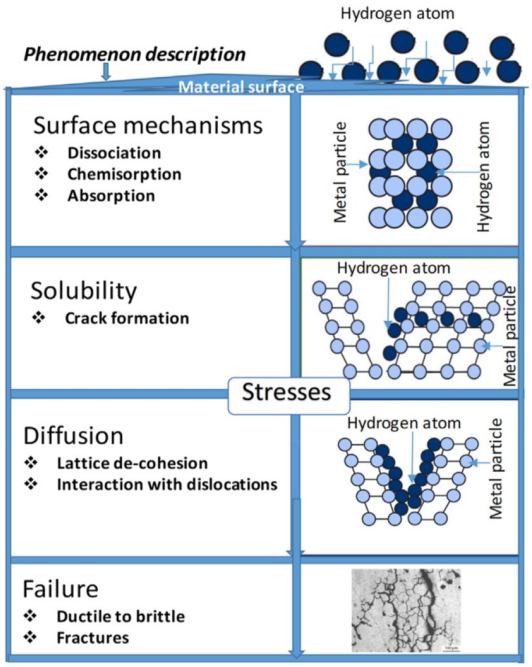


Figure 2.7: Schematic diagram of hydrogen embrittlement mechanism [5]

Testing for hydrogen embrittlement is crucial to guarantee the performance, reliability, and safety of materials and components. Under stress, the process of hydrogen embrittlement, in which hydrogen atoms permeate and gather within the crystalline structure of metals, can result in a sudden and catastrophic failure. In sectors like aerospace, automotive, and oil and gas, where structural integrity and operational safety are key, it is essential to understand and mitigate hydrogen embrittlement.

Failures caused by hydrogen embrittlement can have serious implications. For instance, in the aerospace sector, the failure of a crucial component owing to hydrogen embrittlement can have disastrous repercussions, possibly resulting in fatalities and expensive damage. Like this, hydrogen embrittlement in the automotive industry can endanger both drivers and passengers by undermining the structural integrity of critical parts. Hydrogen embrittlement, which affects equipment and

pipelines in the oil and gas sector, can result in leaks, environmental risks, and economic loss.

Comprehensive testing methods are necessary to effectively mitigate the dangers related to hydrogen embrittlement. These tests are designed to evaluate a material's susceptibility to hydrogen embrittlement and offer valuable information on the behaviour and functionality of hydrogen-exposed materials. The testing procedure simulates real-world operating settings by putting materials to controlled hydrogen environments and stress conditions, enabling precise evaluations of a material's resistance to embrittlement.

Testing for hydrogen embrittlement normally involves several significant procedures. First, it's important to choose the right test samples and materials. The desired use and possible hydrogen exposure should be considered while selecting the materials. Test samples are meticulously prepared and exposed to controlled hydrogen environments, either by exposure to hydrogen gas or immersion in hydrogen-charged electrolytes [18].

After that, test specimens are subjected to mechanical stress, like tension, to determine how susceptible the material is to embrittlement. Depending on the specific application needs and industry norms, other test methods may be used, such as Slow Strain Rate Testing (SSRT), Sustained Load Testing, or Constant Load Testing [19].

Temperature, pressure, and hydrogen concentration are all closely monitored and controlled while the test is being conducted. This enables assessment of the material's mechanical characteristics in the presence of hydrogen, such as strength, ductility, and fracture toughness. For material selection, design validation, and the creation of preventative measures to reduce the hazards of hydrogen embrittlement, exact and trustworthy test data is crucial. Engineers and scientists can discover vulnerable materials, optimize material compositions, and create efficient mitigation techniques by having a thorough understanding of how materials behave in hydrogen environments.

2.5 Hydrogen Embrittlement Testing

Hydrogen embrittlement testing plays a crucial role in ensuring the safety, reliability, and performance of materials and components in various industries. By simulating hydrogen exposure and mechanical stress, these tests enable evaluation of material resistance to embrittlement and inform the design and selection of materials that can withstand hydrogen-related challenges. Hydrogen embrittlement testing is a vital tool for preventing failures, improving safety, and advancing the development of materials and technologies in industries where hydrogen exposure is a concern.

In-situ mechanical testing plays a crucial role in understanding the behaviour and performance of materials under specific environmental conditions. By subjecting materials to mechanical loads in their actual operating environments, it becomes possible to gather valuable data on their structural integrity and durability. This type of testing allows more accurate assessment of material properties, such as strength, ductility, and fatigue resistance, in the presence of factors like temperature, humidity, and chemical exposure.

In the context of hydrogen embrittlement, *in-situ* mechanical testing provides insights into the materials' susceptibility to hydrogen in their intented application. Conducting *in-situ* mechanical testing, allow the evaluation of H_2 effects on the materials' properties, gaining a deeper understanding of hydrogen embrittlement mechanisms and develop strategies to mitigate its detrimental effects. *In-situ* mechanical testing is an indispensable tool in investigating and addressing the challenges posed by hydrogen embrittlement, ultimately leading to the development of more robust and reliable materials for hydrogen-related applications.

To begin the project of a chamber for hydrogen tests was performed a literature review to consider existing *in-situ* testing solutions, understand their requirements and understand potential problems and errors. Therefore, an examination of existing apparatus, with diverse types of requirements for the specific test and various methods of hydrogen gas production, was conducted to gather the necessary information for the initial stages of the design. The simplest solutions found are those that do not involve any external chamber for the H_2-rich environment, i.e., the specimen itself serves as a chamber to hold the hydrogen gas. Solutions like this can be found in Ogata, 2008 [20] and in Boot et al., 2021 [21], which have different working apparatus.

2.5.1 Specimen as chamber solutions

In Ogata, 2008 [20] it can be found a solution for testing from cryogenic temperatures to ambient temperature. This test was developed for tensile tests conducted from 25 to 298 K, specifically at 25, 77, 100, 120, 150, 190 and 298 K. In the different ranges of temperature, the specimen was surrounded by different elements. In the tests from 25 to 70 K, the specimen was surrounded by evaporated helium gas; at 77 K it was in a liquid nitrogen bath; from 100 to 170 K, the specimen, was surrounded by nitrogen gas; and from 190 to 298 K the specimen was cooled by alcohol.

In all of these temperatures, the reduction of area ratio is the key parameter used to assess the effects of hydrogen embrittlement. A ratio of one indicates no embrittlement effect, while a smaller ratio indicates a bigger effect of hydrogen embrittlement. Hydrogen gas is inserted into a hollow cylinder, after evacuation of the air inside the pipes. Although this apparatus is not used for high hydrogen pressure, this solution can be quite safe even if it is used with high pressure H_2. The apparatus used in this solution, as well as its test specimen, are shown in the figure 2.8.

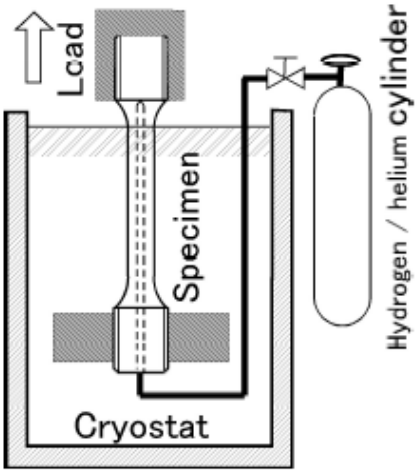


Figure 2.8: Apparatus presented in Ogata, 2008 [20]

Other approach to this specimen as chamber solutions is presented in Boot et al., 2021 [21], where the aim was to recreate the structure of a pipeline, so the specimen principle is similar to the one presented in Ogata, 2008 [20], a hollow specimen. This work is about an *in-situ* tensile setup that could be simply developed and accessible, with a maximum volume of hydrogen of 0.1 L to assure the safety of the system and so it could be easily operated without requiring special facilities. The purpose of this study was to study the influence of hydrogen embrittlement in the pipelines but also in its welds, with H_2 pressures up to 100 bar, at room temperature.

In this method, the hollow specimen is threaded in both ends, as it is shown in figure 2.9, and the hydrogen in inserted at the bottom, as shown in figure 2.10 **(b)**. This was designed to perform slow strain-rate tests, and the fracture was defined where the load drops 20% from its maximum between two steps. To study the hydrogen embrittlement, it was applied a pre-charging step. In this apparatus we find a reference to the insertion of an inert gas, in this case nitrogen gas, to remove impurities from the test piece and the environment. The nitrogen gas is flushed twice to remove any impurities and then it was also pressurised the environment to the required pressure and monitor that for 10 minutes there is no leakage to ensure the safety of the test. At Boot et al., 2021 [21], the variable controlled was the gas pressure, being 100 bar the maximum pressure in study. This apparatus also allows a less expensive way to perform hydrogen embrittlement testing, as previous, and, releasing just 6 mL of hydrogen gas upon the fracture of the sample, it is safe to test the specimens. The apparatus assembly can be seen in the picture of the figure 2.10 **(a)**.

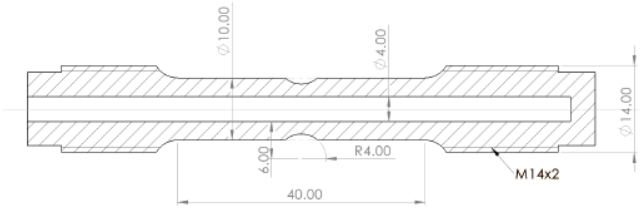


Figure 2.9: Technical drawing of the sample geometry used in Boot et al., 2021

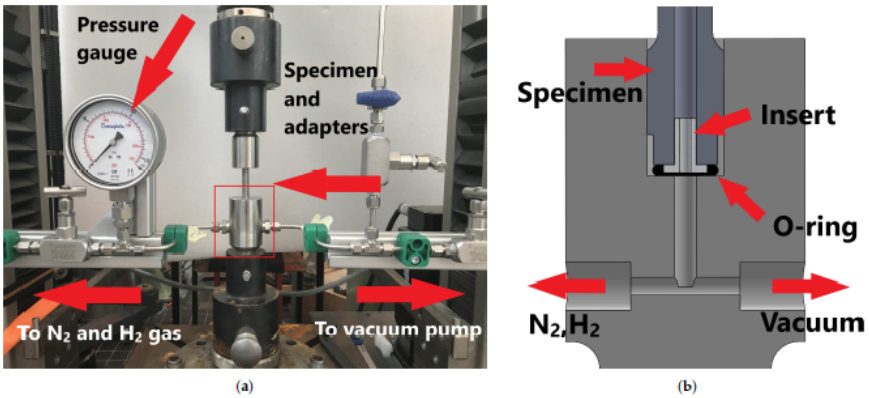


Figure 2.10: **(a)** Picture of the specimen and adapters in the tensile tester. **(b)** Section of the test area, displaying the bottom adapter and the connection with the specimen [21]

2.5.2 External to the specimen chamber solutions

At Zwick Roell two solutions for Hydrogen Embrittlement testing are presented, which are developed because of a partnership with the Materials Testing Institute at the University of Stuttgart. The test machines use several hydraulic load frames and there is an autoclave attached [22].

In one of the apparatus the test chamber is in the form of a pressure vessel, which is lowered and sealed in a way that the specimen is tested inside of it.

In the other one, the test specimen is attached directly inside of the chamber, which is a metal hollow cylinder with very thick walls and closed in one of the ends, being closed by other thick wall piece of metal. The closure of this apparatus is assured by screwing nuts onto pre-existing threaded cylinders in the test chamber.

These solutions are made for tests performed at temperatures from 4 to 563 K, for liquid or gaseous hydrogen, at pressures up to 400 bar, in specific cases up to 1000 bar, with nominal dynamic force up to 100 kN. The systems presented by Zwick Roell are used to preform tensile tests, fatigue tests and fracture mechanics test. The tests performed on this apparatus include, among others, tests to examine fracture mechanics on CT specimens, slow strain rate behaviour, or fatigue properties using notched threaded-end specimens, and it is considered that the slow strain rate test (SSRT) is a very important test for evaluate the hydrogen embrittlement in the materials [22].

The origin of hydrogen to these Zwick Roell solutions is not referred, however, the hydrogen

is not generated inside the chamber and is introduced by some other method. Both apparatuses configurations are presented in figure 2.11.



Figure 2.11: Apparatus presented by ZwickRoell **(a)** where pressure vessel is lowered and **(b)** with thick walls metal cylinder chamber [22]

A different approach is proposed by Shimadzu [23], where the hydrogen gas is generated inside the chamber.

Shimadzu has as objective study the impact of hydrogen in hydrogen fuel cells and its tubing, and to study its effects in hydrogen stations [23]. So, in order to study the effects that a fuel cell is subjected, two different tests are made. The objective of one system is to simulate the elevated temperature and high humidity environment typically found in a fuel cell using a constant temperature and humidity chamber. However, this aspect is not relevant to the subject under study, which focuses on the design of a testing system for a rich hydrogen atmosphere at temperatures around 20 °C [24]. The other test is applied to study the effect of hydrogen embrittlement of the metals.

To study the hydrogen effects, it is performed slow strain-rate tests, as stated before, the most important to acknowledge the hydrogen effects. To perform those tests a hydrogen test chamber is used, and hydrogen gas is generated inside the chamber, figure 2.12. The H_2 is generated by the electrolysis of water, having as by-products H_2 and O_2, being that all the components are submerged in a water bath. To perform the electrolysis of water is used a potentiostat and some sacrifice metals, but there is no mention of which ones, generating hydrogen gas that stays in the water bath to directly accomplish the hydrogen embrittlement in the test specimen [23]. The test specimen is threaded in both ends before being fastened in the water bath, and this sample has a geometry approximately similar to the one described in ASTM F519 [19].

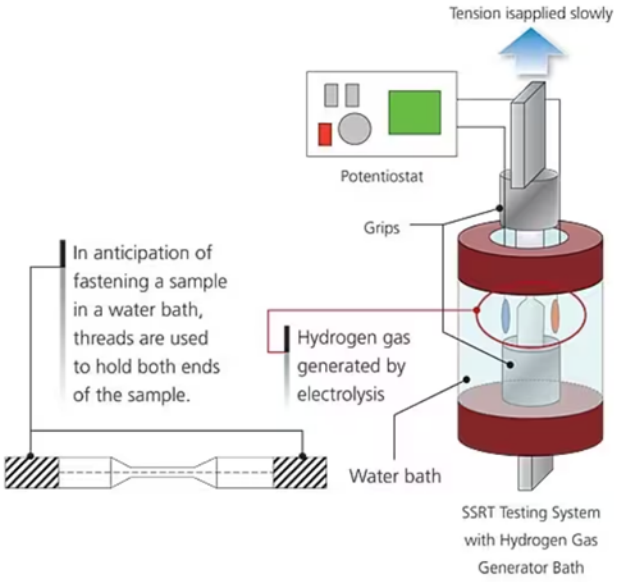


Figure 2.12: Schematics of the apparatus presented by Shimadzu and the used specimen [23]

Ghent University [25] developed a project with the aim of development a methodology and set-up for fracture toughness testing, with special focus on single notch tension tests, because is where representative values for the fracture toughness of thin walls structures. The university researcher, Margo Cauwels, developed this apparatus to perform the test in two pipeline steels, one vintage and one modern steel grade.

In the solution presented by Ghent University we find a similar apparatus to the one previously presented by Shimadzu [23]. The test is performed inside a liquid bath where the specimen is submerged, and the hydrogen gas is generated on site during the test, as schematized in figure 2.13. In this test there is no reference of the geometry of the test sample, only that it will be applied an axial tension, griped in both ends of the specimen. The generation of H_2 will be made by electrolysis of H_2SO_4, that has as by-products H_2 and SO_4, and the H_2 rich environment is formed *in-situ*, inside of the chamber [25]. The difference between the Ghent University apparatus and the Shimadzu one is the liquid bath, one being H_2SO_4 and the other being water, H_2O, respectively.

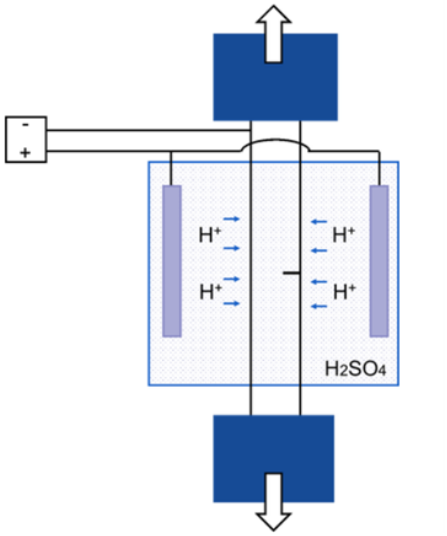


Figure 2.13: Apparatus presented by Ghent University [25]

In Hajilou et al., 2018 [26] it is found an apparatus with a similar function as the ones proposed by Shimadzu [23] and by Ghent University [25], but for nano-scale applications. The chamber is made from glass and has the capacity of sealing all the openings, enabling the permeation cell to be submerged into a water bath, because, similar to the previous solutions, the H_2 is generated by electrolysis inside the chamber. In order to perform the electrolysis, it is used cathodic and anodic cells, Polychlorotrifluoroethylene and Polyoxymethylene, that are positioned in both sides of the testing sample, using platinum wires as counter electrode and silicon gaskets to seal the caps.

The testing procedure implies potentiostats to control the current, and to perform the test a potentiostatic potential of 0 mV was applied in the anodic compartments for 24 h so that the possible diffusible hydrogen present in the sample could be extracted. The exposed area of the sample was 4.4 cm^2 and was polished down to 1 µm on both cathodic and anodic surfaces [26]. This apparatus use $Hg/HgSO_4$ reference electrodes and the potentials were reported with this reference electrode. The apparatus used in this approach and a brief scheme can be seen in the figure 2.14.

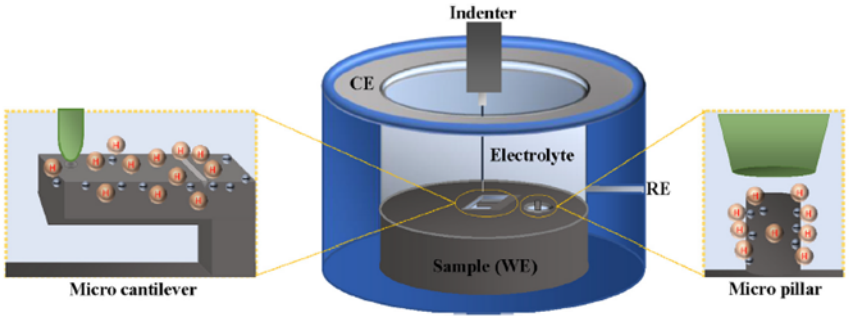


Figure 2.14: Apparatus presented in Hajilou et al., 2018 [26]

The Shimazdzu [23], Ghent University [25] and Halijou et al., 2018 [26] are apparatuses where

the maximum pressure inside the chamber is not as high as the solutions proposed by Yokogawa et al., 2008 [27] and Alvine et al., 2014 [28].

In the industrial processes, very often the materials are subjected to high-pressure and elevated temperatures conditions, and, in order to test the effects of hydrogen embrittlement in these conditions, in Yokogawa et al., 2008 [27] it can be found an apparatus that can meet the requirements of hydrogen testing at elevated pressures and temperatures. This apparatus is designed to be applied with an external load cell, usable for tensile testing, and is designed to be easily adapted to any commercial testing machine and to facilitate the tensile load measurement independently of the stress caused by the gas pressure and the friction at sliding seals.

The apparatus presented by Yokogawa et al., 2008 has 370 mm of diameter by 1200 mm height, and the inside chamber has a diameter of 170 mm by 280 mm height, i.e., approximately 0.05 m^3 of volume, and the predominant material of building is the stainless steel AISI 316. This pressure vessel can sustain pressures up to 50.5 MPa during the test and the maximum load applicable to the specimen is 19.61 kN, with a maximum temperature of 773 K obtained by the internal electric heater of 8 kW capacity. In the side of the vessel there is a circulation of tap water through water jackets to cool the vessel to protect against O-rings thermal degradation. The schematics of this apparatus can be seen in figure 2.15 and it contains a main body with the main chamber where the test occurs and a counter chamber that is connected to the test chamber by a connecting pipe to introduce high pressure gas in this counter chamber so that a compressive load is applied with the same pressure in the counter chamber to assure that no resultant force acts on the specimen before the application of the external load [27]. In this solution there is no reference on the H_2 origin but is clear that the hydrogen gas will be inserted in the chamber, i.e., not generated inside.

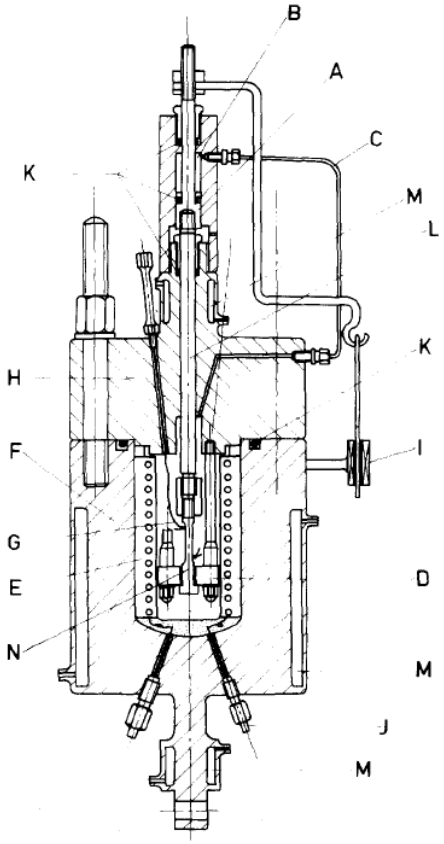


FIG. 1. Schematic diagram of pressure vessel for tensile testing in high-pressure gas at elevated temperature. A—Piston; B—counter chamber; C—connecting pipe; D—stay board; E—electric heater; F—main body; G—thermocouple; H—vessel lid; I—extensometer; J—heater terminal; K—O-ring; L—load rod; M—water jacket; N—specimen.

Figure 2.15: Apparatus presented in Yokogawa et al., 2008 [27]

Hydrogen embrittlement affects metals, but it also can affect some polymers, and, to understand the effect of HE in these materials, Alvine et al., 2014 [28] developed a solution to perform tensile tests for polymers in high pressure hydrogen. The *in-situ* tensile tester works by the application of a load to a specimen while measuring the applied load and the displacement/elongation of the sample. The specimen and device schematics are presented in figure 2.16.

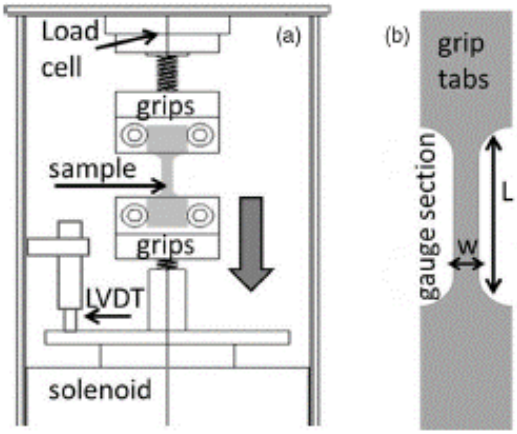


Figure 2.16: Schematics of the apparatus presented in Alvine et al., 2014 with an **(a)** operational schematic of the *in-situ* tensile tester with sample and **(b)** a schematic of a typical "dog-bone" sample. [28]

The apparatus presented in this paper consists in a high-pressure hydrogen autoclave, which has an internal diameter of 123 mm by 305 mm height. The load cell (1) is fixed in the top of the chamber and measure the loads applied in the sample, which is clamped by two grips (2). The solenoid (4) that supply the tensile load in the vertical direction has a maximum force of 530 N and the elongation is measured by the LVDT (3), that measures the displacement of the solenoid core relative to the initial position. This solution allows pressures up to 35 MPa but, even though this is a safety limit, the tests are below the allowable pressure of the vessel rupture disks, to ensure venting before vessel maximum pressure is reached. The maximum temperature reached inside the chamber can be 300 °C, but, because of the plastics components inside, the tests can only be performed with a maximum temperature of 100 °C. After the autoclave sealing Argon inert gas is flushed as least five times to remove oxygen and after that the inert gas is displaced by flushing high purity low-pressure hydrogen at least five times, also, and then followed by pressurization of the chamber with high purity hydrogen to the desired pressure. To assure that the sample are fully saturated the specimen is submitted to at least 20 h of high-pressure hydrogen before testing [28]. This apparatus took in consideration the safety precaution when working with high-pressure hydrogen like oxygen removal, hydrogen-safe materials, high-pressure relief devices, adequate venting, among other, and it can be seen in figure 2.17.

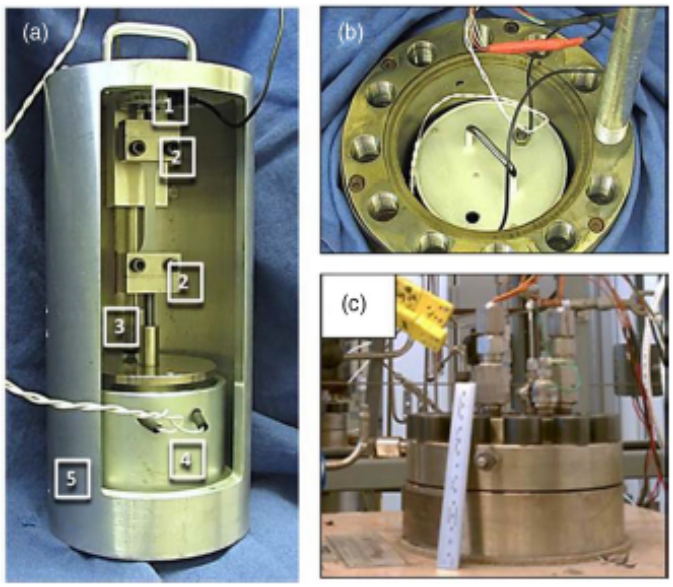


Figure 2.17: Apparatus used by Alvine et al., 2014 with the **(a)** side view of the *in-situ* tensile tester and the key parts, **(b)** the *in-situ* tester resting inside the high-pressure hydrogen autoclave prior to sealing and **(c)** the top of the high-pressure hydrogen autoclave after sealing [28]

2.5.3 Apparatus summary

Based on the eight apparatuses discussed earlier, it is evident that there is no standardized approach for designing a chamber specifically for *in-situ* mechanical testing in hydrogen-rich environments. Each of these solutions has unique characteristics and requires careful consideration.

One common feature among the presented apparatuses is their meticulous approach to provide a safe use of hydrogen, considering its high flammability and inherent risk of leakage. Additionally, many of the solutions involve the use of an inert gas to purge the chamber of oxygen and other particles that could potentially affect the accuracy of the test results. This emphasis on safety and controlling the testing environment underscores the importance of mitigating potential hazards associated with hydrogen and ensuring reliable and valid experimental outcomes.

In terms of hydrogen origin, the existing data show the use of hydrogen already stored in vessels or the production of hydrogen in the chamber where the test will be performed, by a liquid bath that promotes the H_2 formation by electrolysis. The usual pressures for the use of hydrogen, except the solution prepared for high pressures, are around 30 MPa, even if the chambers support more, and the specimens depend on the machine where they are applied and on the need of having a chamber function or not, being most of them with threaded ends.

The autoclave method already has some standards and some guidelines for its application, but it could be high costly, and it can imply long test times, nevertheless, the autoclaves can assure more safety measures to high-pressure and elevated temperatures, having more developed technology and more studies about it . This can be opposed by the shorter test times allowed by the hollow specimen, that also is more economic, but this kind of specimen are not standardized and the relation between the results obtained by the two solution is not yet determined, so, although it

can be manipulated to assure all the safety requirements to hydrogen testing, it is yet to be studied how this solution performs face to the autoclave solution [29].

Chapter 3

Chamber Design

This chapter comprehensively presents the design process of the required chamber, including the rationale behind each step and the justification for the chosen design options. It takes into account the various apparatuses discussed in chapter 2 and their respective design choices.

The design of the hydrogen embrittlement testing chamber takes into consideration the dimensions and specifications of two existing machines in INEGI laboratories, being them the Portable Test Machine v2 (PTM2), seen in figure 3.1, and the High-Speed Machine (HSM), seen in figure 3.2. The chamber is specifically designed to integrate these machines, ensuring compatibility and optimal testing conditions, but it is also applicable to other machines.

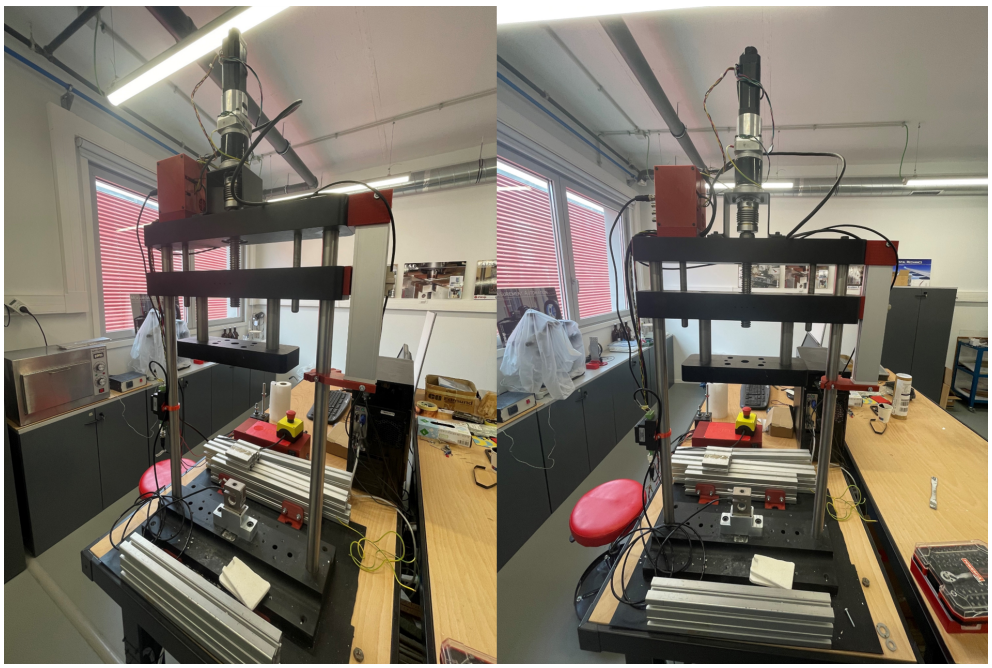


Figure 3.1: PTM2 machine existent in INEGI laboratory

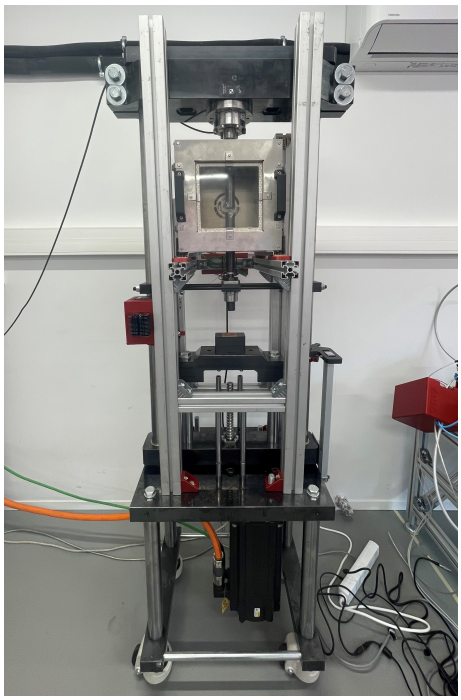


Figure 3.2: HSM machine existent in INEGI laboratory

In this chapter, all of the requirements, subsytems specifications and design choices along with their reasoning are stated.

During the design process of this rich atmosphere testing system, various solutions were carefully considered and evaluated to ensure optimal performance. Each element was thoroughly explored, and the most advantageous solutions were selected to ensure the smooth operation of the apparatus. To aid in the design process, the apparatus was modeled in 3D using Solidworks.

3.1 System Requirements

Understanding and defining the system requirements in great detail is the first step in designing the H_2 rich atmosphere testing system. Given that this project will be working with highly flammable, leak-prone hydrogen gas, it is essential to prioritize and carefully consider all safety issues related to handling this gas. To ensure a safe and controlled environment, strict safety protocols and guidelines become essential.

An extensive analysis of safety precautions and measures is necessary, considering the potential hazards posed by hydrogen gas. This entails putting in place suitable ventilation systems, adding hydrogen sensors for leak detection, and making sure that all safety precautions are followed strictly when handling gas. The testing chamber design must be so that it effectively mitigates risks and ensures a secure operating environment for working with hydrogen gas. As such, it is fundamental to carefully analyze and define the safety requirements for the given system.

Furthermore, it is crucial to define safe operating procedures, and to incorporate into the design safety mechanisms that ensure all required safety precautions are undertaken by the operator when

handling hydrogen gas. This guarantees the best practices, enhancing the project's overall safety. The testing chamber design should be tailored to provide a secure and controlled environment for working with hydrogen gas by giving safety considerations priority right away.

3.1.1 Hydrogen Gas Use Requirements

Strict adherence to safety procedures and precautions is required when using hydrogen gas in a laboratory setting. Due to its high flammability and low ignition energy, handling and using hydrogen safely requires special precautions. It is essential to detect quickly any potential H_2 leak, making use of hydrogen sensors to do so and incoporate adequate ventilation. Furthermore, measurement and log the amount of atmospheric hydrogen during testing is a requirement for safety purposes and to follow the operational requirements.

It is crucial to prioritize an explosion-proof design and carefully pick components that are compatible with hydrogen when designing a system to handle hydrogen gas. Hydrogen gas should never come into contact with oxygen, due to the explosion risk, and anything that could cause a spark should be kept far away from the test area, preferably in a separate room. It is essential to gauge and confirm that the hydrogen concentration inside the test chamber is close to zero before opening the seal to ensure that there is no release of hydrogen into the lab environment. Operators must adhere strictly to all safety precautions and have a solid understanding of hydrogen safety protocols.

The project will maintain a secure environment for working with hydrogen gas by addressing these safety considerations, implementing suitable ventilation and utilizing hydrogen sensors. While operators training is recommended, safety by design will be incorporated in the developed system to mitigate the risks associated with hydrogen's flammability and to ensure the security of laboratory personnel and equipment.

3.1.2 Material Safety Requirements

Hydrogen embrittlement is a detrimental phenomenon affecting many materials, and as such, it is a crucial consideration when design and choosing materials for a test chamber to study this phenomenon. It is crucial to choose a hydrogen-resistant material, to mitigate the risk of leaks, cracks, or fractures. Given that different materials have different compatibility thresholds for pressure and temperature, the selected material should be able to withstand the expected testing temperature and pressure. The use of sensors is key in ensuring that test conditions are within safe levels and required conditions of the test procedures [30].

To ensure accurate test results, it's essential to maintain a clean testing environment. Is important to avoid contamination of the test environment, avoiding dust, oils or greases in the chamber surfaces. To further guarantee a dependable and secure chamber, pressure-resistant seals must be used. To avoid potential explosions or unexpected ignition events, all components must be subjected to stringent maintenance controls, including prompt replacement of any damaged components.

The designed chamber will enable precise and dependable hydrogen embrittlement tests by carefully considering material selection, putting in place pressure-resistant seals, and upholding stringent maintenance control. By taking these precautions, the risk of leaks is reduced, test integrity is preserved, and potential risks related to hydrogen embrittlement induced failure in the testing system components themselves are mitigated.

3.1.3 Present System Requirements

The testing will be carried out at ambient temperature, according to ISO/IEC 17025 [24], around 20 °C and 25 °C, which is within operating temperatures of most engineering materials, not constituting a demanding requirement in the point of view of material selection [31], [32].

The system requires a hydrogen gas generation subsystem, as H_2 gas is not a regular consumable in most mechanical characterization laboratories. As such, it is more convenient and economical to generate *ad-hoc in-situ* H_2 gas.

In this system design, the applied internal pressure is set by the test procedure atmosphere requirements and material's strength. As a first reference value, it will be used the reference of 15 MPa to the maximum pressure obtained inside the chamber, as it was necessary for calculations and some considerations. However, it should be noted that the expected operational pressure will be significantly lower, and its actual value will be determined by the strength of the materials used.

To enable the assembly of the system in the machines, the hydrogen test chamber needs to an opening for specimen loading and setting up, which needs to be properly dynamically sealed. The maximum applied axial load on the specimen by the machines is 20 kN, either in compression or tension. The system must ensure that the sealing is not compromised at maximum applied axial load and that the chamber components do not undergo permanent deformation (plastic deformation) at these loads. In order to fulfil the hydrogen safety regards is important to fulfil all the requirement stated in sections 3.1.1 and 3.1.2 , being important to assure the proper ventilation of the room and the right choice of the H_2 sensor in order to always monitor the hydrogen gas levels present in the atmosphere and enable alarms to be set.

The test chamber may take any form, as long as its dimensions do not surpass the maximum free space in the testing machines in which it will be integrated. To this end the volume is limited by the distance between the machines side pillars and between the top of the base and bottom of the cross-bar. Even though the H_2 test system is set to be machine agnostic and as such capable of being assembled onto a variety of machines, the two previously mentioned existing machines in the INEGI's non linear mechanics laboratory will be used as references.

In the HSM the distance between the side pillars is 450 mm with a maximum distance of 500 mm between the clamps, that have a width of 100 mm. The distance of this machine to the wall is adjustable because it has wheels that enable the easy repositioning of the machine.

The PTM2 has a distance between the side pillars of 400 mm, with a maximum height of 350 mm, and its clamps have a width of 80 mm.

So, the maximum height of the chamber must be lower than 350 mm and, in order to have space to clamp the specimen and space to work, is recommended that the distance between the

chamber walls is around 155 mm. The traveling arm of the PTM2 has a maximum course of 40 mm, 20 mm in each of the axial directions, but the effective course is about 18 mm for each direction. The machines load cell is positioned on the bottom in one of the machines and on the top in another, so the chamber should be designed as to enable assembly in both configurations.

In hydrogen embrittlement testing, it is essential to incorporate an inert gas flush before the start of the test to ensure the atmospheric conditions. The end cap of the chamber must be design with through-holes to enable the introduction and removal of the inert gas and hydrogen. It is crucial to ensure that these holes are properly sealed to prevent any leakage.

The release of the chamber atmosphere must be done to the open outside atmosphere without requiring any special process, as the relatively small quantities of inert gas, N_2, and H_2, used in testing do not pose an environmental hazard. Such release to the open outside atmosphere mitigates any risk of ignition within the laboratory, when opening the chamber.

All of these requirements are crucial consideration in the solution's design. To ensure a systematic organization and easy accessibility of these requirements throughout the project, they have been consolidated in table 3.1. This table serves as a valuable reference, facilitation efficient consultation and improving the understanding and perception of this dissertation's design process.

Table 3.1: Functional and Safety Requirements

Requirement	**Description**
Leakage control	Apply a H_2 concentration sensor to control the chamber environment
Specialized material	Choose hydrogen embrittlement-resistant material
	Apply strict maintenance control to the chamber parts
Avoid explosion risks	Insert an inert gas to remove the O_2 molecules
	Remove anything that can cause a spark from the working laboratory
Avoid contamination	Insert an inert gas to remove impurities from the chamber
Safe work space	Ensure adequate ventilation in the laboratory to mitigate hydrogen gas risks
	Evacuation of the chamber atmosphere to the outside to prevent hydrogen releasing inside the building
	Ensure the chamber sealing until the H_2 concentration inside is zero
Safe testing	Measurement of the testing temperature to ensure the safety of the materials
	Measurement of the testing pressures to avoid excessive pressures that would break the materials
	Apply seals to hold the hydrogen gas inside the chamber
	Apply a pressure relief valve to prevent excessive pressures inside the chamber
	Ensure that all the applied valves or hoses are suitable for hydrogen applications
Machine movement	Create a through-hole proper dynamically sealed to connect the machine for testing
	Ensure that the chamber parts are capable of sustaining a 20 kN axial force without compromising the sealing

3.2 Subsystems and Functional Diagram

Establishing a functional diagram and knowing the system's subsystems are essential for ensuring efficient system operation. A hydrogen test chamber has a number of subsystems that are crucial to achieving the desired functionality. This research identifies five crucial subsystems, including:

- **Hydrogen Gas Generation:** This subsystem involves the provision and management of the hydrogen gas supply. It includes components such as hydrogen generation, regulators, and safety mechanisms to ensure controlled and safe delivery of hydrogen. The flow and volume of hydrogen gas introduced into the chamber are controlled by this subsystem.

- **Sensors:** The management and integration of the various sensors used inside the chamber fall under the purview of the sensors and control subsystem. These sensors could be leaking detectors, pressure sensors, temperature sensors, and chemical concentration sensors for

hydrogen gas. With the help of the subsystem, test conditions can be precisely controlled and analysed in real-time.

- **Valves Sealing:** The mechanisms in charge of creating and preserving the integrity of the chamber seals make up the sealing valves subsystem. During testing, it guarantees proper sealing and reduces the chance of gas leakage.
- **Chamber Atmosphere Releasing System:** After testing, the chamber atmosphere can be safely released and evacuated using the chamber atmosphere releasing system. Vacuum pumps, vent valves, or exhaust systems might be used as mechanisms to ensure controlled and effective gas removal.
- **Inert Gas Flush:** This component regulates the introduction and movement of inert gas inside the chamber. It makes it easier to get rid of any leftover air or contaminants, resulting in a regulated and clean environment for testing.

The design and operation of the hydrogen test chamber can be efficiently coordinated by identifying and defining these subsystems. To achieve precise control, maintain safety, and produce reliable test results, each subsystem is essential. In figure 3.3 a visual summary of the subsystems and some required components is presented.

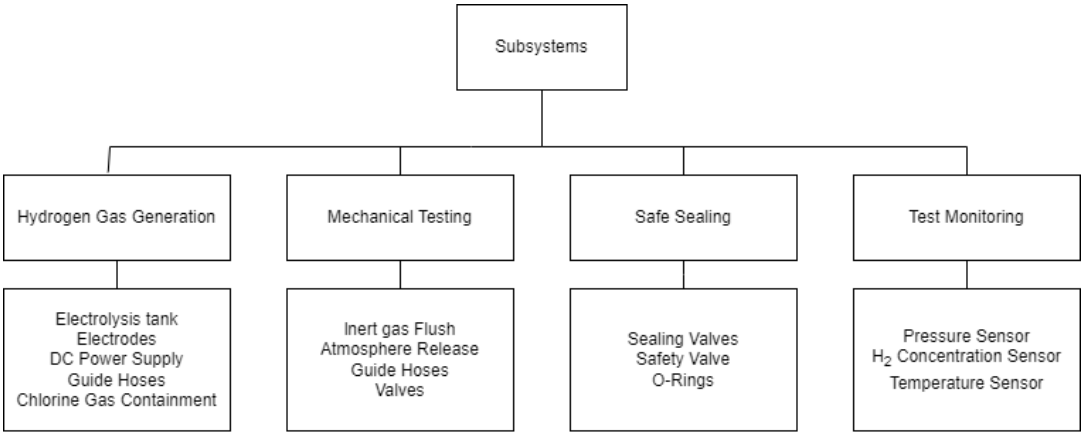


Figure 3.3: Subsystems and applicable components

3.2.1 Hydrogen Source

The hydrogen will be generated *in-situ*, by the mean of saltwater electrolysis. The electrolysis, as referred in section 2.3, can be alkaline, PEM, SOE or AEM. As the temperature for SOE is above 700 °C it is not technically feasible for the intended solution, because it would require a complex system and the test procedures to employ in the solution to be developed do not necessitate larger quantities of hydrogen gas. The hydrogen embrittlement tests will be operated at much lower temperatures, so a cooling system would be required, adding to the complexity of the final solution. The other three solutions can all be implemented in the present design.

Vincent et al., 2018 [17] compared these methods, and it can be seen that although PEM and AEM solutions produce the purest hydrogen, the more mature method is alkaline electrolysis, being PEM technology mature only for small scale applications and AEM technology is still in research and development. As AEM technology is quite recent and is still in development, that is yet no data relative to the system cost. The cost of alkaline electrolysis is approximately 700 to 800 euros (€) less per kilogram (kg) compared to PEM. Alkaline is priced at 1300-800 €/kg, while PEM is priced at 2000-1200 €/kg. Due to its cost-effectiveness and the availability of readily accessible components such as salt and water, as well as the ease of manufacturing or sourcing electrodes, the preferred method chosen for hydrogen generation in this project is alkaline electrolysis. The previously stated information and more relevant information are found in the table 3.2, that provides easy comprehension of these three electrolysis methods.

Table 3.2: Comparison between Electrolysis Solutions, extracted from Vincent et al., 2018 [17]

	Alkaline	PEM	AEM
Electrolyte	20-30% KOH	PFSA	QAPS
Charge carrier	OH	H+	OH
Typical Discharge H_2 pressure (bar)	25-30	30-80	30
Conventional current density (mA cm^{-2})	200-500	800-2500	200 - 500
Demonstrated durability (h)	100 000	100 000-50 000	NA
Hydrogen purity (vol%)	99.3-9.99	99.9999	99.99
Typical current efficiency	50-70.8	48.5-65.5	39.7
Demonstrated rated production(N m^3 h^{-1})	1-760	0.265-30	0.25-1
Specific energy consumption (kW h N m^{-3})	4.5-7.5	5.8-7.3	5.2-4.8
Demonstrated rated power (kW)	2.8-3534	1.8-174	1.3-4.8
System cost (€ kg^{-1})	1300-800	2000-1200	NA
Technology status	Mature	Mature (small scale)	R&D

In Vincent et al., 2018 [17] it can also be found the table 3.3 that summarises the advantages and disadvantages of the alkaline, PEM and AEM electrolysis. As evident from the analysis, alkaline electrolysis, while not boasting the highest performance among the presented solutions, proves to be the most cost-effective and economically viable option. The easily obtained components and the fact that this solution is more mature has the advantage that a lot more solutions can be found in the market, so is the preferable solution for this hydrogen generation.

Table 3.3: Advantages and Disadvantages of the electrolysis processes, extracted from Vincent et al., 2018 [17]

Alkaline	PEM	AEM
Advantages		
Mature technology	Higher performance	Non-noble metal catalyst
Non-PGM catalyst	Higher voltage efficiencies	Noncorrosive electrolyte
Long term stability	Good partial load	Compact cell design
Low cost	Rapid system response	Low cost
Megawatt range	Compact cell design	Absence of leaking
Cost effective	Dynamic operation	High operating pressure
Disadvantages		
Low current densities	High cost of components	Laboratory stage
Crossover of gas	Acidic corrosive components	Low current densities
Low dynamic	Possible low durability	Durability
Low operating pressure	Noble metal catalyst	Membrane degradation
Corrosive liquid electrolyte	Stack below Megawatt range	Excessive catalyst loading

3.2.1.1 Alkaline Electrolysis

The alkaline electrolysis of saltwater, H_2O and NaCl, has as by-products H_2, Cl_2 gaseous, and NaOH in aqueous solution. The semi reactions in the cathode, anode and the full reaction of this electrolysis are:

Dissociation of NaCl: $2\,NaCl \longrightarrow 2\,Na^+ + 2\,Cl^-$

Autoionization of water: $2\,H_2O \longrightarrow 2\,H^+ + 2\,OH^-$

Semi reaction in cathode: $2\,H^+ + 2\,e^- \longrightarrow H_2$

Semi reaction in anode: $2\,Cl^- \longrightarrow Cl_2 + 2\,e^-$

Global Reaction: $2\,NaCl + 2\,H_2O \longrightarrow 2\,NaOH + H_2 + Cl_2$

The H_2, the desired product of the reaction, is formed in gaseous form, so it is easily conducted to the test chamber. The products of the electrolysis reaction, NaOH and Cl_2, are consequently formed in the electrolysis process. These other reaction products are not desirable, and both of them can be harmful, especially Cl_2, so further actions are required to neutralize both.

To perform alkaline electrolysis of saltwater it is required water, salt, electrodes, a vessel to contain the liquid and a power supply. The process of electrolysis involves the use of direct current (DC) power source, an anode and a cathode. In figure 3.4 is presented a schematic of an electrolysis process with some relevant information.

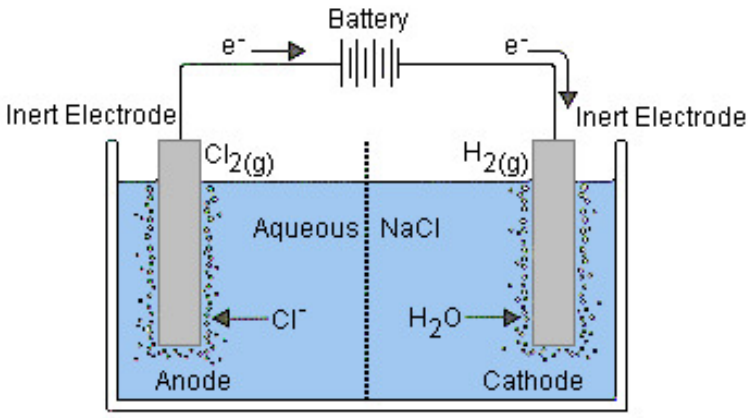


Figure 3.4: Schematic of electrolysis of saltwater [33]

The anode is the positively charged electrode where oxidation occurs and, unlike some sacrificial anodes, in the alkaline electrolysis the anode is intended to be stable and endure the electrolysis process without significant corrosion, having the focus in efficient and controlled electrochemical reactions over sacrificial protection. Some of the materials for the anode in saltwater electrolysis are titanium, platinum, graphite or other non-reactive metals coated with a stable oxide layer. Titanium is the most common choice for anodes in saltwater electrolysis due the high stability of this material in aqueous environments and its significant corrosion resistance [34]. This is primarily attributed to the formation of a protective oxide layer on titanium, which effectively prevents corrosion and ensures the long-term durability of the anode. Platinum also provides excellent performance and durability because it is highly inert and resistant to corrosion [35], [36]. However, platinum is a high-cost material, which limits its general use. Graphite offers good electrical conductivity and resistance to corrosion, so it is suitable for alkaline electrolysis applications, and even though this material is not as durable as the other two, graphite is the most cost-effective option for anodes in saltwater electrolysis [37], [38].

The cathode is the negatively charged electrode where reduction occurs, and its material is chosen for its stability, conductivity and resistance to corrosion in the alkaline environment. The cathode is a non-reactive electrode that facilitates the reduction reaction where hydrogen gas is produced. The cathode is not indended to degrade or sacrifice itself in the electrolysis process, serving only as a site for the reduction of ions. Some cathode materials used in alkaline electrolysis of saltwater include stainless steel, nickel, platinum, graphite or other non-reactive metals. These materials are selected for their ability to endure the electrolysis process without significant corrosion or degradation, ensuring the efficiency and longevity of the electrolysis system. Stainless steel is a popular choice for cathodes in saltwater electrolysis because it has a good cost-effectiveness ratio and provides a good performance in several applications. This is due to the corrosion resistance and durability of the stainless steel [39]. Nickel is also commonly used because it offers great conductivity and has a good corrosion resistance, and this makes it suitable for efficient electrochemical reaction in the alkaline electrolysis environment [39]. Platinum,

when applied as the anode, provides excellent performance and durability because it is highly inert and resistant to corrosion, being limited by its high cost [36]. The graphite is a good economical choice for the saltwater electrolysis cathode, as it is for the anode, because graphite offers good electrical conductivity and resistance to corrosion, being again the most cost-effective option [37], [38].

Is important to identify which of the electrodes will be connected to which pole of the power supply so the correct material is used in the right place. Also, since each electrode is responsible for a specific reaction, either oxidation or reduction, it is crucial to identify the electrode that generates H_2 gas. This information is essential for effectively directing the gas flow into the chamber.

It is also important to identify in which electrode the production of Cl_2 occurs because, as stated before, this is a very harmful gas, and it cannot be released directly into the atmosphere and is a health and safety hazard [40]. The chlorine can be detected by the odour in concentrations as low as 0.1 – 0.3 ppm, and from 1 ppm up dangerous health symptoms start to surface. At 1 – 3 ppm starts the irritation of the mild mucus membrane that can be tolerated for about an hour, and from 5 – 15 ppm the irritation is moderate. At 30 ppm it causes immediate substernal chest pain, shortness of breath and cough, that becomes toxic pneumonitis and/or acute pulmonary oedema at 40 – 60 ppm. The concentration of this gas poses higher levels of danger the highest the concentration in the air, and at concentrations about 400 ppm, it is generally fatal in exposures over 30 minutes, and the time decreases for only a few minutes at concentrations above 1000 ppm [40]. Cl_2 neutralization brings additional risks, so it should be contained and disposed by trained professionals outside the laboratory.

NaOH, present in an aqueous solution can cause irritant contact dermatitis or corrosion, so it needs to be conducted safely and disposed correctly. This substance can be disposed through competent authorities with correct disposal or by the neutralization of this substance [41]. To correctly neutralize the sodium hydroxide, a weak acid can be added, such as citric acid or vinegar, while stirring. The acid must be added in small quantities to prevent a rapid reaction, and the pH is tested to confirm that the solution has a pH almost neutral, between 6 and 8. Once neutralized it can be diluted with a large volume of water and when it is not considered harmful or hazardous it can be disposed of down the drain, after checking the local regulations and guidelines to assure that it is permissible in the area in study [42]. After this disposal plenty of water should run down the drain to flush it away and further dilution happens.

3.2.1.2 Electrolysis system requirements

The electrolysis system consists of a number of important parts that must operate in tandem to enable the electrolysis process in a controlled manner. An electrolysis tank, a power source, electrodes, and guide pipes are some of these parts. Each element is essential to the effective production of the desired products through electrolysis.

The central vessel in which the electrolysis reaction occurs is the electrolysis tank. It is made to hold the electrolyte solution and make it easier to separate the chlorine and hydrogen gases.

The power supply, which provides the required electrical energy to power the electrolysis process, is a crucial component of the electrolysis system. To start the chemical reactions at the electrodes, it must be able to deliver the necessary voltage and current levels.

In the tank's electrolyte solution, the electrodes are submerged. To ensure effective and long-lasting electrolysis performance, it is essential to choose the right electrode materials. As for both anode and cathode the best cost-effectiveness option is found using graphite, as stated in 3.2.1.1 this was the material applied to the electrodes used in this alkaline electrolysis solution.

The flow of gases created during electrolysis is directed using guide pipes. Guide pipes ensure the safe transfer of hydrogen gas produced during electrolysis from the tank to the intended storage or utilization location. In order to ensure efficient containment and transport, these pipes should be made to withstand the unique characteristics of hydrogen gas, such as its flammability and potential for leakage. The hoses used to this effect are presented in section 3.12.

The electrolysis system can be designed and optimized to achieve the desired results with efficiency, reliability, and safety in mind by comprehending the roles and interactions of these various components. The successful operation of the electrolysis system depends on careful consideration of material selection, system parameters, and operational requirements.

During the test procedure, is required that the electrolysis continue to happen to maintain the constant concertation of hydrogen in the environment, to restore the quantity of hydrogen that will embrittle the materials.

3.2.1.3 Electrolysis tank

The electrolysis process requires a vessel where the saltwater and electrodes are contained, and the guide pipes are connected. There are diverse solutions ready to perform electrolysis, but for alkaline electrolysis of saltwater the best and most practical solution is the H-Type Electrochemical Cell, that consists of two independent compartments connected through a diaphragm in a H shape. This type of equipment features a replaceable membrane seal and gas inlet and outlet. The solution will require two holes in each compartment cap, one for the electrode and the other for the gas to exit.

The H-Type Cell chosen was the Ossila's solution, which is a H-Type Electrochemical Cells with a volume of 100 mL [43]. The maximum cell volume was the option due to the requirement to maintain the electrolysis process during all the test procedure, as stated in section 3.2.1.2, to ensure tank is not opened during the test to not create an unnecessary risk by releasing any harmful gas.

The maximum solubility of NaCl in water is 357 mg/mL at 25°C, approximately the ambient temperature [44], but assuming that the saltwater will have approximately the same concentration of the seawater, which is 3.5% of NaCl, or 35 mg/mL, the NaCl mass in the solution will be:

$$m(NaCl) = 35 \times 100 = 3500 \text{ mg} = 3.5 \text{ g} \tag{3.1}$$

Obtaining the elements molar masses in the periodic table:

$$M(NaCl) = 22.9 + 33.45 = 58.44 \text{ g/mol} \tag{3.2}$$

$$n(NaCl) = \frac{m}{M} \approx 0.06 \text{ mol} \tag{3.3}$$

Knowing that for each H_2 mole produces, the same amount of Cl_2 is required,

$$n(H_2) \approx 0.06 \text{ mol} \tag{3.4}$$

$$M(H_2) = 2.016 \text{ g/mol} \tag{3.5}$$

$$m(H_2) = M \times m = 0.1212 \text{ g} \tag{3.6}$$

Also calculating the Cl_2 mass:

$$n(Cl_2) \approx 0.06 \text{ mol} \tag{3.7}$$

$$M(Cl_2) = 66.90 \text{ g/mol} \tag{3.8}$$

$$m(Cl_2) = M \times m = 4.014 \text{ g} \tag{3.9}$$

With the 100 mL tank and with 3.5 g of salt used, it is possible to obtain 0.1212 g of H_2, which should be enough to obtain the required 500 ppm concentration, that will be the maximum H_2 concentration in testing, as seen in section 3.2.2. In case of the full solubility, repeating the equations from 3.1 to 3.6, the maximum H_2 quantity obtained with this solution is approximately 1.24 g, more than enough for the required application.

The Cl_2 quantity obtained in both these cases, will be 4.014 g and 41.07 g, for 3.5 g of salt and to the maximum solubility, respectively, which is important to understand which containment option must be used.

The Ossila's solution assembly is shown in figure 3.5 and the dimensions for product code C2012F1 are presented in the schematic in figure 3.6.



Figure 3.5: Ossila Electrolysis H-Type Tank, Diaphragm and Lids [43]

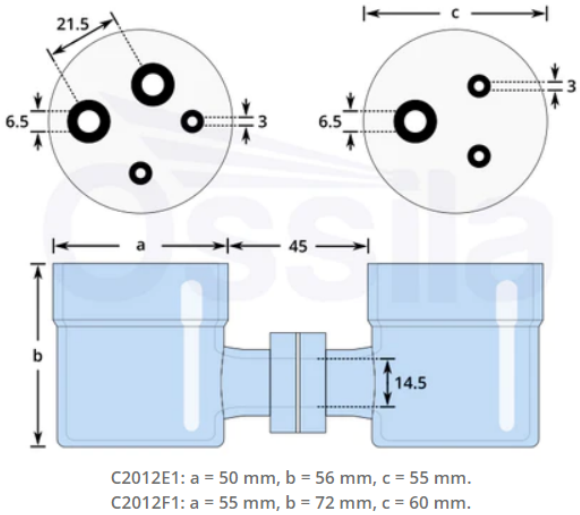


Figure 3.6: Ossila Electrolysis H-Type Tank Schematics [43]

3.2.1.4 Electrodes

The electrodes used for the alkaline electrolysis can be different for the anode and the cathode. The more common choices for anode are titanium and graphite and for the cathode are stainless steel and graphite. Ossila provides different types of electrodes, that are already designed to fit in the holes already made in the H-Type electrolysis tank, so it is a good option chose the electrodes available in the same supplier.

Due to the excellent cost-effectiveness of graphite both anode and cathode electrodes will be from graphite. The electrodes hole in the previously presented equipment is 3 mm, so the 3 mm diameter graphite working electrodes are the chosen electrode [38]. The specifications of the graphite electrode, with the dimensions in mm, are presented in figure 3.7, where n is equal to 3.

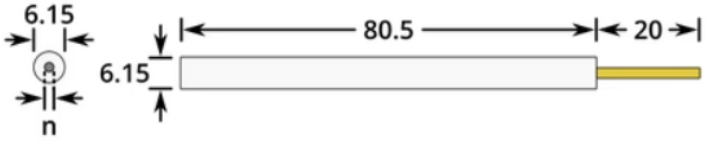


Figure 3.7: Schematics of the Electrode from Ossila [38]

3.2.1.5 Electrolysis Power Supply

As previously staded in section 3.2.1.2, the alkaline electrolysis required a DC power supply. The DC power supply assures that the negative charged electrode will always be the one that facilitates the H_2 formation, and the current amplitude is the property that will define the electrolysis process, because the quantity of hydrogen gas produced by the alkaline electrolysis will depend on the current and its application time.

There are different power supply devices, but to control the electrolysis and the H_2 generation, a controllable and variable power source device is desired.

Bench Top Power Supply (figure 3.8), manufactured by the RND lab is, as indented, a controllable and variable power source device. This solution is also a programmable DC power supply, which can bring an advantage to the automation of the apparatus. This product, with the reference RND 320-KA3005P [45], has a voltage range from 0 to 30 V and a current range from 0 to 5 A, having USB and RS232 interfaces. The output power of the source is 150 W, and the input voltage is 230 V.



Figure 3.8: DC adjustable power supply [45]

3.2.1.6 Chlorine Gas Containment

Chlorine gas is a by-product of saltwater electrolysis and is produced naturally during the process. But given the potential hazard of chlorine gas, it is important to put the right containment measures in place to protect both people and the environment.

A guide pipe will be safely attached and made airtight to the compartment where Cl_2 is produced in order to effectively contain chlorine gas. The chlorine gas is channelled through this pipe

and away from the electrolysis chamber. In order to prevent any unintentional releases of chlorine gas into the environment, it is essential to make sure the connection is strong and leak-proof.

The container designated for collecting chlorine gas will be attached to the other end of the guide pipe. In order to safely contain the gas without the risk of leaks or escapes, this container must be sealed. It's crucial to choose a container that can withstand the pressure created by the chlorine gas and is chemically compatible with the gas.

The collected chlorine gas in the container must be properly disposed of after the saltwater electrolysis test is finished. Chlorine gas disposal should be handled by qualified organizations in charge of handling and getting rid of hazardous materials safely. This guarantees adherence to environmental regulations and reduces any possible risks brought on by chlorine gas.

Strict adherence to safety precautions is essential throughout the entire process. To prevent exposure, workers handling chlorine gas should put on the proper personal protective equipment, such as gloves, goggles, and respiratory protection. To avoid the accumulation of chlorine gas concentrations that could be harmful, all operations should be carried out in a well-ventilated area.

Implementing these measures and adhering to the right safety procedures will enable the containment and disposal of chlorine gas produced during saltwater electrolysis, minimizing potential risks and ensuring the safety of people as well as the environment.

3.2.2 Sensors

To ensure precise control and monitoring of gas concentrations, pressure, and temperature inside the chamber, sensors integration is essential. These sensors play a crucial role in mechanical testing, by providing the intended measurements, enabling the assessment of test specifications, variables, and data interpretation. In the case of hydrogen embrittlement testing, where the chamber requires the presence of an inert gas and controlled hydrogen concentration, three sensors can be needed: one for hydrogen gas, one for the pressure control and another for the inert gas reading.

To measure the pressure inside the chamber, a sensor specifically designed for hydrogen embrittlement testing is required. Hydrotechnik offers a range of sensors suitable for H_2 applications, and the chosen sensor is the HT-H2-TPSE Pressure and Temperature Sensor [46], figure 3.9, which can measure pressures up to 1000 bar, with the upper level defined by request. The sensor applied to this solution is the sensor with the 0 – 60 bar range, that exceeds the 5 MPa (50 bar) limit for this application, as seen in section 3.5.3. Additionally, it operates within a temperature range of -35°C to 100°C, providing a wider functionality range than necessary [46]. This sensor provides both pressure and temperature readings, offering valuable additional information for the precise definition and execution of the performed tests. The total error for the pressure is approximately 0.5% of Full Scale (FS), i.e., 0.3 bar, and for the temperature is approximately 2.0% FS, i.e., 2.7 °C.



Figure 3.9: Pressure and Temperature Sensor, H_2 Resistant [46]

Prior to introducing hydrogen gas, it is crucial to confirm the chamber is well-sealed to mitigate any risks associated with working with hydrogen. This confirmation is performed with the inert gas flushing, presented in section 3.2.5, and the pressure reading obtained from the pressure sensor can be used as an indirect measure of the quantity of inert gas present in the chamber. By monitoring the pressure changes, it is possible to infer the amount of inert gas inside the chamber. The pressure sensor serves a crucial role in detecting leaks and ensuring the chamber's integrity, and with this indirect reading number of required sensors reduce to two. Its main functions are to ensure the chamber integrity and that the chamber is tightly sealed before introducing hydrogen gas and during the test procedure, thereby minimizing the risks associated with working with hydrogen. By accurately detecting the presence of the inert gas, the sensor confirms the integrity of the chamber and helps avoid potential dangers caused by leaks.

To ensure test safety, the hydrogen concentration inside the chamber must not exceed 5% according to safety guidelines [47]. However, for effective hydrogen embrittlement testing, it is not necessary to reach such high hydrogen concentrations. Embrittlement can occur with values as low as 100 ppm [48], and for hydrogen embrittlement testing, concentrations around 100 ppm are typically used to simulate low atmospheric levels of hydrogen gas. The maximum concentration of H_2 allowed for hydrogen embrittlement tests is 500 ppm according to ASTM G142, 2016 [18].

During the hydrogen embrittlement testing in mechanical chambers, the concentration of hydrogen (H_2) is typically controlled up to 500 ppm [18]. This means that the remaining volume in the chamber, needed to achieve the desired pressure, is filled with the inert gas. Therefore, as previously stated, two sensors will be used, one for measuring the quantity of hydrogen gas and another for monitoring the pressure, which also allows the indirect control of N_2 leakage by controlling the chamber's pressure.

Hydrogen gas sensor should be capable of detecting concentrations ranging from 0 to 500 ppm, with a display resolution of 1 ppm, at least. EC Sense offers a hydrogen gas module, presented

figure 3.10, that can accurately measure hydrogen concentrations from 0 to 1000 ppm [49], which falls within the desired range, having a display resolution of 0.1 ppm. The sensor measures gas concentration by utilizing electrochemical reactions at the working electrode, which produce a measurable current indicative of the gas concentration. This sensor's readings are not influenced by the presence of N_2, the inert gas used in the chamber, ensuring accurate measurements without interference. To place this sensor it was also designed a piece, figure 3.11, to further connection of the sensor with the end cap in the opposite side of the gas entrance. The technical drawing of this part is presented in appendix J.



Figure 3.10: Hydrogen Gas Module 0-1000 ppm [49]

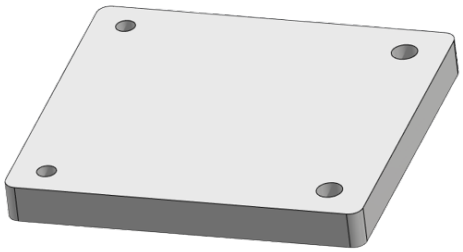


Figure 3.11: Sensor placement part

Using these sensors, the hydrogen gas sensor and the pressure and temperature sensor, accurate monitoring of gas concentrations and pressure can be achieved, ensuring the successful execution of hydrogen embrittlement tests.

3.2.3 Valve Sealing

Valves will be used to regulate the hydrogen and the inert gas supplies, to ensure the containment of the chamber's environment and to release the chamber atmosphere. When working with hydrogen, it is important to consider specific factors in the selection of valves, as all valves need to be compatible with hydrogen gas use. The material of each valve needs to be compatible with the use of hydrogen because it is also subjected to hydrogen embrittlement. The standard ISO/TR 15916 Basic considerations for the safety of hydrogen systems [50] suggests stainless steel AISI 316/L as a suitable material for the metal valve components, and for the non-metal components it suggests Teflon (PTFE) as adequate [51].

Hydrogen valves can be of various types, depending on their use. In this design, as stated, valves to regulate the hydrogen flow will be required, to prevent hydrogen leaks and as pressure relieve. In figure 3.12 a brief summary of different valves and their use is presented, which was used to assist valve selection.

Type of Valve	Use Cases
Hydrogen Needle Valve	Hydrogen fueling stations, Pressure fluid handling system, Compression systems
Hydrogen Ball Valve	Electrolysis, Hydrogen storage
Hydrogen Check Valve	Hydrogen Refilling stations, Fuel cells, Hydrogen processing, Process system control and shut-off
Hydrogen Pressure Relief Valve Valve	Hydrogen boilers and plants, Pressure tanks, Process technology, Storage and transportation of hydrogen
Hydrogen Flow Control Valves	Hydrogen fuel cell test systems, Hydrogen fueling, storage and manufacturing systems
Hydrogen Shut-off Valves	Hydrogen Storage and transportation

Figure 3.12: General use of each valve type [52]

To ensure the containment of the chamber environment it will be necessary a valve that can be closed in order to sustain the inside environment and that can be opened when is necessary to release it. These requirements can be ensured by a ball valve. To regulate the hydrogen flow and to prevent its leakage ball valves can again be a good solution, and they can be controlled both manually and automatically. To relieve pressure it will be needed a pressure relief valve, and to prevent any gas return to outside of the chamber in the test procedure or from the atmosphere release, check valves will be applied.

3.2.4 Chamber Atmosphere Release

To safely release the atmosphere from the chamber, a ball valve is connected to an external guide pipe, that will lead the chamber atmosphere to outside the building. Before the chamber can be opened, it is necessary to ensure that all the gas inside is completely evacuated. This can be achieved using a vacuum pump, which will effectively remove any remaining gases. In order to determine when the chamber is fully emptied, it is important to monitor the readings of the hydrogen sensor. The sensor values should be continuously monitored, and the chamber should only be opened when the sensor readings indicate zero hydrogen presence. This ensures that the chamber is indeed empty, minimizing any potential risks associated with residual gas.

In the inert gas flushing the system will be opened and closed three times, before and after each flush, and it is required that the system is closed before the 10 minutes leakage test, and then the vacuum pump will be required to act again in order to generate vacuum inside the chamber before the test and to ensure that there are no other elements inside that will distort the result of the tests. The testing can only start when all the gases inside the chamber are evacuated. This is measured by the pressure sensor, that is used to control the N_2 concentration, and is required that this sensor measures the value zero, or a near value, because the absolute zero pressure is very difficult to obtain.

3.2.5 Inert Gas Flush

The inert gas, in this case N_2, will be supplied from an external source rather than being generated on site. This will be stored in a vessel and connected to the apparatus. The inert gas will be flushed three times in a controlled amount to eliminate impurities and reduce the presence of O_2 molecules, minimizing the risk of explosions.

After the flush process, it will be performed the chamber leakage test. To this test, it will be released a specific amount of nitrogen and the chamber pressure will be monitored for 10 minutes. This system will need to be connected to a valve, required to also be H_2 ready, that will enable this containment. After this time, the atmosphere release can be activated, and the inert gas valves will be opened when required to pressurize the test chamber and, in perfect conditions, it will not be open any more time during the duration of the test.

3.2.6 Fuctional Diagram

A functional diagram is a representation of how the product works, used to specify its performance and the sequence of actions. The functional diagram does not specify how the operation will happen, only representing the working flow and is a good schematic to help the development of a solution.

In the desired solution the first task is to seal the chamber, by mounting it in the machine and assembling the parts and valves that assure the solution sealing. Assuming that all the other parts are already connected the next step is to perform the inert gas flush and the leakage test, followed by the monitoring of the values obtained by the sensor. Then, the power supply is activated, and

the electrolysis starts, and when the sensor inside of the chamber reads the desired H_2 value the test can begin. When the test is over the power supply is turned off and the atmosphere inside the chamber can be released. Finally, when the quantity of the hydrogen inside reaches zero the chamber can be opened safely. In figure 3.13 can be seen the functional diagram schematics.

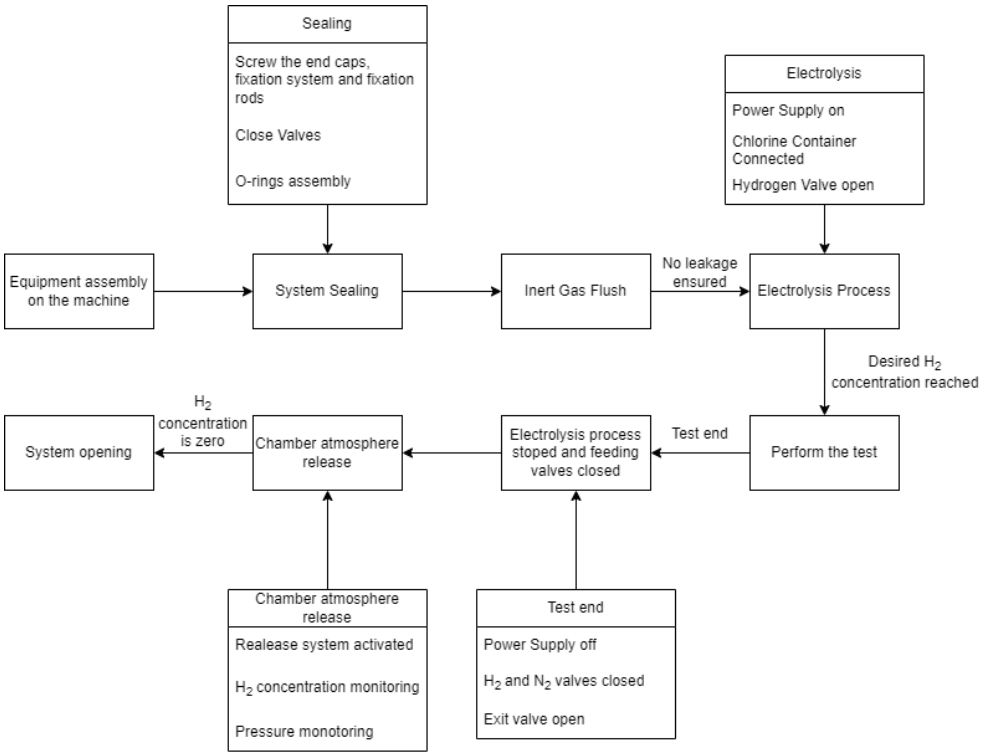


Figure 3.13: Functional Diagram Schematics

3.3 Conceptual Design

To start the chamber project, some chamber designs were studied. A potential design approach found was the BlueRobotics Watertight Enclosure, even though it is not an apparatus designed for the application in any kind of mechanical tests. The Watertight Enclosure for ROV/AUV (6" Series) [53] solution showed potential to be adapted to the intended goal. This chamber is composed of an acrylic tube, an O-ring flange, end caps and O-rings. This solution, despite its appealing design, is not appliable to hydrogen embrittlement testing.

This BlueRobotics solution is designed to enclosure electrical systems assembled inside, for under water exploration, sustaining external pressure that keep the tube closed, not to maintain the caps closed when an internal pressure is applied.

Also, the components of this solution are not hydrogen embrittlement resistant, the opposite of the chosen materials from this design, because the wall are from acrylic and the end caps and O-ring flanges are made from aluminium [53].

As the materials are not fit to be applied in the present design, some alternatives were found but the end solution looks a lot like this BlueRobotics container.

In figure 3.14 can be seen a picture of the BlueRobotics tube and end caps, with some applied features, and in figure 3.15 is presented the 2D technical drawing of the solution.

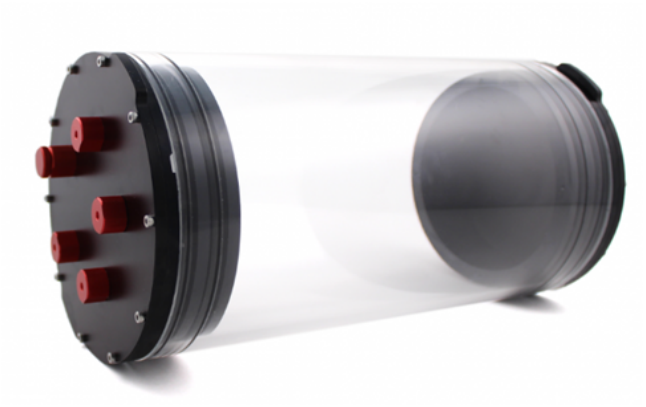


Figure 3.14: BlueRobotics Watertight Enclosure for ROV/AUV (6" Series) product view [53]

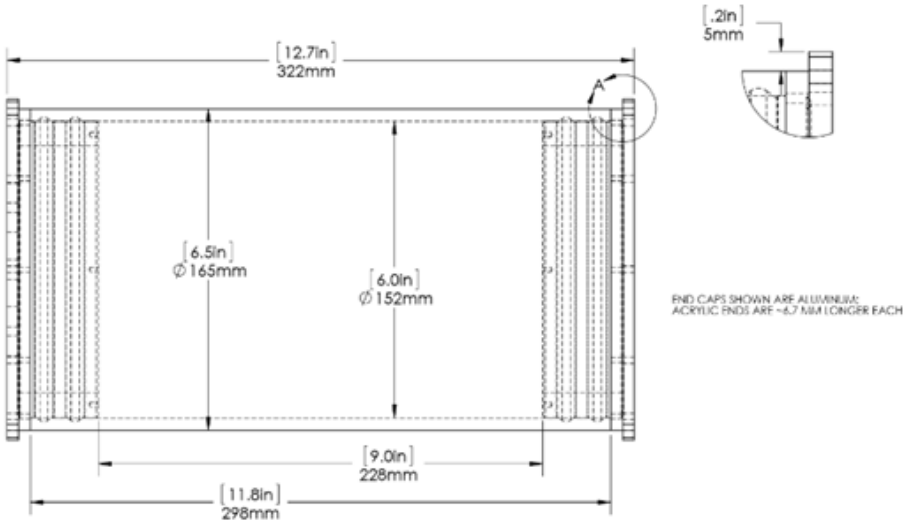


Figure 3.15: BlueRobotics Watertight Enclosure for ROV/AUV (6" Series) 2D technical drawing [53]

3.4 Final Design

To assist in the clarity of the design presented in sections 3.5 to 3.14, figure 3.16 shows an exploded view of the solution, labeling the parts to easily reference in the following sections. The numeration is similar to the bill of materials (BOM), appendix K, and here is presented a shorter version in table 3.4, with the design components to provide a better understanding.

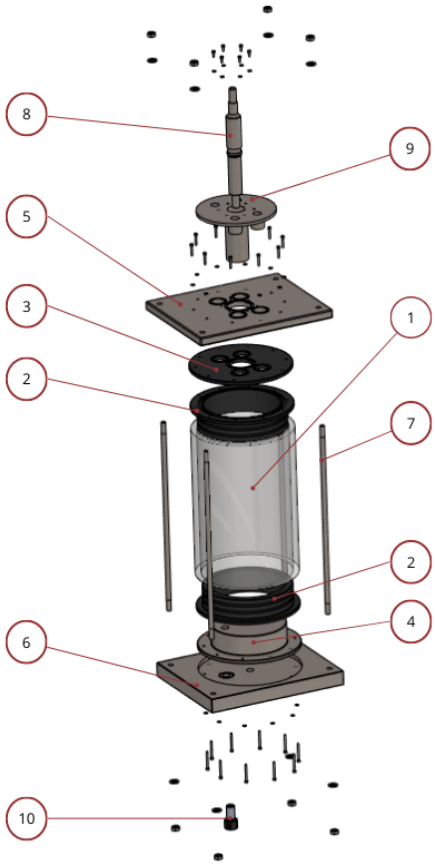
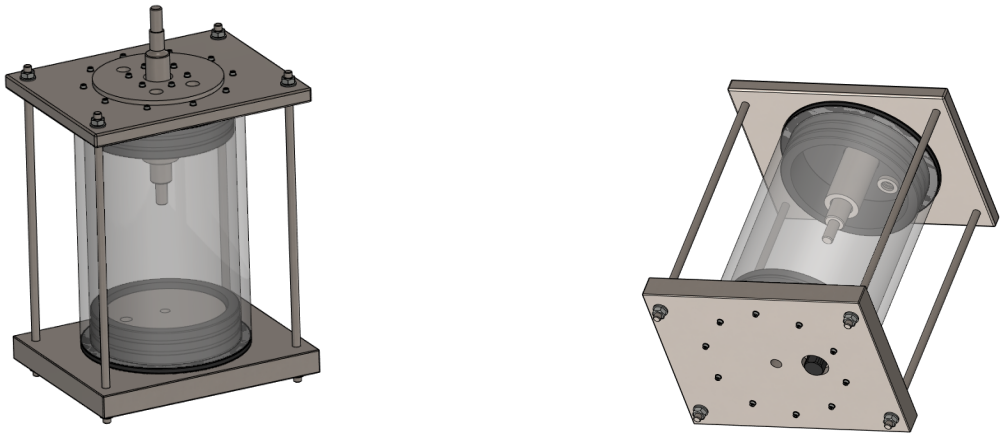


Figure 3.16: Exploded view of the final solution, with labeled parts

Figure 3.17 shows the final design of the chamber, with all the components stated in table 3.4 assembled. In the following sections the design processes and chosen components are stated.



(a) (b)

Figure 3.17: Final Solution Design

Table 3.4: Bill of Materials

Item	Reference	Description	Quantity
1	HTchamber.2023.001 ChamberTube	Fused Quartz Tube Φ175mm Supplier: Optical Solutions	1
2	HTchamber.2023.002 Flange	O-ring Flanges Manufacture	2
3	HTchamber.2023.003 EndCapThrough	End Cap - Dynamic Section Manufacture	1
4	HTchamber.2023.004 EndCapLoadCell	End Cap - Load Cell connected Manufacture	1
5	HTchamber.2023.005 FixationPartThrough	Fixation part - Dynamic Section Manufacture	1
6	HTchamber.2023.006 FixationPartLoadCell	Fixation part - Load Cell connected Manufacture	1
7	HTchamber.2023.007 RodFixatio	Rod - End Threaded M8 - Fixation Manufacture	4
8	HTchamber.2023.008 DynamicRod	Rod for Dynamic Sealing Manufacture	1
9	HTchamber.2023.009 Bushing	Bushing for dynamic rod and hoses Manufacture	1
10	WLP-M14-9.5MM-HC	Power cables penetrator Supplier: BlueRobotics	1
11	Cylinder head screw DIN 912 M3x8 51050_030_008(High)	Cylindrical Head Screw Steel 10.9 M3x8	6
12	Cylinder head screw DIN 912 M3x18 07015_030_018(High)	Cylindrical Head Screw Steel 10.9 M3x18	10
13	Cylinder head screw DIN 912 M3x30 07015_030_030(High)	Cylindrical Head Screw Steel 10.9 M3x30	10
14	Washer DIN 125-1 A 3_2 38130_030_001(High)	Plain Washer DIN 125-1A Steel Zinc Plated 140 HV M3	26
15	Washer DIN 125-1 A 8_4 38130_080_001(High)	Plain Washer DIN 125-1A Steel Zinc plated 140 HV M8	8
16	Hexagon nut DIN 934 M8 01300_080_001(High)	Hexagon Nut DIN 934 Steel Zinc plated 8 M12	8

3.5 Chamber Tube Design (1)

As stated in section 3.1.2, the testing chamber has to be able to resist to the hydrogen embrittlement and to the pressure that will be imposed in the inside of the vessel to perform the tests. The vessel can have any shape, but given the reliance on optical measurement devices in current testing procedures, it is required that the chamber be optically transparent, enabling image acquisition with cameras outside of the chamber.

3.5.1 Chamber Walls Material

Due to the low pressures inside of the chamber, it was decided to design a transparent chamber in a single component. For this purpose, three materials were identified, acrylic, glass and quartz cylinders. Acrylic is not the ideal solution because it is more permeable to gases, including hydrogen, and despite acrylic's resistance to reacting with or absorbing hydrogen, over time small amounts of H_2 might diffuse through the walls. Also, mechanical strength of acrylic is lower that the other materials, and it can deform when subjected to the internal pressure of the chamber. Glass and quartz are the best suited candidates, both have good chemical compatibility, but quartz is highly chemically inert, which can be a better choice for certain reactive substances. In terms of thermal stability both of them are adequate, but quartz is more resistant to rapid temperature changes [54], which is not the intended use of this chamber design. Both of them are transparent and impermeable to gas, but quartz has a better performance in these categories because the optical properties of the quartz are superior, which is advantageous for the use of this apparatus because it must have the capacity of being used in precise optical measurements (also performing well if spectroscopic analysis is needed), and also quartz has lower gas permeability than most glass types, which is important to ensure long-term stability of the gas environment and higher degree of gas containment. Quartz is generally stronger and more resistant to mechanical stresses, and even though the pressure inside is not high, maximum 15 MPa, it may offer better mechanical stability and durability over glass [54]. Even though quartz is less economical than glass, its proprieties overcome the price difference, so the quartz will be the chosen material to the walls of the chamber.

3.5.2 Chamber Format

Other important option taken is the chamber format, which was reduced to two options, either cylindrical or cuboid. Fused quartz, the chosen material for the chamber, has a refractive index around 1.45 [55], and, as it has a high refractive index, it can potentially induce some refraction and distortion. A cylindrical quartz offers advantages in terms of focusing and minimizing distortion, but, even so, the potential refraction and distortion induced by quartz can not be ignored. A straight quartz wall may provide easier camera positioning, but the refractive property of quartz needs to be taken into account, furthermore, it is essential to ensure appropriate lighting conditions in order to minimize distortion.

Ultimately, the choice between a cylindrical or cuboid quartz chamber depends on camara setup and the specific properties that are in test. To avoid the need for additional lighting to ensure the proper functioning of the optical system, a cylindrical shape was chosen. This design choice ensures that the position of the camera is the only variable at play. This arrangement does not pose any issues, aligning with a solution similar to that of BlueRobotics [53]. Therefore, the design of the end caps and O-ring flanges can also be adapted from the BlueRobotics solution, incorporating the necessary features and streamlining the overall design process.

3.5.3 Chamber Dimensions

After the selection of the chamber material and shape, the dimensions were defined. As previously stated, the maximum height of the whole solution is around 350 mm, so, considering that the solution will require end caps and fixation parts, the maximum height of the solution chosen was 260 mm. The thickness of the walls is another key variable to consider in the design. Optical Solutions [56] offers a range of tubes with outer diameters ranging from 3 to 450 mm. Chamber's inner diameter will be about 155 mm, so, it is necessary to calculate the required thickness of the chamber walls. To determine the minimum thickness of the test chamber to withstand the required pressure of 15 MPa the Barlow's Formula [57] will be used, which is commonly used to verify if the operation pressures are supported by the pipes or pressure vessels. The Barlow's Formula is:

$$P = \frac{2 \times S \times t}{D} \Leftrightarrow t = \frac{P \times D}{2 \times S} \tag{3.10}$$

Where S is the maximum allowable stress, that is 50 MPa [58], D is the outer diameter, P is the applied internal pressure (15 MPa is the reference value), and t is the wall thickness.

To solve this equation 3.10, the outer diameter needs to be defined in function of the wall thickness, with $D = d + 2 \times t$, where d is the inner diameter, being 155 mm the value previously defined in this chapter.

$$t = \frac{P \times (d + 2 \times t)}{2 \times S} \Leftrightarrow t = \frac{P \times d}{2 \times S - 2 \times P} \tag{3.11}$$

$$t = \frac{15 \times 155}{2 \times 50 - 2 \times 15} \Leftrightarrow t = 33.21 \text{ mm} \tag{3.12}$$

To use a 33 mm thickness wall, it is required to custom manufacture the quartz glass, directly with the manufacturer, as it is not an usual commercialised size, and the refraction properties of the quartz can bring problems to the image capture. The commercially available quartz tubing typically offers a maximum wall thickness of 10 mm. In Optical Solutions is found quartz tubing with a wall thickness of 10 mm and outer diameters ranging from 50 to 450 mm [56]. So, in order to get a 10 mm thickness wall, the outer diameter must be 175 mm.

This will not be in accordance with Barlow's Formula, which means that the 10 mm thickness tubing should not be able to resist to an internal pressure of 15 MPa. Therefore, it is needed to recalculate the maximum pressure that would be withstand with these conditions.

For the 10 mm thickness it is needed to know the safety limit of the pressure inside, so, using the Barlow's Formula, equation 3.10, again, but this time to calculate the pressure.

$$P = \frac{2 \times S0 \times t}{d + 2 \times t} \Leftrightarrow P = \frac{2 \times 50 \times 10}{155 + 2 \times 10} = 5.71 \text{ MPa} \tag{3.13}$$

Even though this pressure is much lower than the reference one, the test can still occur at this pressure and the pressure is not supposed to even reach 5.71 MPa, so none problem was raised with this limitation.

So, the design solution is presented in figure 3.18.

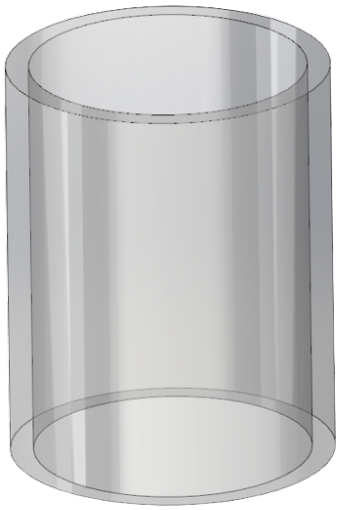


Figure 3.18: 3D CAD of the chamber walls

3.5.3.1 Hydrogen gas quantity regarding the imposed limitation

For the calculated pressure, the maximum quantity of gas inside the chamber can be calculated, and assuming that the behaviour of the gas inside the chamber is similar to an ideal gas:

$$PV = nRT \tag{3.14}$$

where P is the gas pressure, V the chamber volume, n the number of moles, R the molar gas constant, which is 8.314 J/molK, and T the temperature in Kelvin, assuming 20 °C, the temperature is 293.15 K.

$$V = \pi \times \left(\frac{0.155}{2}\right)^2 \times 0.22 = 4.151 \times 10^{-3}\ \mathrm{m}^3 \tag{3.15}$$

From the constant and temperature values and equation 3.13 and 3.15, equation 3.14 can be solved in order to n.

$$n = \frac{PV}{RT} \Leftrightarrow n = \frac{5.71 \times 10^6 \times 4.151 \times 10^{-3}}{8.314 \times 293.15} = 9.725\ \mathrm{mol} \tag{3.16}$$

So, as referred to in section 3.2.2, assuming that the maximum quantity of hydrogen is 500 ppm, the equation 3.17 can be obtained.

$$n(H_2) = \frac{500}{10^6} \times n = 4.8625 \times 10^{-3}\ \mathrm{mol} \tag{3.17}$$

As $M(H_2) = 2.016$ g/mol:

$$m(H_2) = M \times n = 2.016 \times 4.8625 \times 10^{-}3 \approx 10 \times 10^{-3}\ \mathrm{g} \tag{3.18}$$

this confirms what was said in section 3.2.1.3, that the H-type tank is an usable solution.

3.6 End Caps design (3 and 4)

The end caps of the BlueRobotics solution are made from aluminium alloy, which is a material usually susceptible to hydrogen embrittlement, so although the design may be similar, the material needs to be changed. In Yokogawa et al., 2008 [27] it is stated that the constituent material of the majority of the chamber components is AISI 316 stainless steel, which is a steel that is very resistant to hydrogen embrittlement, as was studied by Ogata, 2008 [20], that developed the apparatus presented in section 2.5.2 to test the properties of the stainless steels AISI 304, 304L and 316L. The tests performed in this study confirmed that 316L resists to hydrogen embrittlement, only showing proprieties lost at 190 K [20], but that temperature will not be applied in the intended use of the solution, and even at that temperature, the resistance is better than the other materials in test. So, due to the advantages that the use of the stainless steel AISI 316L brings, that will be the chosen material for application in the end caps.

The two end caps are not going to have the same geometry because one would need to have a through-hole to be connected to the moving part of the machine and the other will have to connect the clamp with the load cell, so it is required that each cap has its own attributes. The end caps will have a cylindrical shape, similar to the BlueRobotics ones, and with a diameter equal to the external diameter of the fused quartz tube, of 160 mm. The end caps will have 10 holes with 3 mm of diameter in which the M3 screws will pass to connect with the fixation parts and with the O-ring flanges.

One of the end caps (4) will be screwed to a M12 threaded connection on the outside, and the clamp that will be connected to the cap inside will also be screwed with a M12 threaded connection, so this end cap will require two M12 threaded holes, guaranteeing that the hole does not goes through all the cap and that in the middle of these holes a sufficient quantity of material exists so it contains the interior atmosphere without leaking. This end cap will need to have a salience that enters the chamber, to guarantee that this end cap will be able to withstand the force applied by the machine, so a reinforcement is recommended to prevent any deformation of the cap, even that the force applied is not too high and that the AISI 316L stainless steel has good mechanical properties. To assure that any problem that can be caused by this force is mitigated, the salience will be 35 mm height with a 127 mm diameter, a smaller diameter than the O-ring flange, with dimensions in section 3.8 to avoid contact problems, and in this feature is where one central inside M12 hole will be present, and any other information about the fabrication process of this piece is presented in appendix D and its CAD can be observed in figure 3.19.

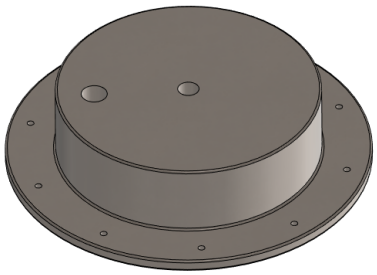


Figure 3.19: 3D CAD of the end cap connected to the load cell

As stated, one end cap (3) will require a through-hole , so it was defined a 40 mm diameter hole in the middle of one end cap where the dynamic part will pass and an O-ring gland will also be placed in this end cap, to assure the correct isolation of the gas inside the chamber. The O-ring gland will have to be dimensioned, which is presented in section 3.10.1.

The end cap with the through hole will have a gland with 2 mm height, and outside diameter of 50 mm, with a groove width of 4 mm. To the chamber gas circulation, four more holes will be required, each with 23 mm diameter.

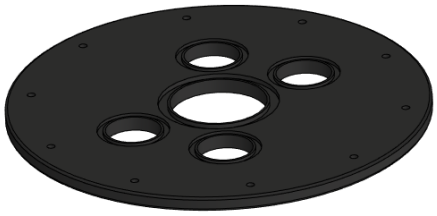


Figure 3.20: 3D CAD of the end cap with a through-hole

Both of these end caps are then made of stainless steel AISI 316L and they are going to be ordered from a supplier, so manufacturing designs were made, and they can be found in appendix C or section 3.14.

3.7 Fixation Solution (5, 6 and 7)

As stated in section 3.3 the solution of BlueRobotics that is being adapted to a test chamber is not suited for positive internal pressure, so a fixation system of the end caps will be needed. The end caps will be connected to these parts by the means of ten M3 screws, so it is necessary that both possess ten 3 mm diameter holes where these screws can go through, and both fixation parts will have different features to match the end cap where they will fix. The fixation parts will consist in an initial rectangular piece with dimensions of 200 mm by 250 mm where the features will be

applied, and the material of these parts will also be AISI 316L stainless steel, because specially the part connected to the dynamic part of the machine will be subject to hydrogen embrittlement, so it is important that the constituent material can resist to this embrittlement.

The all fixation system is presented in figure 3.21, and the different parts are explained in the sections 3.7.1 to 3.7.3.

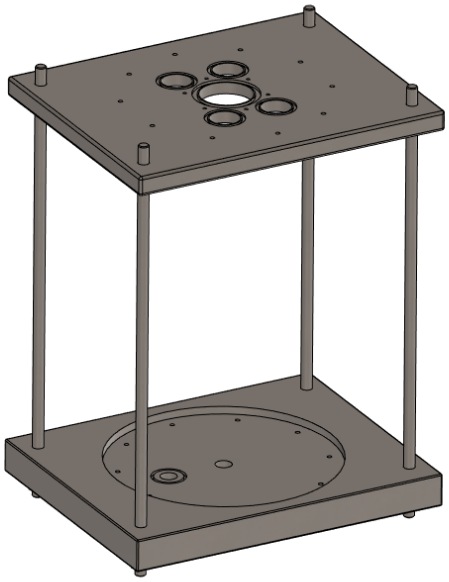


Figure 3.21: Fixation System assembled

3.7.1 Fixation part of the through hole end cap design (5)

The part that will connect with the end cap where the dynamic part will pass through needs to have a hole that match the dimension of that feature and threaded holes where the dynamic sealing will connect. This fixation part will have a 15 mm thickness with a circular indentation of diameter 175 mm with a depth of 6 mm, which dimensions are the diameter of the end cap and its thickness, so it fits in an easier way. The hole where the dynamic sealing pass will have a diameter of 40 mm, so the dynamic bushing exterior diameter will be adjusted to this option.

The connection between these features is made by the means of six M3 screws. The respective threaded holes were designed in this fixation piece, along with the through holes required by the bushings designs. As hydrogen can leak through these holes, O-rings will be applied in the upper face of the fixation part, dimensioned in section 3.10.1.

The final design of this fixation piece can be seen in figures 3.22 and 3.23.

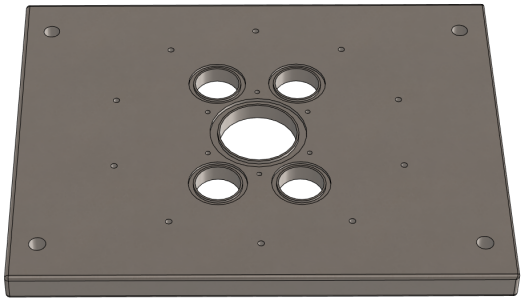


Figure 3.22: 3D CAD of the fixation part of the through hole end cap - top view

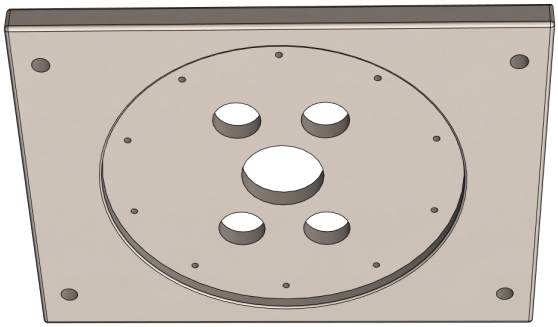


Figure 3.23: 3D CAD of the fixation part of the through hole end cap - down view

3.7.2 Fixation part of the load cell connected end cap design (6)

The other fixation part will be connected to the end cap that is connected to the machine in the load cell, so it will need to have a central hole with a 12 mm diameter, where the M12 screw can pass freely. As this piece will be subjected to the machine force, the thickness of this part will be 10 mm greater than the other, having a 25 mm thickness with a circular indentation of diameter 175 mm with a depth of 6 mm. This piece will have to seal the hydrogen in the penetrator hole, having the gland dimensions in section 3.11. To connect the penetrator, given its size, it will be created an indentation in the bottom surface to insert this piece, with a 30 mm diameter. This features were applied in Solidworks and the fixation part CAD is presented in figures 3.24 and 3.25.

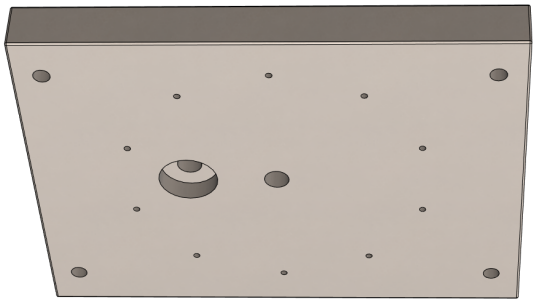


Figure 3.24: 3D CAD of the fixation part of the load cell connected end cap - top view

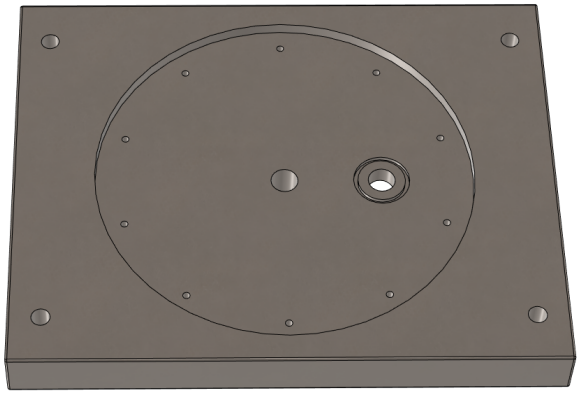


Figure 3.25: 3D CAD of the fixation part of the load cell connected end cap - down view

3.7.3 Fixation Rods design (7)

As seen in figures 3.24 and 3.25, both of the pieces have four holes in the extremities of the rectangular face. These holes exist to enable the passage of four rods that will be inserted in the fixation system to hold the fixation parts in place.

The rods will have a length of 340 mm and a diameter of 8 mm, threaded in both ends, in 20 mm, where nuts will be applied, as seen in figure 3.26. To support the system the rods will have a M8 thread in the end, and even though it was not necessary that the system possess four rods, it was opted to apply this number because of both aesthetic reasons and so that no rods interfere with the camera's field of view. These rods will also be made from AISI 316L stainless steel.



Figure 3.26: 3D CAD of the threaded rods

3.8 O-rings Flanges design (2)

In order to correctly guarantee the complete insulation of the test atmosphere and to prevent leakages from inside the chamber through the top of the fused quartz tube we need to insert some sealing, applying the O-rings dimensioned in section 3.10.3. The O-ring flanges will require ten threaded M3 holes to connect with the fixation solution and the end caps. Both flanges will have the same features, with an external diameter of 175 mm, equals to the end caps diameter. The O-ring flanges will have a geometry similar to the BlueRobotics Enclosure system, but with some different measures and different O-ring glands due to the different material of these O-rings, due to the need to be hydrogen gas resistant. The O-ring flanges will have a total thickness of 46 mm, being 6 mm in the top part, and 40 mm in the part that will perform the sealing of the chamber. Each flange will possess in total three O-rings, two radial and one facial. The two radial O-rings are applied to ensure that hydrogen is contained inside, due to its small particle size, to maintain the high security level, and the facial one is applied avoid the leakage between the flange and the end cap.

With the O-rings dimensions stated in section 3.10.3, a gland for a facial O-ring will be made, with 2 mm height and inside and outside diameters of 137 mm and 147 mm, respectively, and in the sides there will be two recesses with 6 mm depth and 8 mm length. The outside diameter of the salience will be 153 mm and the inside diameter can be 130 mm, like the solution proposed by BlueRobotics. The CAD of this piece can be seen in figure 3.27, and further fabrication designs are presented in appendix B.



Figure 3.27: 3D CAD of the O-ring flanges

For the required application with hydrogen, in static surfaces where the seal is guaranteed by thermoplastics and rubber seals, 0.3 µm is the maximum surface roughness that the material can have where O-rings are applied, so in order to guarantee that the surface is not also too much soft in a way that will affect the sealing, the surface roughness of the O-ring flanges in the O-ring glands will be 0.20 µm [59].

3.9 Dynamic Sealing design (8 and 9)

To ensure that no leaks occur through the hole that connects the moving part of the machine to one the clamps, a dynamic sealing solutions will be applied. The dynamic seals are divided into three categories, reciprocating seals, rotational seals or oscillating seals [60]. As the movement of the machine is only axial, reciprocating seal is the solution applied to the present design and, as the machine implies no contamination of the environment the seal applied will require a pneumatic solution.

Reciprocating seals usually use a piston-and-bore solution, where the piston seal performs a linear movement, maintaining adequate sealing force. To perform the seal there are different options, O-rings are the simplest solution and can be applied in any of the categories. X-rings and low drag D-rings are other possible solutions applied to the dynamic sealing, the first for reciprocating seals and the other to the other two categories [60, 61]. However, O-rings was the chosen solution for the required sealing, due to their simplicity and easy application.

For reciprocating seals one of the more significant aspects to consider is the surface finish, to maintain the O-rings structure and not produce any damage. In Parker Fluid Power Seal Design Guide [59], it can be found an interval of values acceptable for the surface roughness that need to be assured in the dynamic seals. So, for Hydrogen Gas applications, in dynamic surfaces where the seal is guaranteed by thermoplastics and rubber seals, the surface roughness has to be between 0.08 to 0.25 µm [18, 59], so in order to guarantee that the surface is not excessively soft to the

extent that it would affect the sealing, the surface roughness of the dynamic sealing will be 0.20 µm.

A dynamic sealing schematic is presented in figure 3.28, such as the relevant dimensions. The dynamic seal will be exposed to hydrogen, which means the dynamic seal will also be produced with AISI 316L stainless steel. The rod of the dynamic sealing will be subject to the machine axial force, so it is necessary to perform calculations to determine the minimum diameter for this rod. The rod will not be subjected to bending or torsion, so the only relevant calculation will be for the axial tension. The axial tension that is applied to a rod can be defined by the following equation:

$$\sigma_m = \frac{N}{A} \tag{3.19}$$

where N is the normal applied force and A is the critical zone area. In the case of this rod, the critical zone is the end of the rod, where the clamp will be connected. The normal force applied has a maximum value of 20 kN defined by the machines.

Knowing that the yield tensile strength of AISI 316L stainless steel, σ_F, is 205 MPa [55], it is needed to assure that:

$$\sigma_m < \frac{\sigma_F}{SF} \tag{3.20}$$

where SF is a applied safety factor. Applying a safety factor of 2, by equation 3.20 is possible to obtain the maximum axial tension that the rod can be subjected to.

$$\sigma_m < \frac{205}{2} \Leftrightarrow \sigma_m < 102.5 \text{ MPa} \tag{3.21}$$

As rod is cylindrical, the critical section area is given by $A = \pi \times r^2$, where r is the section radius. Applying the result obtained in equation 3.21 in the equation 3.19, the section radius can be calculated.

$$\sigma_m > \frac{N}{A} \Leftrightarrow A > \frac{N}{\sigma_m} \Leftrightarrow \pi \times r^2 > \frac{N}{\sigma_m} \tag{3.22}$$

$$r > \sqrt{\frac{N}{\sigma_m \times \pi}} \Leftrightarrow r > 7.88 \times 10^{-3} \text{ m} \tag{3.23}$$

So, the rod diameter needs to be bigger then 15.76 mm. To guarantee this condition and to assure the rod integrity the diameter of the rod will be 22 mm.

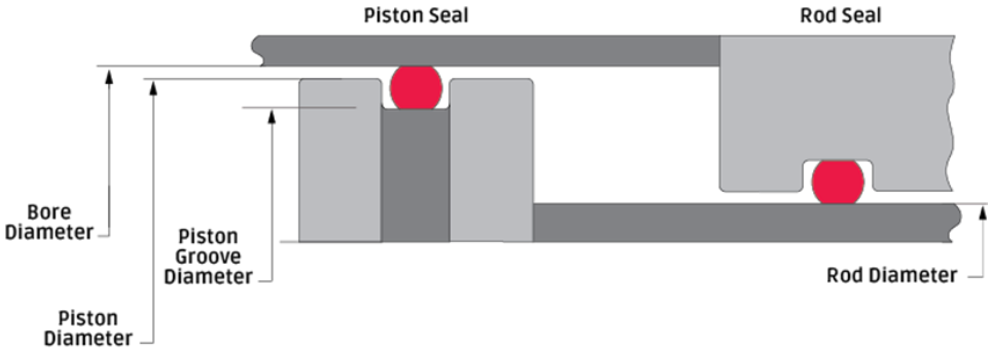
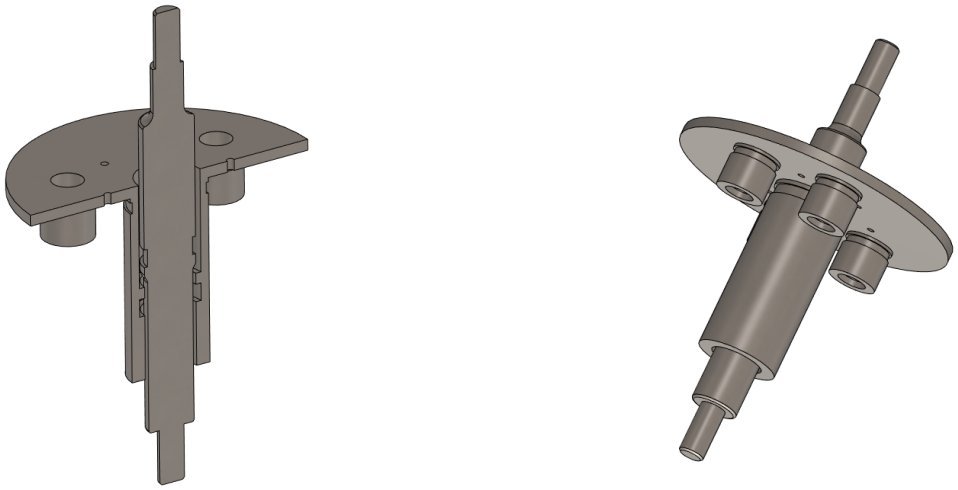


Figure 3.28: Dynamic Reciprocating Seal Schematics

The dynamic reciprocating seal is divided into two parts, a rod (8) that will move linearly and will be connected to the moving part of the machine and to the clamp, and a bushing (9), that will insulate the rod and will be connected to the fixation piece.

The dynamic sealing system will be screwed in the fixation part by six M3 screws, and on the top part of the bushing the diameter will be bigger than the one inside of the chamber, with an outer diameter of 70 mm, in order to possess the six 3 mm diameter holes where the screws will pass through. The features to apply O-rings are dimensioned in section 3.10.4, and the final CAD can be seen in figure 3.29 and further information can be consulted in appendices H and I.



(a) (b)

Figure 3.29: **(a)** Partial view and **(b)** isometric view of the 3D CAD of the Dynamic Sealing metal components

3.10 O-rings sizing

The first thing to do in the O-ring choice is find a suitable material for the hydrogen application. To this determination some O-rings manufacturers were contacted and the recommended guide to

find the right material was the Apple Rubber one [62]. In Apple Rubber can be found an O-Ring Chemical Compatibility Guide, and an exposure rating guide is defined, dividing the material in five categories, that can be seen in the figure 3.30.

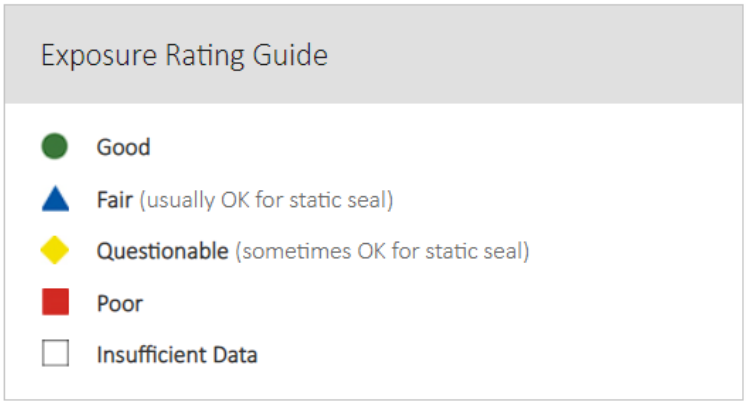


Figure 3.30: Exposure Rating Guide of Chemical Compatibility [62]

The chemical compatibility is defined for a 70 °F (around 20 °C) temperature, which is the standard test temperature, and the guide is therefore useful for material selection. Searching the chemical compatibility for Hydrogen Gas it provides a list of all the suitable materials for the pretended use. The list provided by Apple Rubber to the suitable materials for the application can be seen in the figure 3.31.

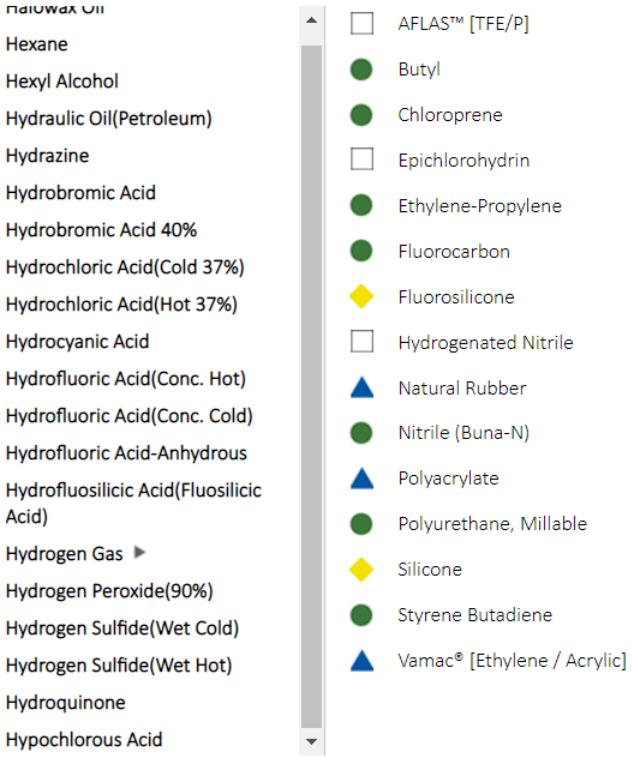


Figure 3.31: Hydrogen Gas compatible materials [62]

Crossing the data of this guide with another guides, like the one available in eFunda [63], figure 3.32, where the scale is similar to the one presented in figure 3.30, but with (4) for good to (0) for no data, the materials in common are Nitrile (Buna-N), Butyl, Ethylene-Propylene, Fluorocarbon and Polyurethan (Millable). From these available materials, in order to simplify the O-ring search, the general chosen material was the Fluorocarbon (FKM).

O-Ring Materials Compatible with Hydrogen Gas (select a material to show its compatible chemicals)		
Aflas (0)	Buna-N (Nitrile) (4)	Butyl (4)
Chemraz (4)	Epichlorohydrin (0)	Ethylene-Propylene (4)
Fluorocarbon (4)	Fluorosilicone (2)	Hypalon (4)
Kalrez (0)	Natural Rubber (3)	Neoprene (4)
Nitrile, Hydrogenated (0)	Polyacrylate (3)	Polysulfide (0)
Polyurethane, Cast (0)	Polyurethane, Millable (4)	Silicone (2)
Styrene Butadiene (3)	Teflon, Virgin (4)	Vamac (4)

Figure 3.32: O-ring materials compatible with H_2 [63]

3.10.1 O-ring between End Cap (3) and Fixation part (5)

To find the suitable O-ring size Apple Rubber also has an O-ring Size Search tool [64], which was used for sizing the O-rings.

As the centre hole will have a 40 mm diameter, the facial O-ring will need an ID bigger than 40. Using the O-ring size search and defining a minimum ID of 50 and maximum of 60. Opting for a normalized size, to the FKM material, by ISO 3601, the chosen ID was the 45.69, with the ISO 3601 reference of ISO 3601 - 133, which have a 2.62 cross section.

After defining the O-ring properties Apple Rubber also provides a tool to calculate the O-ring gland and other dimensions [65], like the gland diameter. To determine the O-ring gland height and diameters, is important to evaluate its squeeze, that for static applications can have values from 10% to 40%, and the volume fill, which values can go up to 90% in static applications. The squeeze of an O-ring and its volume fill can be obtained by the following equations:

$$Squeeze = \frac{CS - H}{CS} \tag{3.24}$$

where CS is the O-rings cross section diameter and H the gland depth

$$Volume\ Fill = \frac{CS_{area}}{CS\ Gland_{area}} = \frac{\pi \frac{CS^2}{4}}{H \times G} \tag{3.25}$$

where G is the groove width.

To apply a facial O-ring between the end cap (3) and the fixation part (5), with internal pressure, the dimensions which need to be set are the outside diameter ($OutD$), groove width and gland depth. To ensure the squeeze value and the volume fill the chosen dimensions were:

$$OutD = 50 \text{ mm} \tag{3.26}$$

$$G = 4 \text{ mm} \quad and \quad H = 2 \text{ mm} \tag{3.27}$$

With these, the inside diameter ($InsD$) can be calculated:

$$InsS = OutD - 2 \times G = 42 \text{ mm} \tag{3.28}$$

Introducing these values in the Apple Rubber tool the verification values, squeeze and volume fill were obtained to assure that the solution is a viable one, and if the values are outside of the allowable value, it can be changed the O-ring or change the attributed values.

As the first values complies with the squeeze and volume fill requirements, with a squeeze of 24% and a volume fill of 73%, the dimensions of the O-ring gland are obtained.

3.10.2 O-ring between fixation part (5) and bushing (9)

The hole present in this fixation part (5) is similar to the end cap (3) one, so the O-ring dimensions are the same as the ones defined in section 3.10.1. The fixation part will then have a facial seal ISO 3601 – 133 O-ring, from FKM, to prevent the hydrogen leak. This means that the gland dimensions will be similar to the previous presented ones, i.e., outside and inside diameters of 50 mm and 42 mm, respectively, with a gland depth of 2 mm, returning the same volumes of squeeze, 24%, and volume fill, 73%, which means that the solution can also be applied.

3.10.3 O-rings applied in the flanges (2)

As the O-rings that are going to be applied in the flanges (2) will be subject to hydrogen embrittlement the chosen material was similar to the previous presented O-rings, Fluorocarbon, FKM. This material will be applied to the facial O-ring, although, to the required measure of the radial sealing, the FKM O-rings were bigger than the required size, so to perform this sealing, the chosen radial O-rings will be from Buna-N (Nitrile Butadiene Rubber), NBR.

The facial seal, between the flanges (2) and the end caps (3 and 4), needs to have an outside diameter smaller than 150 mm, to guarantee the M3 holes safety and that the screws are not subjected to hydrogen embrittlement. So, using this value as a maximum it can be used an ISO 3601 – 255 O-ring, which have an ID of 142.47 and a CS of 3.53.

$$OutD = 147 \text{ mm}, \quad G = 5 \text{ mm} \quad and \quad H = 2.5 \text{ mm} \tag{3.29}$$

Being G the groove width and H the groove depth. With these:

$$InsD = 137 \text{ mm} \tag{3.30}$$

Introducing these values in the Apple Rubber tool the verification values, the squeeze and volume fill obtained were 29% and 73%, respectively. As these values are inside of the interval that assure that the solution is a viable one, the dimensions of the O-ring facial gland are obtained.

The radial O-ring is designed assuming that the flange works like a piston, but in a static seal. To choose the O-ring dimension it was assumed that the ID was bellow 150, and the O-ring chosen is an ISO 3601 – 162, which has an ID of 145.72 and a cross section of 2.62. To the piston O-ring calculation, the attributed parameters are different than the facial ones. To define the dimension of the O-ring, is necessary to establish a value for the bore, piston and groove diameter and the grove width. The bore diameter in this case will be the chamber inner diameter, and to avoid contact between the flange and the cylinder walls, the piston diameter will lower that that value. So, the dimensions are:

$$Bore\ Diameter = 155\ \text{mm} \tag{3.31}$$

$$Piston\ Diameter = 153\ \text{mm} \tag{3.32}$$

$$Groove\ Diameter = 151\ \text{mm} \tag{3.33}$$

$$G = 4\ \text{mm} \tag{3.34}$$

To assess if a piston or rod solution is suitable for a static application, the squeeze value needs to be between 10% and 30% and the volume fill now has a maximum value of 85%. In this application, the stretch is also a relevant factor, and the value needs to be between 1% and 5%. The stretch can be obtained by the formula:

$$Stretch = \left(\frac{Groove\ Diameter}{O-ring\ ID} - 1 \right) \times 100 \tag{3.35}$$

These definitions will result in a squeeze value of 23.7%, stretch of 3.6% and volume fill of 65.3%, which complies with all the requirements, so the O-ring flange is now dimensioned.

3.10.4 O-ring dynamic between dynamic rod (8) and bushing (9)

The rod will have different diameter in the full length, because it will work as piston and rod seal. To define the full proprieties, diameters and widths of the glands, it was used the Apple Rubber tool [65]. To calculate these dimensions, it is needed to separate the analysis in two parts, one to define the rod seal and the other to the piston seal. All of the O-rings used in the dynamic sealing application and in its application to the test chamber will be from FKM material, already defined as hydrogen embrittlement resistant.

Starting with the rod seal, the dimensions that are necessary to be established are the rod, bore and grove diameters and the grove width. As referred to in section 3.10.3, the squeeze, stretch and volume fill have pre-determined allowable interval values. However, in dynamic sealing application the values of squeeze are different from static. In dynamics the squeeze value has a suitable interval of 8% to 30%, maintaining the 1%-5% interval form stretch and a maximum volume fill of 85%.

The O-ring applied to the rod is the ISO 3601 - 316, which has a 21.59 ID and possess a 5.33 cross section. The defined values to ensure that this O-ring is suitable are:

$$Rod\ Diameter = 22 \text{ mm} \tag{3.36}$$

$$Bore\ Diameter = 25 \text{ mm} \tag{3.37}$$

$$Groove\ Diameter = 30 \text{ mm} \tag{3.38}$$

$$Groove\ Width = 8 \text{ mm} \tag{3.39}$$

With these values and applying the equations 3.24, 3.35 and 3.25, the obtained values are:

$$Squeeze = 25\% \tag{3.40}$$

$$Stretch = 1.9\% \tag{3.41}$$

$$Volume\ Fill = 72.2\% \tag{3.42}$$

As these values are inside the allowable interval for squeeze and stretch values and below the maximum volume fill, the bore and grove diameters as well as the groove width for the rod part are defined, so now the values for the piston seal can be determined.

The idea to facilitate the definition of the dynamic seal was to apply the same O-ring to the piston and to the rod, so here the chosen O-ring was again the ISO 3601 - 316, which properties are described above. To the piston seal the measures that are necessary to be established are the bore, piston and grove diameters and the grove width.

The defined values were:

$$Bore\ Diameter = 30 \text{ mm} \tag{3.43}$$

$$Piston\ Diameter = 25 \text{ mm} \tag{3.44}$$

$$Groove\ Diameter = 22\ \text{mm} \tag{3.45}$$

$$Groove\ Width = 8\ \text{mm} \tag{3.46}$$

Applying the equations 3.24, 3.25 and 3.35, the obtained values will be equivalents to the ones obtained in the rod calculations:

$$Squeeze = 25\% \tag{3.47}$$

$$Stretch = 1.9\% \tag{3.48}$$

$$Volume\ Fill = 72.2\% \tag{3.49}$$

As these values are inside the allowable interval for squeeze and stretch values and below the maximum volume fill, the bore and grove diameters as well as the groove width for the piston seal are defined, so all the measures required for the construction of the dynamic sealing are almost defined.

The only missing value is the additional O-ring that will be applied between the bushing (9) of the dynamic sealing and the fixation part (5). To guarantee the system safety, even though two facial O-rings are already defined, a radial O-ring can be applied to the bushing. ISO 3601 – 126 is a good option for the sealing purpose. This O-ring has an ID of 34.59 with a 2.62 cross section. To define this O-ring, it will be assumed a piston seal in a static state, where the values are:

$$Bore\ Diameter = 40\ \text{mm} \tag{3.50}$$

$$Piston\ Diameter = 38\ \text{mm} \tag{3.51}$$

$$Groove\ Diameter = 36\ \text{mm} \tag{3.52}$$

$$Groove\ Width = 5\ \text{mm} \tag{3.53}$$

Calculating the squeeze, stretch and volume fill by the equations 3.24, 3.25 and 3.35:

$$Squeeze = 23.7\% \tag{3.54}$$

$$Stretch = 4.1\% \tag{3.55}$$

$$Volume\ Fill = 52.8\% \tag{3.56}$$

As these results are inside the allowable interval for squeeze and stretch values and below the maximum volume fill, the bore and grove diameters as well as the groove width for the radial seal are defined, and now all the dimensions required for the construction of the dynamic sealing are fully defined.

3.10.5 O-ring between end cap (4) and fixation part (6)

To ensure the isolation of the chamber atmosphere, an O-ring will be introduced between the end cap (4) and the fixation piece (6), so it was chosen another FKM O-ring. To this purpose, and ISO 3601 – 118 O-ring was chosen, which has a 21.89 ID and cross section of 2.62.

Defining the outside diameter, the groove width and gland depth and calculation the squeeze and the volume fill to guarantee the correct sealing.

$$OutD = 26\ \text{mm} \tag{3.57}$$

$$Groove\ Width = 4\ \text{mm} \tag{3.58}$$

$$Gland\ Depth = 2\ \text{mm} \tag{3.59}$$

$$Gland\ Depth = 2\ \text{mm} \tag{3.60}$$

$$Squeeze = 24\% \tag{3.61}$$

$$Volume\ Fill = 75\% \tag{3.62}$$

As the squeeze and volume fill are inside the allowable intervals, the sealing is ensured and the respective glands were applied to the fixation part.

3.10.6 Hoses O-rings sizing

In order to insert the hoses inside the chamber, through holes will be created. The 6 mm type hose has an external diameter of 12,6 mm, which means that the bushing will need to ensure that will not happen leakages. To perform the penetration of the chamber, four bushings will be created, with an O-ring system to perform the gas containment. The O-rings to ensure this sealing will be made of FKM, as almost all the other O-rings used in this chamber design.

To ensure the sealing will be introduced two O-rings between the hose and the bushing, one O-ring between the bushing (9) and the fixation part (5), and two facial O-rings, one in the end cap

(3) and other in the fixation part (5). In the dynamic sealing, the bushing will be connected with the fixation part, so, to avoid using more screws and raise problems with space, the bushings will be manufactured directly in the dynamic seal bushing. The gas circulation will then be performed through this holes and the leakage risk of an extra feature is avoided.

As the hose has a 12.6 mm diameter, the chosen radial O-ring for the inner part is an ISO 3601 – 112, with an ID of 12.37 and 2.62 cross section. To the O-rings definition, a rod in static state was assumed, where:

$$Rod\ Diameter = 12.6\ \text{mm} \tag{3.63}$$

$$Bore\ Diameter = 14\ \text{mm} \tag{3.64}$$

$$Groove\ Diameter = 17\ \text{mm} \tag{3.65}$$

$$Groove\ Width = 3.5\ \text{mm} \tag{3.66}$$

The equations 3.24, 3.35 and 3.25 allow the calculating of the squeeze, stretch and volume fill to verify the correct application of the O-rings. So verifying the solution chosen:

$$Squeeze = 16\% \tag{3.67}$$

$$Stretch = 1.9\% \tag{3.68}$$

$$Volume\ Fill = 70.9\% \tag{3.69}$$

To evaluate is a piston or rod solution is suitable in static state, as referred before, the squeeze value needs to be between 10% and 30%, the volume fill maximum value is 85% and the stretch needs to be between 1% and 5%. So, has the obtained values check all these requirements, the O-ring is adequate.

To apply an O-ring in the outer surface of the bushing, between parts 9 and 5, it will be applied an ISO 3601 – 117, with an ID of 20.29 and 2.62 cross section. To define this O-ring, it will be assumed a piston seal in a static state, where the values are:

$$Bore\ Diameter = 25\ \text{mm} \tag{3.70}$$

$$Piston\ Diameter = 23\ \text{mm} \tag{3.71}$$

$$Groove\ Diameter = 21\ \text{mm} \tag{3.72}$$

$$Groove\ Width = 3.5\ \text{mm} \tag{3.73}$$

Verifying once again the values to confirm the suitability of the solution:

$$Squeeze = 23.7\% \tag{3.74}$$

$$Stretch = 3.5\% \tag{3.75}$$

$$Volume\ Fill = 76.7\% \tag{3.76}$$

As these values are inside the allowable interval for squeeze and stretch values and below the maximum volume fill, the bore and grove diameters as well as the groove width for the radial seal are defined.

To apply the facial seal between parts 5 and 9 and parts 3 and 5, the diameter must not interfere with the screws that connect the dynamic sealing to the fixation part, so it was chosen an ISO 3601 – 024 O-rings, with ID 28.30 and cross section 1.78. Defining the relevant values:

$$OutD = 29\ \text{mm} \tag{3.77}$$

$$Groove\ Width = 2.5\ \text{mm} \tag{3.78}$$

$$Gland\ Depth = 1.4\ \text{mm} \tag{3.79}$$

Verifying the squeeze and volume fill, that for facial O-rings squeeze has an interval of allowance of 10% to 40% and the maximum volume fill is 90%:

$$Squeeze = 21\% \tag{3.80}$$

$$Volume\ Fill = 82\% \tag{3.81}$$

With these values for the O-rings, all the O-rings are now dimensioned, and the bushing are already fixed to the dynamic sealing system bushing to, so the leakage is avoided, and the hoses can safely penetrate into the chamber.

3.11 Sensors Placement

The placement of sensors inside the hydrogen test chamber to track and measure various internal parameters is a key component of its design. The placement of the sensor and the method

of penetrating the end cap without compromising the hydrogen environment must be carefully considered in order to ensure accurate data collection and maintain the integrity of the chamber.

The best place to allocate sensors is on the end cap that is attached to the load cell. This choice is supported by the option that the gas should be inserted at the opposite end from the sensors. By doing this, the possibility of gas leaks close to the sensors is reduced, ensuring accurate and secure measurements.

The sensors were already presented in section 3.2.2, and the the power supply should also be ensured through the passage of power cables in this end cap

A penetrator (9) will be used to make a safe and sealed connection in order to power the sensors housed in the end cap. The penetrator applied for this purpose is the BlueRobotics WetLink Penetrator M14 [66], figure 3.33, made from 7075-T6 aluminium and anodized for enhanced durability and corrosion resistance. The WetLink Penetrator M14 from BlueRobotics has exceptional mechanical strength and is suitable for environments containing hydrogen. Because it is made of 7075-T6 aluminium, it has sufficient strength to withstand the chamber's operating pressure of 5 MPa. This component datasheet can be found in appendix L.

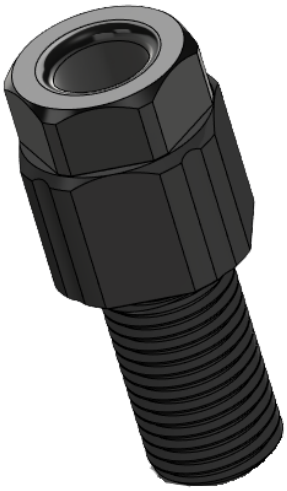


Figure 3.33: BLueRobotics M14 penetrator for the power cables [66]

A seal is already inserted in the BlueRobotics solution, and the seal material is FKM, which exhibits excellent resistance to hydrogen embrittlement and maintains its sealing properties even in demanding conditions. The FKM seal makes sure that the penetrator and end cap are tightly and securely connected, effectively stopping gas leakage [66].

Additionally, Buna-N (Nitrile Butadiene Rubber), which is renowned for its compatibility with hydrogen and resistance to various chemicals, as can be seen in section 3.10, is used to make the O-ring in this penetrator arrangement. The overall integrity of the hydrogen test chamber is enhanced by the Buna-N O-rings ensuring the leak-proof seal [66].

The design ensures accurate sensor measurements while preserving the integrity of the hydrogen environment by strategically placing sensors in the end cap, away from the gas insertion point, and using a penetrator system with a reliable seal. The FKM and Buna-N sealing materials, along with the BlueRobotics WetLink Penetrator M14, offer the required compatibility, strength, and resistance to hydrogen embrittlement to support the safe and effective operation of the hydrogen test chamber.

3.12 Valve sealing and hoses

To perform effective sealing and ensure the containment of the chamber environment, it is crucial to choose valves and hoses that are resistant to hydrogen embrittlement. This is essential to prevent any potential leakage caused by material weakening.

As mentioned in section 3.2.3, the design incorporates various valves, including ball valves, a pressure relief valve, and check valves. These valves will be acquired from external suppliers, and it is important to ensure that they meet the desired requirements for reliability and performance.

In order to connect the valves, hydrogen-resistant hoses capable of withstanding pressures up to approximately 5 MPa, which is the maximum chamber pressure, are necessary. SPIR STAR AG offers hoses with inner diameters of 6 mm and 16 mm, specifically designed for hydrogen use. These hoses have maximum working pressures of 962.5 bar and 600 bar, respectively, exceedingly largely the required working pressures for the test chamber [67].

The valves will be connected to the hoses using threaded connections, with the hoses equipped with MP fittings at the connection points. The insert sizes for the fittings are 3/8" for the 6 mm hose and 3/4" for the 16 mm hose [67]. As the hoses will be much larger than the inner diameter, and as the gas flow will not require elevated speed inside these hoses, the chosen hose is the type 6mm, figure 3.34, so the valve must have a 3/8” port size, which is equivalent to a DN10. It is worth noting that the insert material for the fittings is AISI 316, known for its resistance to hydrogen embrittlement. More information about the hose and the datasheet can be found in appendix M.

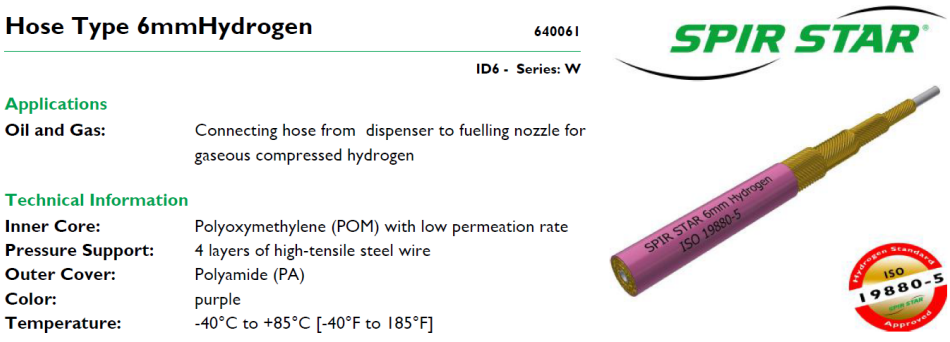


Figure 3.34: Hose Type-6mm SPIR STAR [67]

The selected ball valves are from Habonim, and they are part of the Hydrogen Service High Pressure Floating Ball 3 Piece Threaded-Body series [68]. Specifically, the H24 valve, figure

3.35, is chosen for this project, capable of withstanding pressures up to 414 bar. These valves are designed for automation, certified for fire-safety and emission standards, and feature double body sealing. With a 3/8" full port, they will be applied in the hydrogen source system, inert gas flush, and chamber atmosphere releasing system. The datasheet and information of this valve can be seen in appendix N.

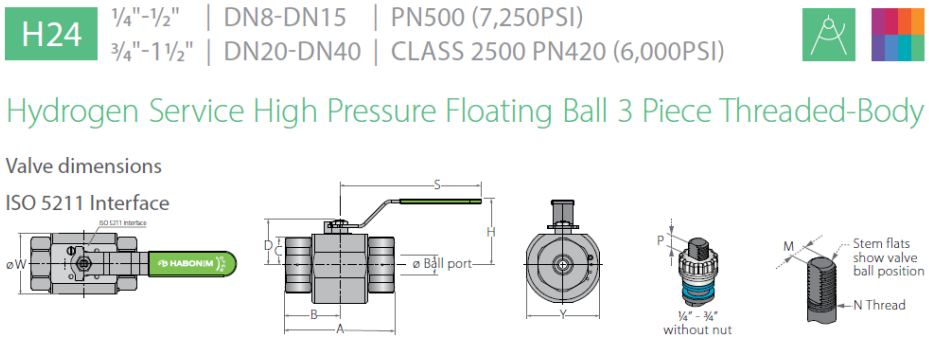
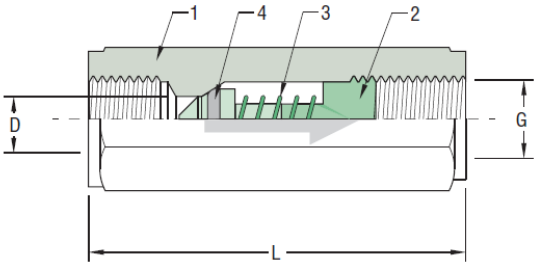


Figure 3.35: H24 Habonim valve [68]

To prevent gas backflow in the chamber entrance and the atmosphere releasing system, check valves will be utilized. Redfluid offers high-performance check valves designed to prevent reflow, with working pressures up to 425 bar, which exceeds the requirements. These check valves also have a 3/8" port size and can handle pressures up to 350 bar, with a spring cracking pressure of 1 bar, being the product code 70.03 [69]. The valve material is AISI 316, ensuring compatibility with hydrogen, 3.36. Three check valves will be required, and they will be connected to the chamber using the appropriate hoses. In appendix O is presented the datasheet and information of this valve.



TECHNICAL FEATURES		
Description		**Material**
1	Body	AISI 316
2	Lock screw	AISI 316
3	Spring	AISI 316
4	Poppet	AISI 316

Figure 3.36: Redfluid check valve and components materials [69]

Additionally, a safety valve, or pressure relief valve, needs to be set to a pressure of 5 MPa to

ensure the safe operation of the chamber and to protect the fused quartz tube. Goetze Armaturen offers a suitable valve that meets these requirements, figure 3.37. The maximum connection size for this valve is 3/8", which is compatible with the used hose. The valve can be adjusted up to 50 MPa and is constructed mainly with AISI 316L stainless steel, with the option of including a metallic or PTFE bellows [70]. Appendix P contains all the relevant information of the safety valve.



Figure 3.37: Gotze Armaturen series 420 pressure relief valve [70]

3.13 Screws, Nuts and Washers

The fixation of all the components in place require the application of nuts in the fixation system and of screws and washers in the fixation system, with the end caps and flanges, and with the dynamic sealing system. The screws, nuts and washer used in this design are obtained from Fabory.

The nuts are applied to the four rods (7) in the fixation system, that use M8 nuts (16), in the eight ends of the rods, two for each rod. The chosen nuts are hexagon nuts from steel zinc plated DIN 934, that will guarantee the fixation of the system and the end caps in place. To apply these M8 nuts it will require a washer between the fixation piece (5 and 6) and each nut, so eight washers are required. Using the supplier that was referred before, it will be used plain washers DIN 125-1A Steel Zinc plated M8 140 HV (15). This combination of washers and nuts are then defined and ready to be applied in the fixation system.

For the connection of the end caps, flanges and dynamic sealing to the fixation parts, M3 screws are used, but different sizes are required. The M3 screws used are the hexagon socket head cap screws, DIN 912, so the M3 screws will have variation lengths of this.

For the dynamic sealing it will be applied six M3 screws, that will pass through the bushing of the dynamic seal system to the fixation piece. The M3 holes in the fixation piece have a depth of 4 mm, and the bushing as a thickness of 5 mm, which means that the screw can have a maximum

length of 9 mm. Choosing a standardized length the nearest value is 8 mm, so to perform the fixation of these two parts, the M3x8 screws DIN 912 Stainless steel (11) are used.

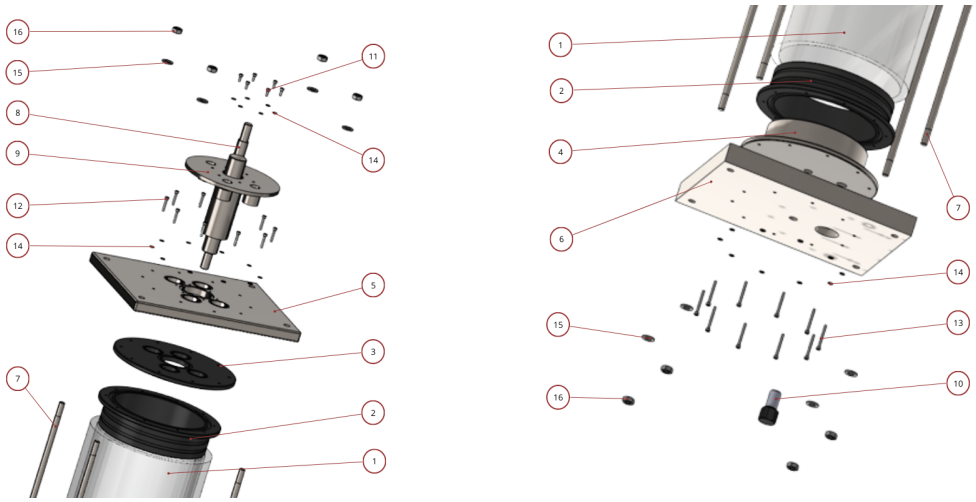
The connection between the fixation part, end cap and flange will not be similar in both ends of the chamber, because the fixation parts have different thickness. The thickness of both end caps and flanges is 6 mm each.

The fixation part connected to the dynamic sealing (5) has a thickness of 15 mm, with an indention where the end cap (3) is applied, and to this thickness is added the flange (2) thickness of 6 mm. This means that the full length of the screw can be up to 21 mm. Choosing a standardized length, and regarding the fact that the holes in the flanges should not pass through all the thickness, the chosen length value is 18 mm, so it will be used M3x18 screws DIN 912 Stainless steel (12) to perform the fixation of the fixation piece, end cap and flange together.

In the other end of the solution, the fixation part (6) has a thickness of 25 mm, having a similar indention to part 5, where the end cap (4) is applied, and to this thickness is added the flange (2) thickness of 6 mm. This mens that the full length of the screw can be up to 31 mm. The standardized length chosen value is 30 mm, regarding the same fact previously stated about the flange holes, so it will be used M3x30 screws DIN 912 (13) Stainless steel to perform the fixation of this section.

In all of the M3 screws used a washer will also be applied between the screw head and the metal part in which it will be applied. The washers will also be supplied by Fabory, and they are similar to the ones applied in the M8 nuts, only reducing the diameter to M3, so the used plain washer will be the DIN 125-1A M3 (14).

The specific place of allocation of the screws, nuts and washers can be seen in figure 3.38, where is observed the allocation of this features in both end of the system.



(a) Through hole section (b) Load cell section

Figure 3.38: Exploded detail view of the screws, nut and washers allocation

3.14 Design for Manufacturing

To achieve the final designed, some parts will be procured but others will require manufacturing, so it is necessary to identify which parts will be manufactured, the required materials and the manufacturing drawings and options needs to be established.

The pieces that are going to be manufactured are the fixation pieces and rods, the dynamic sealing rod and bushing, the ends caps and the O-ring flanges. Almost all of these pieces will be exposed to hydrogen embrittlement, with exception of the fixation rods, but to use the same material to all the parts and as referred before, the material in which they will be manufactured is the AISI 316L stainless steel.

The manufacturing process for these components primarily involves turning, drilling, and milling operations.

Turning is utilized to achieve high levels of concentricity, ensuring precise dimensional control by rotating the workpiece on a lathe while a cutting tool removes material.

Drilling is extensively employed to create holes of various sizes and depths, relying on the rotation of a drill bit and axial force to cut through the material.

In the case of larger holes requiring precise dimensions, milling is employed using a rotating milling cutter with multiple teeth to remove material and achieve the desired shape, size, and surface finish. Additionally, milling is not limited to hole-making but also encompasses other machining tasks such as surface machining, profiling, and contouring.

The fixation pieces will have a similar design, differing mainly in the diameter of the central hole, thickness, and the inclusion of six additional M3 holes for securing the dynamic sealing. The manufacturing process involves cutting the pieces to the desired dimensions and subsequently applying milling techniques. The milling process serves multiple purposes, including achieving the desired surface finish, creating a larger recess in the middle of the piece, and forming the hole for the dynamic seal bushing. The holes required for the rod can be generated either through the milling process or by using drilling techniques. In addition, any remaining necessary holes in this component will be drilled accordingly. Furthermore, the milling process will be employed to correct the surface roughness in the O-ring glands, ensuring a high-quality surface finish. The design 2D drawing of these parts can be found in appendices E and F.

The fixation rods are not difficult to manufacture as they will not require extra cares, being four solid beams with M8 threaded ends. The only important thing to assure in these rods is that the threaded length is enough to correctly place the M8 nuts and washers. Turning will be the manufacture process of this pieces, and the thread in the ends can be manufactured through turning or milling. The rods 2D drawing is presented in appendix G.

Dynamic Sealing metal parts will require extra care in the manufacture because the surface roughness needs to be 0.20 µm. Turning will be the best process to manufacture these parts, because the concentricity is very important for the dynamic sealing to work properly, and the surface roughness can be corrected by milling if needed. The hose bushings inserted in this component will also be fabricated using turning techniques, and ensuring the desired surface roughness will

also require special procedures. This surface roughness is applied to all the bushings and the pull rod, and more precisely details of the parts concerned can be observed in appendices H and I.

Both O-ring flanges are similar, and the most important feature of these pieces is to ensure that the O-ring glands will have a 0.20 µm surface roughness, to avoid material damage in the O-rings. This surface roughness needs to be applied not only to the radial glands but also to the facial gland, to really guarantee the correct sealing of the chamber. The O-ring flanges will be manufactured by turning, and, similar to the dynamic sealing the surface roughness can be corrected by milling if needed. The detailed manufacturing design is presented in appendix B.

The end caps will be very different, being that one of them will only have a 6 mm thickness with a central hole and the 3 mm diameter holes and the other one will have a salience that will ensure the connection of the clamp with the machine. In the end cap with the salience hole that does not goes through the hole piece will be made, so the dimensions of the hole already consider the removal of the machine tool in the manufacturing to avoid failures and to guarantee that the required manufactured piece will have the same dimensions as the designed ones. As high concentricity is required in both the end caps, the main manufacture process of these will be turning, applying milling in the end cap where the dynamic sealing will pass, and drilling the remaining holes of the parts. The milling will also be applied to certain details of these pieces to ensure the high surface quality required. In appendices C and D the detail drawing of both pieces is presented, as well as the manufacturing projected tolerances.

3.15 Chapter Summary

In conclusion, the design entails a combination of parts being procured and others being manufactured. To withstand hydrogen embrittlement, all of the parts that will be produced, such as fixation pieces, rods, dynamic sealing components, end caps, and O-ring flanges, will be made of AISI 316L stainless steel.

The essential specifications for surface roughness, dimensions, and tolerances have been laid out, guaranteeing that the design and manufacturing details for each part contribute to the end goal of the system. These specifications must be followed during the production process to guarantee the components' quality and functionality.

The development project goal is to design a durable chamber for hydrogen embrittlement testing through the careful selection of materials and production techniques. The testing capabilities and safety of the chamber will be further improved by the addition of sensors for measuring gas concentration and pressure.

This chapter has given a general overview of the pieces that need to be created, their designs, and the materials and methods used to make them. These specifics set the groundwork for the project successful completion and enable accurate and controlled testing of hydrogen embrittlement effects.

More information about the system assembly and its user guide can be found in appendix Q.

Chapter 4

Structural Validation

To assess the proposed solution, it is important to analyse the structural integrity. It is crucial to perform a thorough assessment of the design's integrity, ensuring that the project's reliability, safety, and its operation is within specifications. To perform this, it was performed a finite element analysis, by the finite element method (FEM). This analysis was conducted using Abaqus CAE software package, which is a recognized software for numerical analysis, especially for structural modeling.

To create the CAE model in Abaqus, it is required to import the Soldiworks CAD model, and ensure the correct material definitions, boundary conditions, loading and interactions. In this chapter, the strategies used for the analysis setup, as boundary conditions, loadings, constraints, and more simulation parameters, are discussed.

Furthermore, the outcomes of the Abaqus analysis are displayed, along with thorough visualizations and data analysis to assess the effectiveness of the solution. This includes the distribution of stresses, the profiles of displacements, and the critical areas vulnerable to failure or deformation. The structural integrity of the suggested solution can be effectively evaluated by comparing these results to predetermined design criteria and industry standards.

In the end, the structural verification that was conducted in this chapter is crucial to ensuring the dependability and safety of the designed system. Utilizing Abaqus' capabilities enables in-depth understanding of how the solution behaves under various circumstances, enabling knowledgeable decision-making and fostering necessary improvements.

4.1 Modeling Assumptions

As stated before, the objective of this work is to design a durable chamber, and the definitions of the chamber, material justification, dimensions and all the important considerations taken during the design process are presented in chapter 3.

There are several important factors discussed in the previous chapters, but for this analysis, the most crucial elements to consider for a comprehensive structural analysis are the selected

materials, the forces and pressures exerted on the chamber, and the preload set on the bolted connections.

The chosen materials are fused quartz to the chamber walls and AISI 316L stainless steel for almost all the remaining parts of the design, excluding screws, nuts and washers and the power cables penetrator. The materials properties of AISI 316L and fused quartz can be consulted in GRANTA edupack [55] and the most relevant properties are presented in table 4.1.

Table 4.1: Proprieties of AISI 316L and Fused Quartz

Property	AISI 316L	Fused Quartz
Density [kg/m^3]	8000	2200
Young's Module [GPa]	197.5	72.5
Yield strength (elastic limit) [MPa]	205	50
Poisson's Ratio	0.27	0.17
Maximum Service Temperature [°C]	750	1160

In this test chamber, the intended applied maximum forces and pressures are not too high, having the force a maximum of 20 kN, and the pressure will always be maintained in safe level, below 5 MPa.

Another factor worth considering is the screws preload, which refers to the intentional application of an initial axial force or tension to a screw during installation. This force creates a clamping force between the joined parts, which helps to prevent loosening and improves the joint's resistance to external forces and vibrations [71]. Preload is a characteristic of each screw, defined by its metric and the thread type, increasing with the metric increment, and achieving higher values with fine thread than with coarse thread, for the same diameter. This parameter is crucial to evaluate the structural validation of the solution, to ensure that the fixation is correct, and no unexpected errors will occur due to excessive force in the screws or not correct holding. The preloads of the various screws used in this project can be consulted in the figure 4.1.

TABLE OF PRELOADS AND TIGHTENING APPROXIMATE VALUES

METRIC	mm allen	mm hex.	mm coarse thread	resistant section mm2	friction coefficient	COARSE THREAD 8.8 PRELOAD N	8.8 TORQUE Nm	10.9 PRELOAD N	10.9 TORQUE Nm	12.9 PRELOAD N	12.9 TORQUE Nm
M2	1,5	4	0,40	2,07	0,10	976,9	0,51	1.373,6	0,43	1.648,6	0,52
					0,14	899,0	0,57	1.284,3	0,52	1.517,1	0,63
M2,5	2	5	0,45	3,39	0,10	1.627,0	0.63	2.288,0	0.88	2.745,6	1,05
					0,14	1.499,8	0,77	2.109,1	1,08	2.531,0	1,30
M3	2,5	5,5	0,50	5,03	0,10	2.439,9	1,09	3.431,0	1,53	4.117,2	1,84
					0,14	2.251,9	1,84	3.186,7	1,88	3.800,0	2,26
M3,5		6	0,60	6,78	0,10	3.276,4	1,68	4.607,5	2,38	5.528,9	2,84
					0,14	3.022,8	2,05	4.250,6	2,88	5.100,7	3,47
M4	3	7	0,70	8,78	0,10	4.230,6	2,30	5.849,6	3,52	7.139,5	4,22
					0,14	3.901,9	3,08	5.487,0	4,30	6.584,4	5,16
M5	4	8	0,80	14,20	0,10	6.923,1	4,83	9.735,7	6,93	11.682,8	8,82
					0,14	6.393,7	6,04	8.991,1	8,50	10.769,3	10,20
M6	5	10	1,00	20,10	0,10	9.748,4	8,47	13.710,1	11,92	16.452,2	14,80
					0,14	8.998,2	10,37	12.653,7	14,59	15.184,4	17,51
M7		11	1,00	28,90	0,10	14.269,1	13,94	20.065,9	19,60	24.079,1	23,52
					0,14	13.199,2	17,21	18.561,4	24,20	22.273,6	29,04
M8	6	13	1,25	36,60	0,10	17.894,2	20,41	25.163,7	28,70	30.196,5	34,44
					0,14	16.531,2	25,07	23.247,0	35,26	27.896,5	42,31
M10	8	16	1,50	58,00	0,10	28.489,0	40,22	40.052,7	56,58	48.075,3	67,87
					0,14	28.334,6	49,52	37.033,3	59,64	44.439,9	83,58
M12	10	18	1,75	84,30	0,10	41.533,2	68,86	58.406,1	98,63	70.087,3	116,20
					0,14	38.408,0	84,84	54.011,2	119,31	64.813,5	143,17

Figure 4.1: Preload table of some metric screw sizes [72]

All the model's pieces will be subjected to an axial force of 20 kN, and as seen in the figure 4.1 the preload force of the screws applied should be enough to not occur any disconnection problem. The dynamic rod is held by a M12 screw and the load cell section by a M12 and ten M3 screws, so no issue regarding the screws is foreseen. However, validation is required.

4.2 Critical Sections

After defining the important parameters to analyse is necessary to establish the critical section of the design and perform its structural analysis. The critical section is the specific location where the critical effects of the applied load are expected, being crucial to ensure that the deformation of this section does not occur, because is where the highest stress, strain and deformation effects concentrate, making the overall structural integrity and performance of the element analysis crucial.

Focusing on the critical section allows the accurately evaluation of the behaviour and capacity of the elements under different loading conditions. This attentive analysis helps to determine if the safety standards are met, where are the potential failures and it helps the dimension optimization or elements reinforcement, to prevent these major failures.

Identifying the critical sections is fundamental to the correct structural design, and this analysis provides valuable information's about the performance and reliability of the project. Through this analysis the decision-making about materials selection, design modification, safety measures, and design limitations are correctly ensured.

As stated before, in section 3.1.3, the machine maximum force is applied by the movable part of the machine, which is connected to the dynamic sealing, which was already dimensioned to

sustain this applied force (section 3.9), and the reaction force will be applied in the chamber part connected to the load cell. The maximum safety pressure reached in the chamber is also defined, in section 3.5, which is a parameter relevant to simulate in order to verify the design structural integrity.

After identifying the critical pressure and forces, three key sections have been determined. The first section is the dynamic sealing rod, which is connected to the machine and one clamp, experiencing the maximum force exerted by the machine. This section is crucial as it enables the application of forces to the specimens. The second section is comprised of the chamber walls, which are subjected to internal pressure. These walls are critical due to their mechanical properties, which are less resistant than steel. The final section includes three components connected to the load cell: the fixation part, the end cap, and the O-ring flange. This section is also exposed to the machine's maximum force and is of utmost importance to ensure its integrity and prevent any risk of fracture or hydrogen leakage. The relevant dimensions of these components can be found in appendices D, F, and B. Considerations for preloads include M12 and M3 coarse thread screws selected from the 10.9 class.

The rod is connected to the machine by the mean of a M12 screw, and the three pieces of the load cell connected critical section are the means of ten M3 screws, of the 10.9 class, and the fixation of the chamber to the machine is made by one M12 screw, connected to the end cap and the fixation piece. The definition of this screws preloads is necessary, to evaluate if the applied force will not fracture the screws and fail the connection of the pieces and ruining the chamber sealing. Within the surfaces in contact in these connections a 0.10 friction coefficient will be assumed, to assume the lowest friction condition. Defining the values corresponding to this assumption of the figure 4.1. In appendix H the manufacturing design of this piece is presented, where the relevant dimensions can be consulted.

The other critical section, the fused quartz tube, subjected to the pressure of the inside environment, does not have any fixation around. This tube is then subjected to a pressure on its inside wall, in all its length between the O-ring flanges. The relevant dimensions of this chamber can be seen in section 3.5.

Having the critical sections defined the software Abaqus can now be used to perform the FEM analysis.

4.3 Modeling Strategy

Defining the critical sections is a key aspect to the detailed modelling of the system, simplifying the FEM analysis. In this chapter are presented some of the employed modelling techniques to accurately represent the applied forces and pressure to this critical section, in representation of the test chamber.

In order to simplify some structures, assumptions were made during the analysis, applying some boundary conditions and loading scenarios to correctly perform the FEM analysis.

The critical sections are then the pieces connected to the load cell because it is the place where the maximum force will be applied, and the quartz glass tube, because of the less strong material and the internal pressure applied.

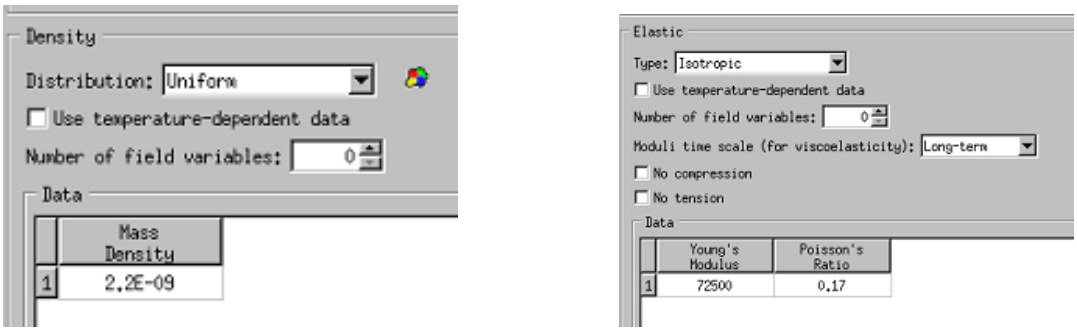
In order to input property values into Abaqus, it is necessary to ensure that all units are consistent. Since the designs were uploaded in mm, it is important to use mm as the reference unit for all remaining values. To obtain the final stress results in MPa, the density should be defined in tonne per mm^3 and Young's Modulus in MPa. An example of different Abaqus units relation can be seen in figure 4.2.

	International System	Micromechanics	Mesomechanics 1	Mesomechanics 2	Mesomechanics 3	Macromechanics
	Fundamental magnitudes					
Length	$\boldsymbol{m}$	μm	mm	mm	mm	m
Mass	$\boldsymbol{kg}$	g	g	ton	kg	$kton$
Time	s	ms	ms	s	ms	s
	Derivate magnitudes					
Force	$\boldsymbol{N}$	mN	N	N	kN	MN
Stress	$\boldsymbol{Pa}$	GPa	MPa	MPa	GPa	MPa
Energy	$\boldsymbol{J}$	nJ	mJ	mJ	J	MJ
Density	$\boldsymbol{kg/m^3}$	$10^{15}\ kg/m^3$	$10^{6}\ kg/m^3$	$10^{12}\ kg/m^3$	$10^{9}\ kg/m^3$	$10^{6}\ kg/m^3$
Water density	$\boldsymbol{10^3}$	10^{-12}	10^{-3}	10^{-9}	10^{-6}	10^{-3}

Figure 4.2: Relation of units system to Abaqus [73]

4.3.1 Fused Quartz tube analysis

The fused quartz tube was the first structural element to be studied, to ensure that the internal environment will not fail the chamber wall, resulting in total leakage and potential safety hazard. The definition of the most relevant proprieties of fused glass, namely the mass density, Young's Modulus and Poisson's ratio, are presented in table4.1, applied in Abaqus as presented in figure 4.3. The tube CAD was uploaded from Solidworks and modeled as an isotropic deformable solid. The quartz tube mesh is presented in figure 4.4. In this section, 24960 elements were used, specifically the C3D8R elements.



(a) (b)

Figure 4.3: Fused Quartz properties inserted in Abaqus software

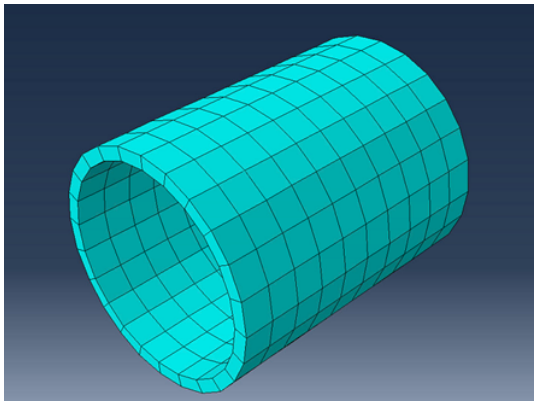


Figure 4.4: Quartz Tube mesh

As loading condition, a 5 MPa internal pressure was applied on the internal wall.

For boundary conditions, all axial displacements were restrained at bottom and top surfaces of the tube, in accordance with the physical system restraints.

The loading and boundary conditions is shown in figure 4.5.

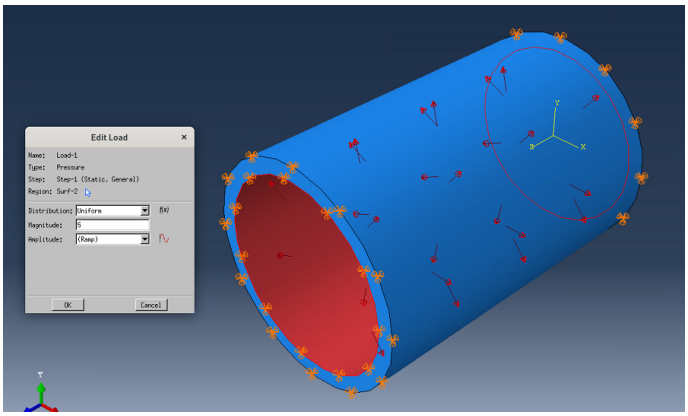


Figure 4.5: Quartz Tube applied internal pressure

With the model defined, the resulting von Mises stress field in MPa (figure 4.6) and displacement in mm (figure 4.7) were assessed.

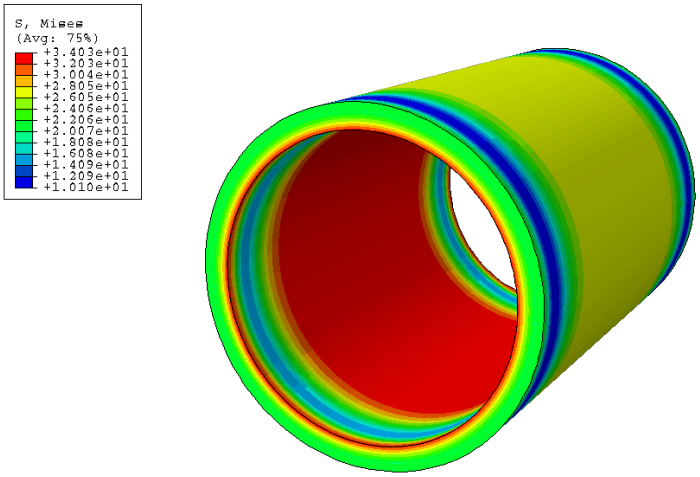


Figure 4.6: Chamber wall resulting stresses in MPa

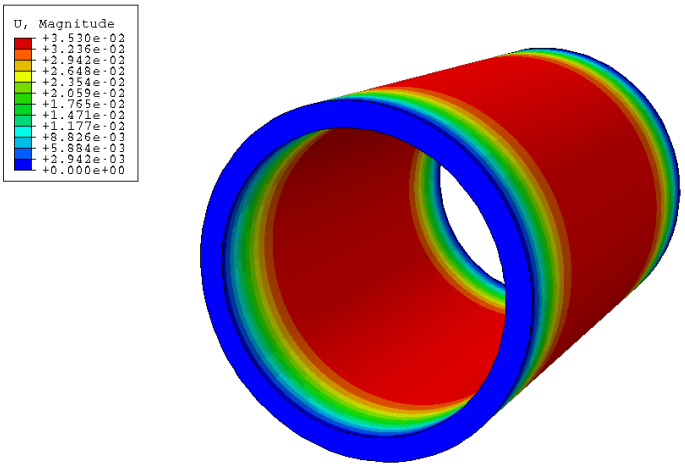


Figure 4.7: Chamber wall resulting displacements in mm

4.3.2 Load Cell connected section analysis

As stated previously, the parts connected to the charge cell are subjected to the highest loading and it requires numerical validation to ensure a safe design. This critical section is composed by the O-ring flange, end cap and fixation part connected to this cell, and these parts will be connected through various bolted connections.

These components were modeled in AISI 316L stainless steel, and the relevant properties to this analysis are presented in table 4.1.

The geometry of these pieces is complex, having more than one feature by part, which can complicate the Abaqus meshing process. To simplify this process and to execute an also correct analysis some simplifications can be applied to the pieces.

The first simplification possible is to remove the screws, washer and nuts, creating face partitions where the washers and nut contact, applying the respective force to that feature. To realise this simplification, a reference point is created in the center of the circumferential partition, and is coupled to the circular area where the washer contact will happen. The same principle is applied to the nuts contact. An example of this application is presented in figure 4.8.

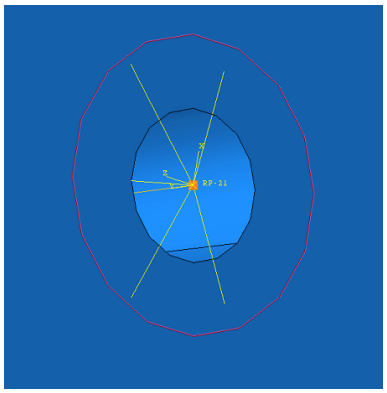
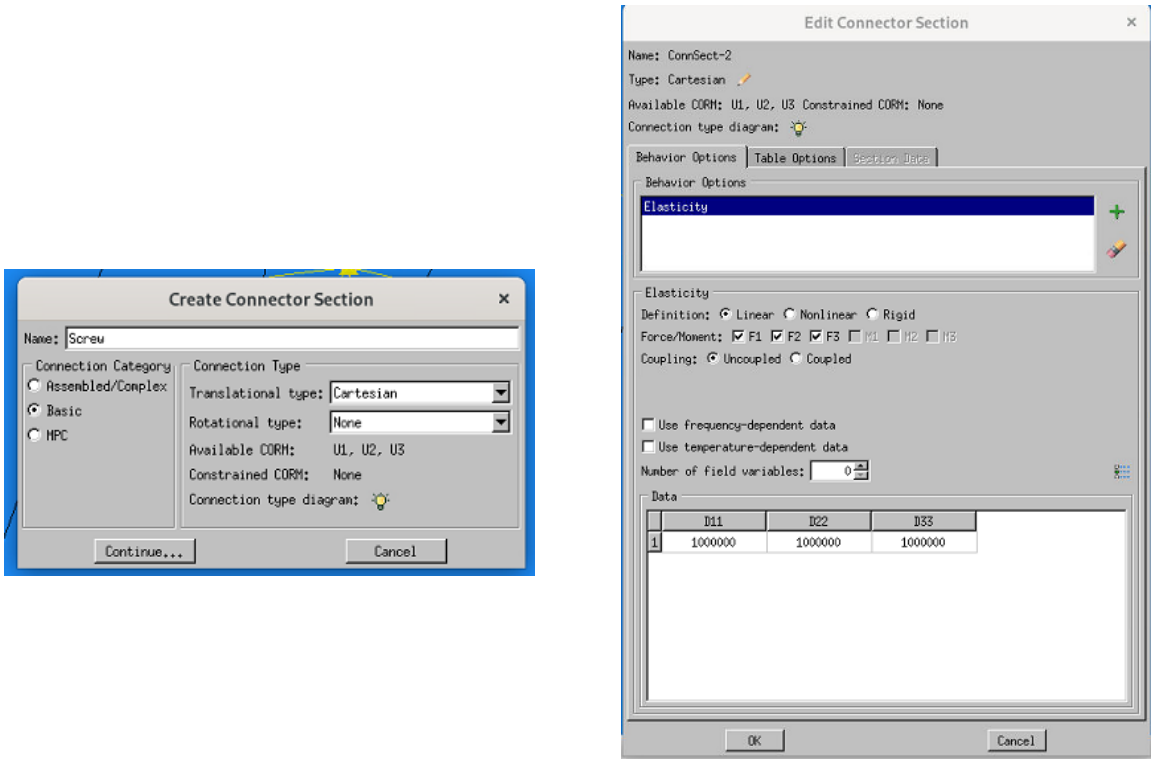


Figure 4.8: Example of the coupling constrain application

To eliminate the bolts, is used the preload to define the fixation provided by them. The definition of the preload firstly requires a wire that connect to two reference points, and then this wire will be defined as a solid part. To define this connection is created a connector section, defining its category as basic and the translational type as cartesian, as seen in figure 4.9a. After the categorization of the connection the behaviour of the section is defined as an elasticity behaviour, and to ensure that all the forces are applied to the screws, the stiffness will be defined as an exaggerated value, figure 4.9b.



(a) (b)

Figure 4.9: Connector Section properties defined in Abaqus to simulate the screws

The bolts apply forces in the washers and the threaded holes are in the flange piece, where the screw ensure the fixation. This connector section is then applied to the wires created to unite the bottom surface of the fixation part and the flange holes, simplifying the model analysis but ensuring that all the required connection are present.

It will also be applied a contact interaction between the elements contacting surfaces, to simulate the contact in Abaqus, to represent the pieces assembly. The contact properties applied were the conditions presented in figure 4.10.

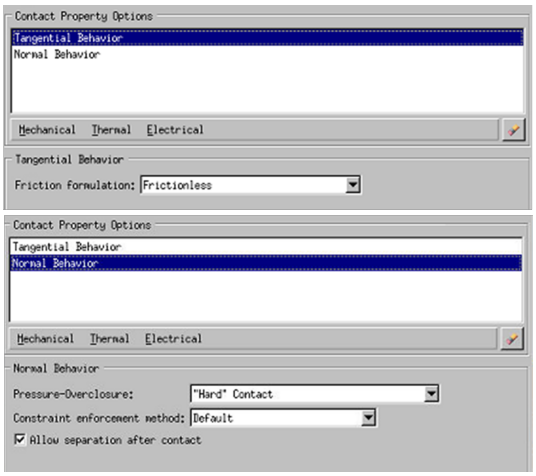


Figure 4.10: Contact propertied applied between surfaces

This simplification can be applied to the present critical section and, after meshing the parts, the configuration of this properties is the one seen in figure 4.11. A total of 387044 C3D10 elements were used in this section, with 260258 elements in the fixation part, 93499 elements in the end cap, and 33287 elements in the flange.

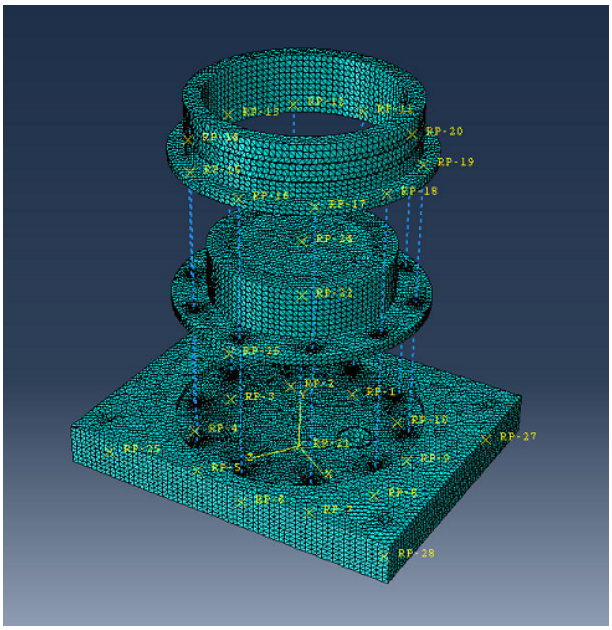


Figure 4.11: Interactions and mesh of the load cell connected section

To apply the loads three steps are created, the initial one, where the boundary conditions and the simplification are applied, the preload step, that will create connector forces to the connector section previously defined, and the test step, in which the maximum force applied by the machine will be defined.

In the initial step is then defined the boundary condition. The fixation part will be connected to the machine in the central part of the piece, by the mean of a M12 screw, that end in the end

cap. So, to apply the boundary condition it will be considered the fixation part fixed in the bottom, connected to the central hole, and the end cap fixed in the central hole, in the bottom surface, simulating also this M12 connection.

Next, the definition of the bolts preload is applied in the preload step. The preload is set for each bolt connection type (M3 and M12) following the figure 4.1. These preloads are applied to the wires, defined as cartesian, as a connector force. The force is defined concerning the screw applied, in figure 4.12 is presented an example of this connector force application in a M3 hole.

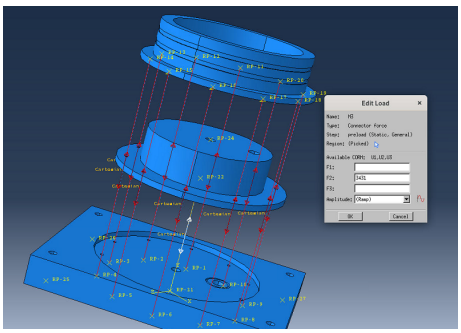


Figure 4.12: Introduction of M3 preload in Abaqus

Finally, in the last step is defined the force applied to the chamber, in the reference point created in the upper surface of the end cap, connected to the surface where the screw will contact. This force applied will be the tension force, with a value of 20 kN, as presented in figure 4.13, and this ends the load definition of this critical section.

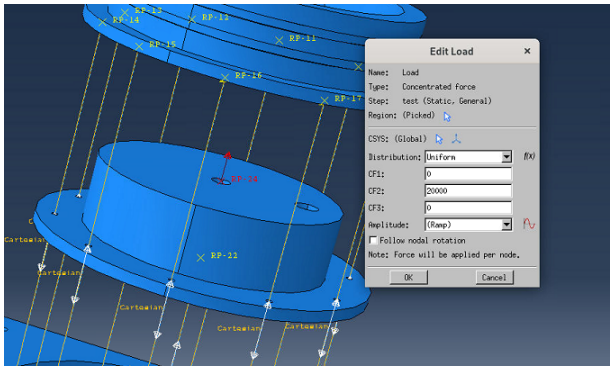
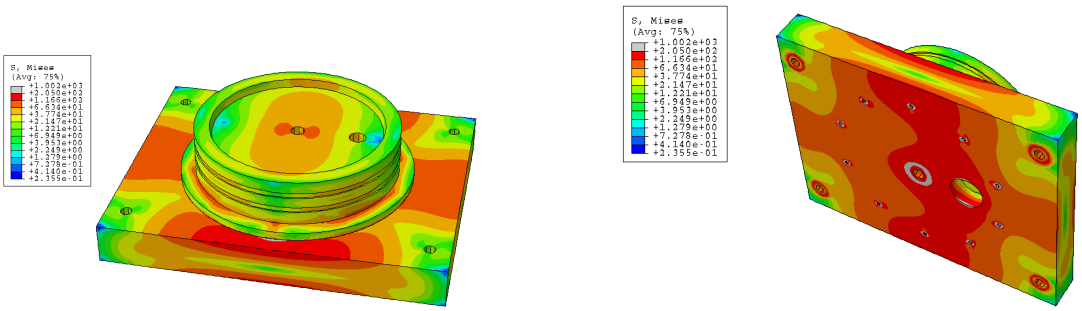


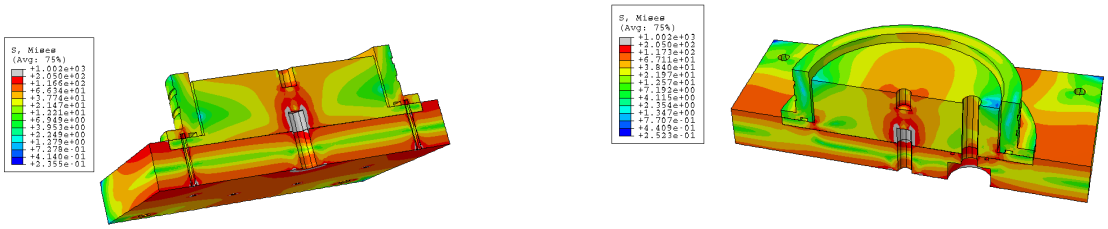
Figure 4.13: Axial maximum force applied in Abaqus simulation

The parts were subsequently translated to their respective locations, and the simulation was conducted. A job was created to obtain the results for this section. With all parameters defined, Abaqus calculated the desired property values. The definitions previously presented develop the results presented in figures 4.14 and 4.15. To rigorously evaluate the results, the maximum stress to represent will be 205 MPa, as the yield strength elastic limit of this material, having the stress above that at grey colour to correctly interpretate the simulation.



(a) (b)

Figure 4.14: Load Cell connected section stresses in MPa



(a) (b)

Figure 4.15: Cut views of the Load Cell connected section stresses in MPa, in different planes

4.3.3 Dynamic Sealing Rod analysis

The last analysed critical section is the dynamic sealing rod, which is subject to the maximum force applied by the machine.

This rod is manufactured in AISI 316L stainless steel, which properties were already presented in table 4.1.

This piece has two M12 threaded ends, one to connect to the machine movable piece and other in the other end to connect to the clamp, in which the specimen will be attached.

To simplify the analysis of this section both M12 were reduced to circumferences in the ends of the piece with a reference point tied to this circumferential area, as the solution used in the section 4.3.2.

This component is connected to the test machine through a M12 bolted connection, and given that the preload is approximately three times larger than the applied load, it will be set as restrained on all degrees of freedom in this section. At the other end, the concentrated force is defined as the maximum machine force, with 20000 N in the axial direction. These defined conditions are presented in figure 4.16.

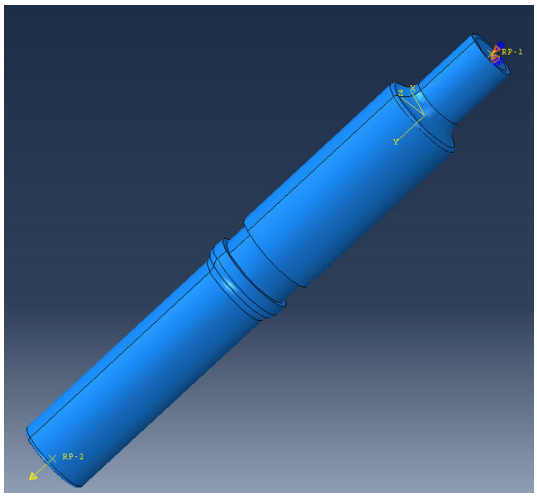
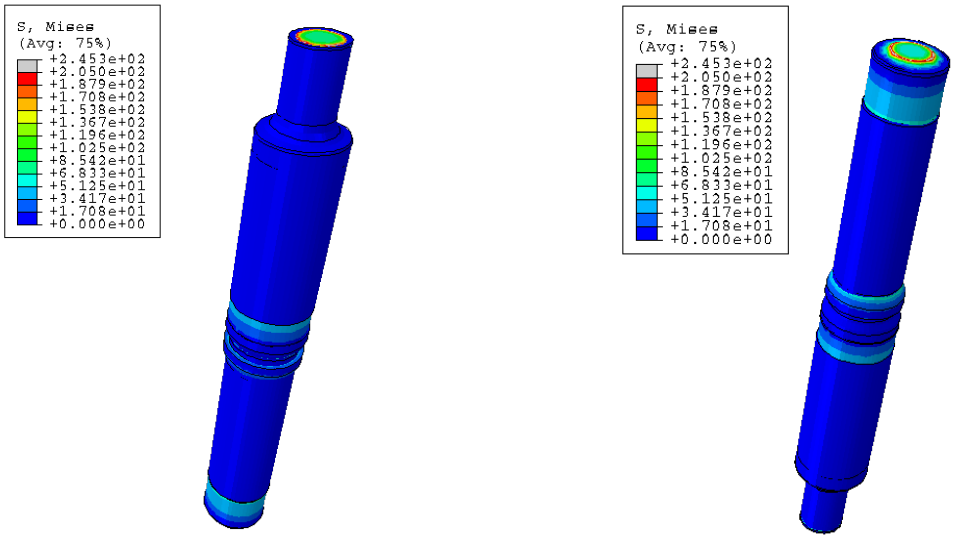


Figure 4.16: Boundary Condition and Force applied to the Rod

After defining all the conditions, the mesh for the part was created using 265882 C3D10 elements. The job for conducting the FEM analysis is now prepared and ready for submission. This analysis will provide the desired values for stresses and displacements, which are presented in Figures 4.17 and 4.18, respectively.



(a) Machine Connected Section (b) Clamp Connected Section

Figure 4.17: Stresses applied in dynamic rod, in MPa

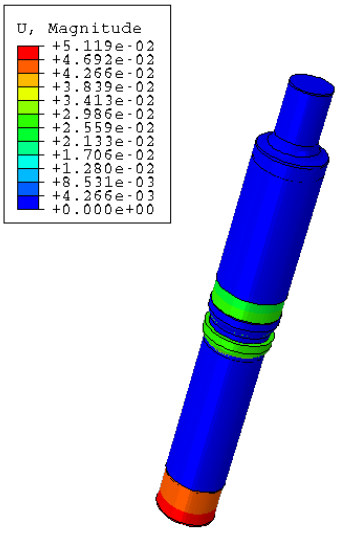


Figure 4.18: Dynamic Rod resulting displacements in mm

4.4 Simulations Results Discussion

To validate that the test chamber will not incur any permanent deformation the maximum stress level were checked against the materials yield strength and safety coefficients were calculated.

Separating the critical sections, this analysis becomes easy, so comparing each section with the applied material, in this chapter, the validation of the solution is discussed.

The important aspect to evaluate the solution is the maximum stress value obtained, which will be compared with constituent material elastic limit yield strength, needing to obtain a maximum stress below that value, to ensure that the solution will not enter a plastic behaviour.

In this section the critical sections will be analysed separately, performing each structural analysis directly.

4.4.1 Quartz Tube Results Analysis

As presented in figure 4.7 and 4.6, the displacement of the quartz tube is in the micrometres scale, and the obtained maximum stress value can be compared with the material elastic yield strength, having both values presented in table 4.2.

Table 4.2: Quartz Tube stress values obtained in Abaqus and the material property

Property	Stress [MPa]
Von Mises Maximum Stress - Abaqus	34.03
Fused Quartz Yield Strength Elastic Limit	50

Table 4.2 verify that the previous sizing of the quartz tube to ensure its safety is correct, and this thickness can be validated as the chamber wall. The maximum stress is substantially below the material yield strength. The safety factor value is 1.47, the ratio between the Abaqus result

and the elastic limit yield strength, and this factor will be higher because the pressures will never reach 5 MPa.

With the Abaqus results, is then possible to verify that the quartz glass tube is adequate for this design and that it will sustain pressure at least up to 5 MPa, so the wall can be composed of fused quartz and the dimensions are the ones already defined.

4.4.2 Load Cell Connected Section Results Discussion

In figure 4.14 it can be observed that the stress values of this section are very elevated, which is not a good situation. Defining the maximum stress as the yield strength all a lot of elements of the simulation take the colour grey, which means that they will enter the plastic behaviour, what is not intended. The maximum stress value is compared with the material elastic yield strength in table 4.3.

Table 4.3: Load Cell connected stress values obtained in Abaqus and the material property

Property	Stress [MPa]
Von Mises Maximum Stress - Abaqus	1002
AISI 316L Yield Strength Elastic Limit	205

As seen in table 4.3, the maximum stress value obtained in this simulation is much higher than the yield strength, so the AISI 316L can not be the applied material in this critical section.

In figure 4.14 it can be seen that there are a lot of places where the stresses are above the yield strength elastic limit, which means that those elements would enter a plastic behaviour, which is supposed to be avoided. The stresses are really high, and even though AISI 316L is a resistant material, it is possible that the material would fracture with this situation, because the tensile strength for this material has a maximum value of 560 MPa. The principal piece subjected to this aspect is the fixation part and there are also some elements of the end cap that are subjected to higher stresses, in the M12 connection.

Having these results, the solution is to change the material that compose the fixation part. As the three parts are subject to hydrogen embrittlement, the hydrogen safety material is still required. As the stresses resultant in these pieces are elevated, a material with an elevated yield strength elastic limit is necessary, while it keeps the high resistance to hydrogen embrittlement.

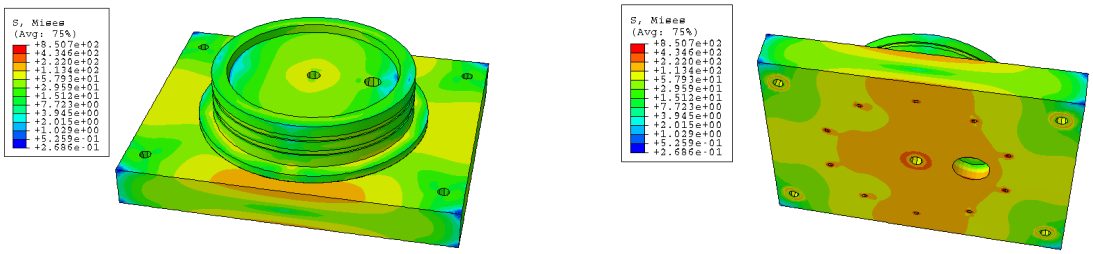
One material that has become significant in hydrogen applications is the Cobalt-based superalloy, MP35N. This alloy possesses a crystal structure that offers exceptional resistance to embrittlement caused by hydrogen. To apply a material in this application is important that its yield strength elastic limit is a very high value, and the MP35N can be cold drawn and aged, which increases this limit. So, the option for these pieces was the MP35N cold drawn and aged, at 1000°F (537.78°C), whose yield strength is more than nine times bigger than the AISI 316L one. The properties of this MP35N can be found in the table 4.4, that display also the AISI 316L properties to easy comparison.

Table 4.4: Proprieties of MP35N and AISI 316L

Property	MP35N	AISI 316L
Density [kg/m^3]	8430	8000
Young's Module [GPa]	234.8	197.5
Yield strength (elastic limit) [MPa]	1999	205
Poisson's Ratio	0.45	0.27
Maximum Service Temperature [°C]	399	750

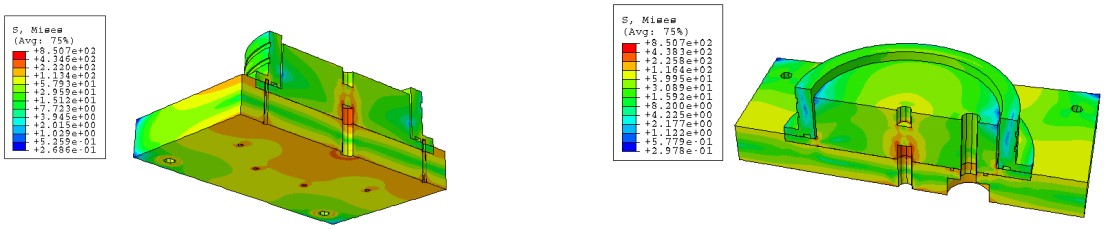
The new simulation preserves all the simplifications and definitions outlined in section 4.3.2, with the sole modification being the revised material properties specified.

Adjusting the material and running the new simulation with the adjusted material, applying this MP35N cold drawn and aged to all the pieces, it is obtained the results presented in figures 4.19 and 4.20.



(a) (b)

Figure 4.19: Load Cell connected section stresses in MPa, MP35N



(a) (b)

Figure 4.20: Cut views of the Load Cell connected section stresses in MPa, MP35N

These results are consistent with the MP35N application, as the maximum stress is around 850 MPa, which means that a safety factor around 2.35 can be achieved, defined as the ratio between the elastic limit and the Abaqus obtained stress, meaning the elastic limit is higher than the resultant stress. The stress maximum value obtained in Abaqus and the material yield strength elastic limit can be observed in table 4.5.

Table 4.5: Load Cell connected section maximum stress value obtained in Abaqus and the MP35N property

Property	Stress [MPa]
Von Mises Maximum Stress - Abaqus	850.7
MP35N Yield Strength Elastic Limit	1999

Is important to refer that the maximum stresses are found in the proximity of the M12 screw connection, in the fixation part and in the end cap, which is normal to happen. However, is important to refer that the screw connection with the piece is really simplified, and in reality the reaction will be distributed to a full surface and not a circumferential area, which means that the piece can be subjected to less forces in that section. Still, this simulation is a good reference and ensure some safety to the present design.

4.4.3 Dynamic Sealing Rod Results Discussion

Figures 4.17 and 4.18 shows the obtained values for the displacement and stresses to which the dynamic rod is subjected. By the values presented figure 4.17 the maximum stress to which this piece is subjected can be compared to the material yield strength, as can be seen in table 4.6.

Table 4.6: Dynamic Sealing Rod stress values obtained in Abaqus and the material property

Property	Stress [MPa]
Von Mises Maximum Stress - Abaqus	245.3
AISI 316L Yield Strength Elastic Limit	205

Comparing the displayed values, it is evident that the maximum stress exceeds the yield strength of AISI 316L. This indicates that AISI 316L is not suitable for this particular application. Moreover, both ends of the structure exhibit stresses that surpass the elastic limit, with all of them concentrated at the threaded connection.

The material of this section needs to be adjusted, still being required the hydrogen embrittlement resistance. As the stresses on the rod section are not as high as those on the section connected to the load cell, the material used for this section does not need to have such a high elastic limit. Therefore, a stainless steel cold worked, such as AISI 316LVM, can be applied. This steel is more resistant and ensures safe use with hydrogen.

The properties of this AISI 316LVM can be found in the table 4.7. The AISI 316L properties are again displaced to easily compare the materials properties.

Table 4.7: Proprieties of AISI 316LVM cold worked and AISI 316L

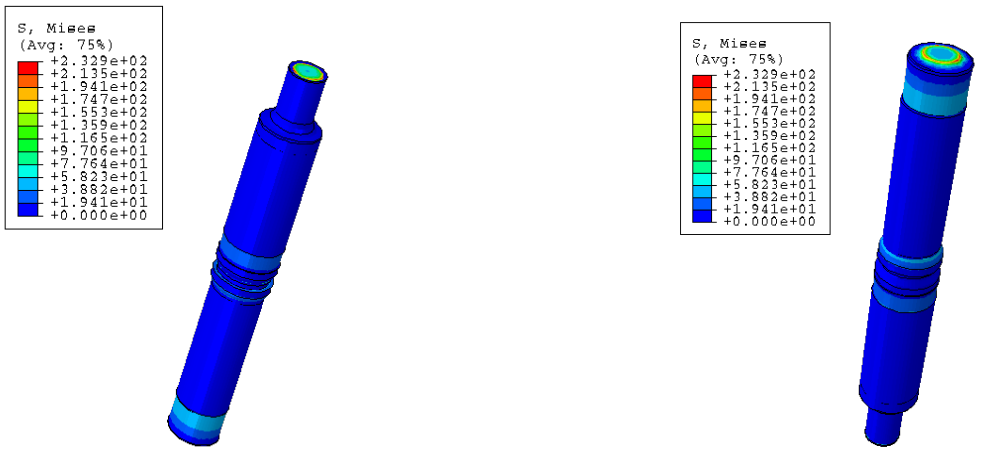
Property	AISI 316LVM	AISI 316L
Density [kg/m^3]	8000	8000
Young's Module [GPa]	187.5	197.5
Yield strength (elastic limit) [MPa]	793-945	205
Poisson's Ratio	0.27	0.33
Maximum Service Temperature [°C]	312	750

The yield strength of the AISI 316LVM depends on the cold worked percentage, so this parameter will be chosen when the information about the maximum stress is obtained. The parameter changes with the cold worked percentage is presented in figure 4.21. The tensile strength of this stainless steel is also higher, with a range from 862 to 1241 MPa [74], This material have better mechanical properties, and it was chosen to solve the fracture problem.

Condition	% Cold Worked	0.2% Yield Strength		Ultimate Tensile Strength		% Elongation in 4D	% Reduction of Area	HRC Hardness
		Ksi	MPa	Ksi	MPa			
Annealed	N/A	36	248	85	586	57	88	88 HRB
Cold Worked	35	115	793	125	862	18	72	26
	48	120	827	145	1000	16	69	32
	52	123	848	150	1034	16	65	34
	60	128	883	160	1103	16	62	36
	70	130	896	170	1172	15	60	38
	80	137	945	180	1241	13	57	40

Figure 4.21: AISI 316LVM properties depending of the cold worked percentage [74]

Simulating the same conditions applied and defined in section 4.3.3 but changing the material properties to the AISI 316LVM shown in table 4.7, the results are the one shown in figures 4.22 and 4.23.



(a) Machine Connected Section (b) Clamp Connected Section

Figure 4.22: Stresses applied in dynamic rod in MPa, AISI 316LVM

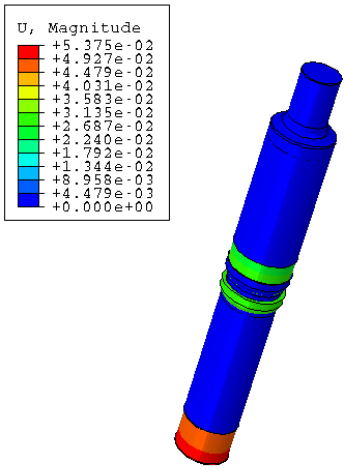


Figure 4.23: Dynamic Rod resulting displacements in mm, AISI 316 LVM

Comparing the values obtained with the AISI 316LVM relevant properties it can be seen that the problems are solved, by a big safety factor, because comparing the values, as presented in table 4.8, the yield strength is approximately four times bigger than the stress applied in the pieces.

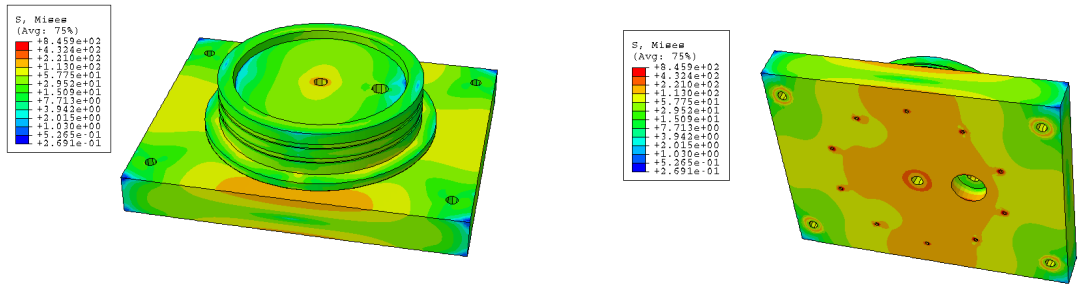
Table 4.8: Dynamic Sealing Rod stress values obtained in Abaqus and the AISI 316LVM property

Property	Stress [MPa]
Von Mises Maximum Stress - Abaqus	232.9
AISI 316LVM Yield Strength Elastic Limit	793-945

As with the AISI 316LVM no issues are presented, this will be the material applied to this dynamic rod, and the dimensions of this dynamic rod do not present any relevant problem. The cold worked percentage, by figure 4.21, can assume any value.

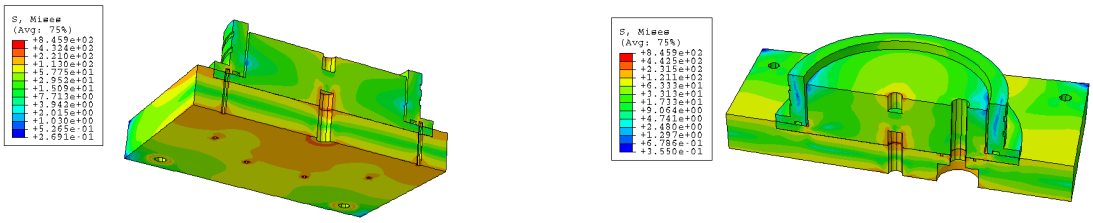
4.5 Compressive force simulation

To further expand the solution safety, it was performed a simulation with the compressing force, having the same maximum value of 20 kN. The definitions applied were the similar to the ones stated in section 4.3.2, changing the load direction, applying a negative value in the load definition. This simulation was performed to the MP35N material, and the results are presented in figures 4.24 and 4.25.



(a) (b)

Figure 4.24: Load Cell connected section stresses in MPa, compression



(a) (b)

Figure 4.25: Cut views of the Load Cell connected section stresses in MPa, compression

The maximum stress obtained in Abaqus with this compression definition and the material yield strength elastic limit are presented in table 4.9.

Table 4.9: Load Cell connected section maximum stress value obtained in Abaqus with compressive force and the MP35N property

Property	Stress [MPa]
Von Mises Maximum Stress - Abaqus	845.9
MP35N Yield Strength Elastic Limit	1999

This results are once again consistent with the MP35N application, as the safety factor obtained in these conditions is higher than 2.35, meaning the elastic limit is much higher than the resultant stresses.

4.6 Structural Validation summary

Having solved all the problems that the AISI 316L presented by the limitations of its mechanical properties is now ensured that the test chamber will resist to the intended application.

The defined critical sections can withstand the maximum force exerted by the machine, and the chamber will remain sealed, ensuring no issues with machine operation.

The simulation of both traction and compression in the load cell section confirms the stability of this critical component. This indicates that the proposed solution is suitable for the intended applications and can be safely implemented on the target machines.

Material changing is not a ideal solution to solve the structural concerns. This path was only followed due to time limitations, to enable results to be obtained. The ideal solution was to further analyse the critical section of the parts, where the higher stresses are concentrated, and redesign certain features. Major structural issues are present in the hole that enable the assembly of the chamber to the machines, so the first step to improve the structural integrity would be redesign the assembly method, distributing the forces over a larger area.

In conclusion, all pertinent aspects have been thoroughly examined and verified in the chapter on structural validation. The integrity, performance, and compliance of the structure have all been examined and validated, even though the ideal solution is not applied. The structure's strength and dependability to withstand anticipated loads are idem confirmed by the validation results, ensuring its safety and functionality.

A thorough understanding of the structure's response has been attained by closely examining crucial sections, using exacting testing procedures, and taking a variety of loading conditions into account. The design satisfies the necessary performance criteria because the validation process successfully found and addressed any potential flaws or areas of concern.

The structural validation's successful conclusion gives rise to confidence in the structure's ability to serve the intended purpose. It demonstrates the careful planning, in-depth investigation, and thorough assessment that have been made throughout the project.

In summary, the meticulous structural validation process has ensured that the design complies with the requirements, giving rise to confidence in its dependability and safety. The completion of

in-depth analysis and verification is reflected in this chapter, which marks a significant milestone in the project.

Chapter 5

Conclusion

In the final chapter of this dissertation, the final conclusions from the research conducted in this work are presented. Additionally, suggestions for future works and developments are provided, aiming to further advance the hydrogen testing field and to improve the chamber design to aid the hydrogen technology evolution.

This chapter summarizes the key findings and insights gained throughout the research process, providing a culmination to the dissertation. By presenting the conclusions and work suggestions, it brings a sense of closure to the study, while opening ways to further investigation and improvement of the design of hydrogen embrittlement testing chambers.

5.1 Final Conclusions

The hydrogen economy development entails various technological challenges, particularly with the hydrogen transportation and storage. A significant obstacle to the advancement of hydrogen solutions is hydrogen embrittlement, the deterioration of materials' mechanical properties.

Standards and studies addressing the hydrogen embrittlement testing and associated challenges have provided valuable insights into hydrogen gas, H_2, properties and related issues. This dissertation has in consideration all the significant progress made this far in this field.

The research brought the perception on the potential of hydrogen as a clean energy carrier and emphasized the necessity of trustworthy testing procedures to guarantee the security and dependability of hydrogen infrastructure. Ultimately, this study's findings, have the potential to enhance the reliability and integrity of hydrogen related systems.

The literature review performed in the first step contributed to the final solution consideration, having principally retained hydrogen safety measures and significant hydrogen embrittlement resistant materials.

Through this, the hydrogen chamber was developed, involving careful consideration numerous factors, such as material selection, safety protocols and all the specific requirements and potential applications of the chamber. Those consideration include the machine applied forces, machine connections, operating temperature, pressures, and other relevant factors.

By meticulously addressing these design considerations, this dissertation ends with a successfully creation of a specialized test chamber, that can offer a controlled environment, measuring hydrogen quantities and inside pressures, to evaluate the behaviour and performance of the intended specimen in hydrogen-rich environments.

All the safety risks associated with hydrogen use where recognized and safety features where applied, such as, numerous O-rings, hydrogen ready valves, and other important components. The material limitations where also noted, and sensors and a safety valve are applied, avoiding any risks with this solution use.

In the design process, some general conclusions are taken, for example, safety requirements that need to be acknowledge before the parts definition and the several impacts that an element as hydrogen can have in the options that are defined through all the design process.

The structural validation, conducted by using FEM analysis, has enable the correction of the chamber materials and avoided problems that could have appeared during the machine usage, which could have caused a disastrous situation. The final simulation, with the adjusted material, proves the effectiveness and reliability of the test chamber, simulating the conditions to which the solution will be exposed to.

Although, using a different material to address the identified issue was not the ideal solution, it was a necessary step within the given time constraints to rectify significant challenges.

Therefore, with this validation process, the test chamber has been proven capable of accurately sustain hydrogen-rich environments in the conditions that the design will be used, enabling the researchers to apply this solution to test the hydrogen embrittlement precisely in the intended materials. Such a reliable and manufacturable testing chamber will contribute to a deeper understanding of the hydrogen effects, and it will aid the development of the hydrogen technologies.

Is important to refer that this chamber was designed for appliance of an axial force, with a maximum value of 20 kN, and the pressure inside should never surpass the 5 MPa, to ensure some safety factor to the chamber application.

Moreover, the successful design of the test chamber enables a significant milestone in the hydrogen embrittlement associated challenges, promoting the sustainable and safety use of hydrogen as an energy source.

In conclusion, the mechanical test chamber, to replicate hydrogen-rich environments to hydrogen embrittlement studies, can make substantial contributions to advancing the hydrogen embrittlement understanding and its impact on different materials or systems. The design of the specialized hydrogen test chamber, coupled with the manufacturing designs and the capability of its production, establishes a reliable solution to conduct experiments to the technological development. Hopefully, the developed work in this dissertation will play a crucial role in the evolution of hydrogen infrastructures, supporting its safety and efficient operations, ultimately contributing to a better future, cleaner and opening path to more sustainable energies.

5.2 Future Works

Progress of the hydrogen solutions is desired, so in this section some possible future works are suggested.

As discussed in chapter 4.6, it is acknowledged that changing the material is not the ideal solution to address the structural analysis concerns. The best way to solve this would be redesign the fixation between the chamber and the machines, not assembling these two components only by the means of a M12 screw. Instead, a more effective approach would involve redesigning the connection between the chamber and the machines, moving away from solely relying on an M12 screw for assembly. By distributing forces over a larger area, it should be possible to reduce the thickness of the component or explore alternative, cost-effective materials.

Expand the applicability of the chamber beyond the two referenced machines is equally desirable. Conducting a comprehensive study on the requirements of different machines and conducting research to optimize the chamber's implementation would significantly contribute to the understanding of hydrogen embrittlement.

Moreover, this study can evolve to incorporate mechanical chambers for various tests, not limited to axial force applications. Developing different tubes to accommodate diverse solutions and incorporating interchangeable parts into the design would be intriguing paths to explore.

Furthermore, extending automation to safety measures would be prudent. Implementing a system that only allows the power supply to activate when all valves and chamber components are fully closed would prevent the generation of hydrogen gas before achieving full closure.

Finally, the ultimate recommendation is the actual production and application of this test chamber to conduct hydrogen embrittlement testing. By gaining a better understanding of the effects of hydrogen embrittlement on materials, this effort contributes to a healthier and more sustainable future.

These suggested areas of future work aim to boost the knowledge and application of hydrogen embrittlement research, encouraging advancements in the field and facilitating the transition to a cleaner and more sustainable energy, contribution to the low-carbon economy.

References

[1] Marie Dejonghe. Hydrogen: A Deus Ex Machina for Today's Energy Crisis? *Ghent University*, January 2023. Available at https://www.ugent.be/ps/politiekewetenschappen/gies/en/research/publications/gies_papers/2023-global-energy-crisis/hydrogen-a-deus-ex-machina-for-today2019s-energy-crisis.

[2] Farnoosh Farhad, David Smyth-Boyle, and Xiang Zhang. Fatigue of X65 steel in the sour corrosive environment—A novel experimentation and analysis method for predicting fatigue crack initiation life from corrosion pits. *Fatigue & Fracture of Engineering Materials & Structures*, 44(5):1195–1208, 2021. Available at https://onlinelibrary.wiley.com/doi/pdf/10.1111/ffe.13423.

[3] Natasha Nguyen. Hydrogen Blending as a Pathway Toward U.S. Decarbonization. *National Renewable Energy Laboratory (NREL)*, 24 January 2023. Available in https://www.nrel.gov/news/program/2023/hydrogen-blending-as-a-pathway-toward-u.s.-decarbonization.html.

[4] Sandeep K. Dwivedi and Manish Vishwakarma. Hydrogen embrittlement in different materials: A review. *International Journal of Hydrogen Energy*, 43(46):21603–21616, 2018. Available at https://www.sciencedirect.com/science/article/pii/S0360319918331306.

[5] Paul C. Okonkwo, El Manaa Barhoumi, Ikram Ben Belgacem, Ibrahim B. Mansir, Mansur Aliyu, Wilfred Emori, Paul C. Uzoma, Wesam H. Beitelmal, Ersin Akyüz, Ahmed Bahgat Radwan, and R.A. Shakoor. A focused review of the hydrogen storage tank embrittlement mechanism process. *International Journal of Hydrogen Energy, Volume 48, Issue 35*, pages 12935–12948, April 2023. Available at https://doi.org/10.1016/j.ijhydene.2022.12.252.

[6] N. N. Sergeeva, A. N. Sergeeva, S. N. Kutepova, A. G. Kolmakov, and A. E. Gvozdeva. Mechanism of the hydrogen cracking of metals and alloys, part ii (review). *Inorganic Materials: Applied Research*, 10(1):32–41, 2019. Available at https://www.researchgate.net/publication/332929622_Mechanism_of_the_Hydrogen_Cracking_of_Metals_and_Alloys_Part_II_Review.

[7] William Lee Jolly. Hydrogen. *Encyclopedia Brittannica*, 6 June 2023. Available at https://www.britannica.com/science/hydrogen.

[8] Michelle Fung. Energy density of hydrogen. *The Physics Factbook*, 2005. Available at https://hypertextbook.com/facts/2005/MichelleFung.shtml.

[9] Inc. WHA International. Hydrogen in industry, September 2020. Available at https://wha-international.com/hydrogen-in-industry/#_ednref1. Accessed on March 2023.

[10] Nathan Skillen, Helen Daly, Lan Lan, Meshal Aljohani, Christopher W. J. Murnaghan, Xiaolei Fan, Christopher Hardacre, Gary N. Sheldrake, and Peter K. J. Robertson. Photocatalytic reforming of biomass: What role will the technology play in future energy system. *Current Chemistry*, 380:33, 2022. Available at https://www.researchgate.net/publication/361405771_Photocatalytic_Reforming_of_Biomass_What_Role_Will_the_Technology_Play_in_Future_Energy_Systems,.

[11] National Grid. The hydrogen colour spectrum, February 2023. Available at https://www.nationalgrid.com/stories/energy-explained/hydrogen-colour-spectrum. Accessed on march 2023.

[12] Linshuo Dong, Shuize Wang, Guilin Wu, Junheng Gao, Xiaoye Zhou, Hong-Hui Wu, and Xinping Mao. Application of atomic simulation for studying hydrogen embrittlement phenomena and mechanism in iron-based alloys. *International Journal of Hydrogen Energy*, 47(46):20288–20309, 2022. Available at https://www.sciencedirect.com/science/article/pii/S0360319922016895.

[13] A.O. Oni, K. Anaya, T. Giwa, G. Di Lullo, and A. Kumar. Comparative assessment of blue hydrogen from steam methane reforming, autothermal reforming, and natural gas decomposition technologies for natural gas-producing regions. *Energy Conversion and Management*, 254:115245, 2022. Available at https://doi.org/10.1016/j.enconman.2022.115245.

[14] Learn and Grow. Gasification process, October 2016. Avilable at https://www.youtube.com/watch?v=DOLjl_93K9k&ab_channel=LEARNANDGROW. Accessed on March 2023.

[15] Hikaru Maeda Taro Shimonosono, Hikari Imada and Yoshihiro Hirata. Separation of hydrogen from carbon dioxide through porous ceramics. *Materials*, 9, 930, 2016. Available at https://www.ncbi.nlm.nih.gov/pmc/articles/PMC5457225/.

[16] Hydrogen and Fuel Cell Technologies Office. Hydrogen production: Electrolysis. Available at https://www.energy.gov/eere/fuelcells/hydrogen-production-electrolysis. Accessed on March 2023.

[17] Immanuel Vincent and Dmitri Bessarabov. Low cost hydrogen production by anion exchange membrane electrolysis: A review. *Renewable and Sustainable Energy Reviews*, 81:1690–1704, 2018. Availabe at https://www.sciencedirect.com/science/article/pii/S1364032117309127.

[18] ASTM G142. Standard test method for determination of susceptibility of metals to embrittlement in hydrogen containing environments at high pressure, high temperature, or both. 2016.

[19] ASTM F519. Standard test method for mechanical hydrogen embrittlement evaluation of plating/coating processes and service environments. 2017.

[20] T. Ogata. Hydrogen embrittlement evaluation in tensile properties of stainless steels at cryogenic temperatures. *AIP Conference Proceedings*, 986:124–131, 2008. Available at https://pubs.aip.org/aip/acp/article/986/1/124/847433/HYDROGEN-EMBRITTLEMENT-EVALUATION-IN-TENSILE.

[21] T. Boot, T. Riemslag, E. Reinton, P. Liu, C.L. Walters, and V Popovich. In-situ hollow sample setup design for mechanical characterisation of gaseous hydrogen embrittlement of pipeline steels and welds. *Metals*, 11:1242, 2021. Available at https://doi.org/10.3390/met11081242.

[22] Zwick Roell. Materials and components testing under the influence of hydrogen. Available at https://www.zwickroell.com/news-events/case-studies/mpa-ha-hc/. Accessed on March 2023.

[23] Schimadzu, Analytical Instruments Used for Hydrogen Fuel Quality Control. Strength testing in a hydrogen environment. Available at https://www.shimadzu.com/an/industries/automotive/automotive-electrification/strength-testing-in-a-hydrogen-environment/index.html. Acessed on April 2023.

[24] ISO/IEC 17025. General requirements for the competence of testing and calibration laboratories. 2017.

[25] Ghent University. Hydrogen-material interaction. Available at https://www.ugent.be/ea/match/sms/en/research/hydrogen_material_interaction.htm. Accessed on March 2023.

[26] Tarlan Hajilou, Malin S.B. Hope, Amin H. Zavieh, Nousha Kheradmand, Roy Johnsen, and Afrooz Barnoush. In situ small-scale hydrogen embrittlement testing made easy: An electrolyte for preserving surface integrity at nano-scale during hydrogen charging. *International Journal of Hydrogen Energy*, 43(27):12516–12529, 2018. Available at https://www.sciencedirect.com/science/article/pii/S0360319918313570.

[27] Kiyoshi Yokogawa, Seiji Fukuyama, Murao Mitsui, and Kiyokatsu Kudo. Pressure vessel for tensile testing in high-pressure gases at elevated temperatures. *Review of Scientific Instruments*, 49(1):50–51, August 2008. Available at https://pubs.aip.org/aip/rsi/article-pdf/49/1/50/8367491/50_1_online.pdf.

[28] K. J. Alvine, T. A. Kafentzis, S. G. Pitman, K. I. Johnson, D. Skorski, J. C. Tucker, T. J. Roosendaal, and M. E. Dahl. An in situ tensile test apparatus for polymers in high pressure hydrogen. *Review of Scientific Instruments*, 85(10), October 2014. Available at https://pubs.aip.org/aip/rsi/article-pdf/doi/10.1063/1.4899315/13631248/105110_1_online.pdf.

[29] Zwhick Roell. Hydrogen influence on metals: Hydrogen embrittlement. Available at https://www.zwickroell.com/industries/energy/hydrogen-influence-on-metals-hydrogen-embrittlement/. Accessed on March 2023.

[30] Office of Energy Efficiency & Renewable Energy. Safe use of hydrogen. *Hydrogen and Fuel Cell Technologies*. Available at https://www.energy.gov/eere/fuelcells/safe-use-hydrogen. Accessed on April 2023.

[31] Omnexus. Max continuous service temperature. Available at https://omnexus.specialchem.com/polymer-properties/properties/max-continuous-service-temperature. Acessed on May 2023.

[32] TEADIT. Metallic materials. Available at https://www.allsealsinc.com/teadit/TypicalMetalProperties.pdf. Accessed on April 2023.

[33] Bodner Research Web. Electrolytic cells. Available at https://chemed.chem.purdue.edu/genchem/topicreview/bp/ch20/faraday.php#top. Accessed on April 2023.

[34] W. Zhang, E. Ghali, and G. Houlachi. Review of oxide coated catalytic titanium anodes performance for metal electrowinning. *Hydrometallurgy*, 169:456–467, 2017. Available at https://www.sciencedirect.com/science/article/pii/S0304386X1730109.

[35] Z. A. C. Ramli and S. K. Kamarudin. Platinum-based catalysts on various carbon supports and conducting polymers for direct methanol fuel cell applications: a review. 13(410), 2018. Available at https://link.springer.com/article/10.1186/s11671-018-2799-4#citeas.

[36] Ossila. Platinum disc working electrode. Available at https://www.ossila.com/en-eu/products/working-electrode. Accessed on April 2023.

[37] Zuozhao Zhai, Lihui Zhang, Tianmin Du, Bin Ren, Yuelong Xu, Shasha Wang, Junfeng Miao, and Zhenfa Liu. A review of carbon materials for supercapacitors. *Materials & Design*, 221:111017, 2022. Available at https://www.sciencedirect.com/science/article/pii/S0264127522006396.

[38] Ossila. Graphite working electrode. Available at https://www.ossila.com/en-eu/products/graphite-working-electrode?variant=43341041434840. Accessed on April 2023.

[39] D. E. Hall. Electrodes for alkaline water electrolysis. *Journal od the Electrochemical Society*, 128(740), 1981. Available at https://iopscience.iop.org/article/10.1149/1.2127498/pdf.

[40] Carl W. White and James G. Martin. Chlorine gas inhalation. *Proceedings of the American Thoracic Society*, 7(4):257–263, 2010. Availble at https://www.atsjournals.org/doi/abs/10.1513/pats.201001-008SM.

[41] Department of Health and Human Services. Niosh skin notation (sk) profile | sodium hydroxide (naoh). *Centers for Disease Control and Prevention, National Institute for Occupational Safety and Health*. Available at https://www.cdc.gov/niosh/docs/2011-150/pdfs/2011-150.pdf.

[42] William Anderson. Titration of vinegar lab answers. 2020. Available at https://schoolworkhelper.net/titration-of-vinegar-lab-answers/. Accessed on April 2023.

[43] Ossila. H-type electrochemical cells. Available at https://www.ossila.com/en-eu/products/h-type-electrochemical-cells?variant=43328693305560. Accessed on April 2023.

[44] Sigma-Aldrich. Sodium chloride. Available at https://www.sigmaaldrich.com/deepweb/assets/sigmaaldrich/product/documents/179/430/71386dat.pdf. Accessed on April 2023.

[45] Distrelec. Rnd 320-ka3005p - bench top power supply, 30v, 5a, 150w, programmable, rnd lab. Available at https://www.distrelec.biz/en/bench-top-power-supply-30v-5a-150w-programmable-rnd-lab-rnd-320-ka3005p/p/30061864. Accessed on April 2023.

[46] Hydrotechnik. Ht-h2-tpse dual pressure and temperature sensor. Available at https://www.hydrotechnik.co.uk/sites/default/files/2022-07/ht-h2-tpse-dual-pressure-temperature-sensor-datasheet.pdf.

[47] PennEHRS (Environmental Health & Radiation Safety). Fact sheet: Hydrogen gas use in anaerobic chambers. April 2018. Available at https://ehrs.upenn.edu/health-safety/lab-safety/chemical-hygiene-plan/fact-sheets/fact-sheet-hydrogen-gas-use-anaerobic.

[48] Internation Atomic Energy Agency. Intercomparison of techniques for inspection and diagnostics of heavy water reactor pressure tubes. *Determination of Hydrogen Concentration and Blister Characterization*, March 2009. Available at https://www-pub.iaea.org/MTCD/publications/PDF/te_1609_web.pdf.

[49] EC Sense, Easy Gas Sensors. Hydrogen gas module 0-1000ppm - TB600C-H2-1000. Available at https://ecsense.com/wp-content/uploads/2021/03/1592924401-TB600C-H2-1000ppm_Technical_Specification_20200612.pdf. Accessed on April 2023.

[50] ISO/TR 15916. Basic considerations for the safety of hydrogen systems. 2015.

[51] RedFluid. Is my ball valve suitable for hydrogen? hydrogen as key to the future, February 2022. Available at https://redfluid.es/en/hydrogen-ball-valve/. Accessed on April 2023.

[52] Hyfindr. Hydrogen valve, February 2022. Available at https://hyfindr.com/hydrogen-valve/. Accessed on April 2023.

[53] BlueRobotics. Watertight enclosure for rov/auv (6 series). Available at https://bluerobotics.com/store/watertight-enclosures/6-series/wte6-asm-r1/. Accessed on April 2023.

[54] Task Rok. Thermal shock vs tensile strength: A comparison study, March 2018. Available at https://highlyeducatedti.com/blogs/information/thermal-shock-vs-tensile-strength. Accessed on April 2023.

[55] Ansys GRANTA EduPack software. Ansys, Inc., Cambridge, UK, 2020.

[56] Optical Solutions. Quartz tubing. Available at https://www.opticalsolutions.it/en/quartz/quartz-tubing/. Accessed on April 2023.

[57] American piping products. Barlow's formula. Available at https://amerpipe.com/reference/charts-calculators/barlows-formula/. Accessed on April 2023.

[58] Heraeus. Properties of fused silica. Available at https://www.heraeus.com/en/hca/fused_silica_quartz_knowledge_base_1/properties_1/properties_hca.html#tabs-608478-6. Accessed on April 2023.

[59] Parker. Fluid power seal design guide. *Catalog EPS 5370*, 2014. Available at https://www.parker.com/content/dam/Parker-com/Literature/Engineered-Polymer-Systems/5370.pdf. Accessed on April 2023.

[60] Apple Rubber. Seal types and gland design : Dynamic seal types. Available at https://www.applerubber.com/seal-design-guide/seal-types-and-gland-design/dynamic-seal-types/. Accessed on April 2023.

[61] Parker. Dynamic sealing. Available at https://promo.parker.com/promotionsite/seal-solutions-guide/us/en/home/Dynamic-Sealing. Accessed on April 2023.

[62] Apple Rubber. O-ring chemical compatibility guide. Available at https://www.applerubber.com/chemical-compatibility-guide/. Accessed on April 2023.

[63] eFunda, engineering fundamentals. O-ring compatibilities. Available at https://www.efunda.com/designstandards/oring/oring_chemical.cfm?SM=none&SC=Hydrogen%20Gas#mat. Accessed on April 2023.

[64] Apple Rubber. O-ring size search. Available at https://www.applerubber.com/oring-size-search/?email=&unit=mm&id1=20&id2=25&w1=0.20&w2=100&standard_number=&material=VT&standard=iso_number&results=100&submitted=1#results. Accessed on April 2023.

[65] Apple Rubber. O-ring glande calculator. Available at https://www.applerubber.com/oring-gland-calculator/. Accessed on April 2023.

[66] BlueRobotics. Wetlink penetrator. Available at https://bluerobotics.com/store/cables-connectors/penetrators/wlp-vp/. Accessed on April 2023.

[67] Spir star. Hose type 6mm hydrogen. Available at https://www.spirstar.de/productfinder_uploads/spirstar_germany/pdf/SPF_EN_Hose_Type_6mmHydrogen.pdf. Accessed on April 2023.

[68] Habonim. Hydrogen service ball valves, product catalog. Available at https://esitechgroup.com/wp-content/uploads/2021/06/Habonim_Hydrogen-Service_Brochure_24052021.pdf. Accessed on April 2023.

[69] Redfluid. Valves & accessories, vertic serie. Available at https://hyfindr.com/wp-content/uploads/2022/11/Hydrogen-Check-Regulating-Valves-Redfluid.pdf. Accessed on April 2023.

[70] Gotze Armaturen. Type test approved safety valves angle-type for industrial applications. Available at https://hyfindr.com/wp-content/uploads/2022/01/3.05_Series-420_en.pdf. Accessed on April 2023.

[71] Industrial Indicators. Fundamentals of basic bolting. Available at http://www.smartbolts.com/fundamentals/. Accessed on May 2023.

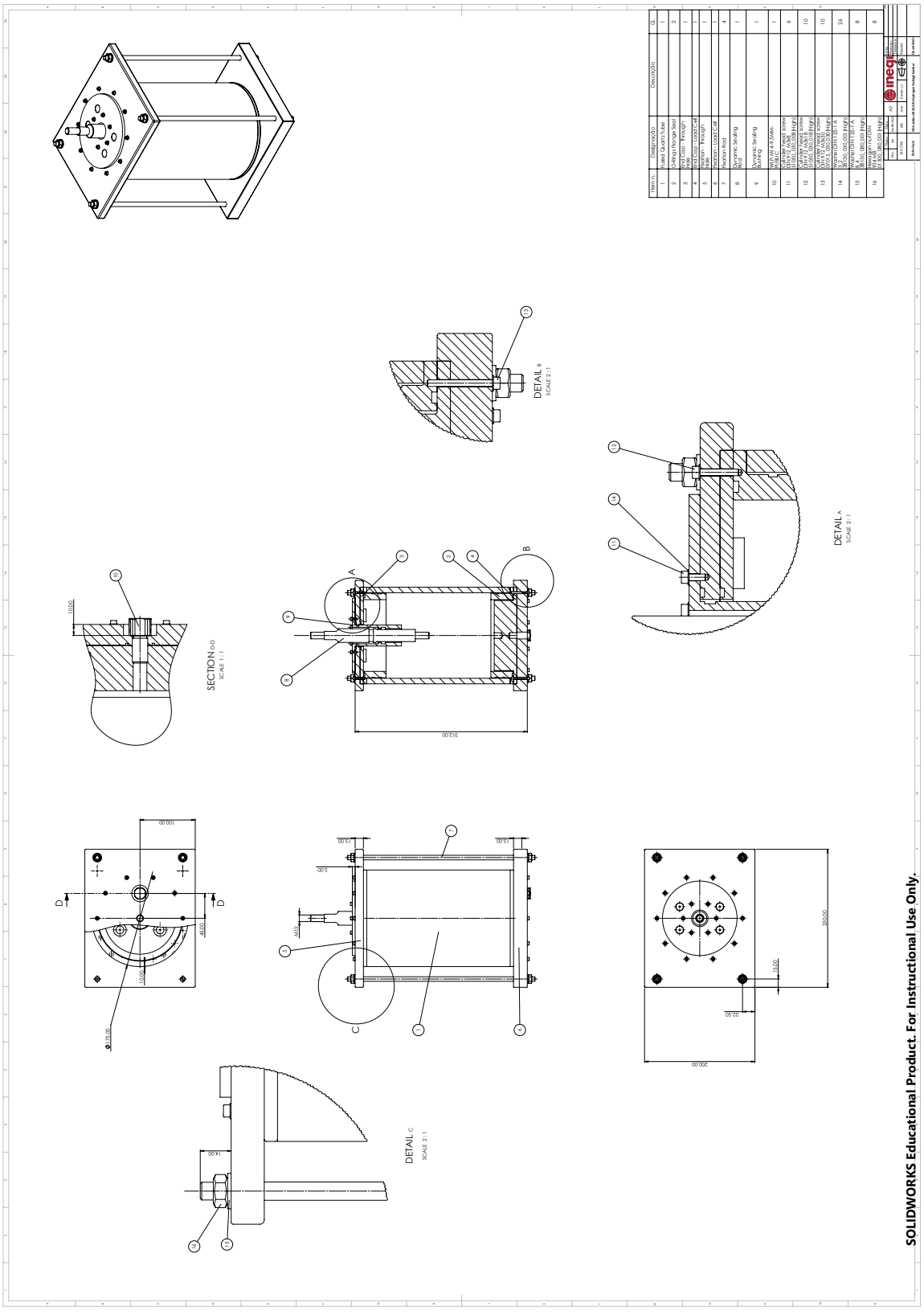
[72] TSF. Table of preloads and tightening approximate values. Available at https://www.tsftsh.com/docs/documentation/Precargas%20Web.pdf. Accessed on May 2023.

[73] Miguel. How to avoid errors with the units in abaqus, February 2021. Available at https://tecnodigitalschool.com/how-to-avoid-errors-with-the-units-in-abaqus/. Accessed on June 2023.

[74] United Performance Metals. 316LS / 316LVM surgical stainless bar - ASTM F138. Available at https://www.upmet.com/products/stainless-steel/316lslvm. Accessed on June 2023.

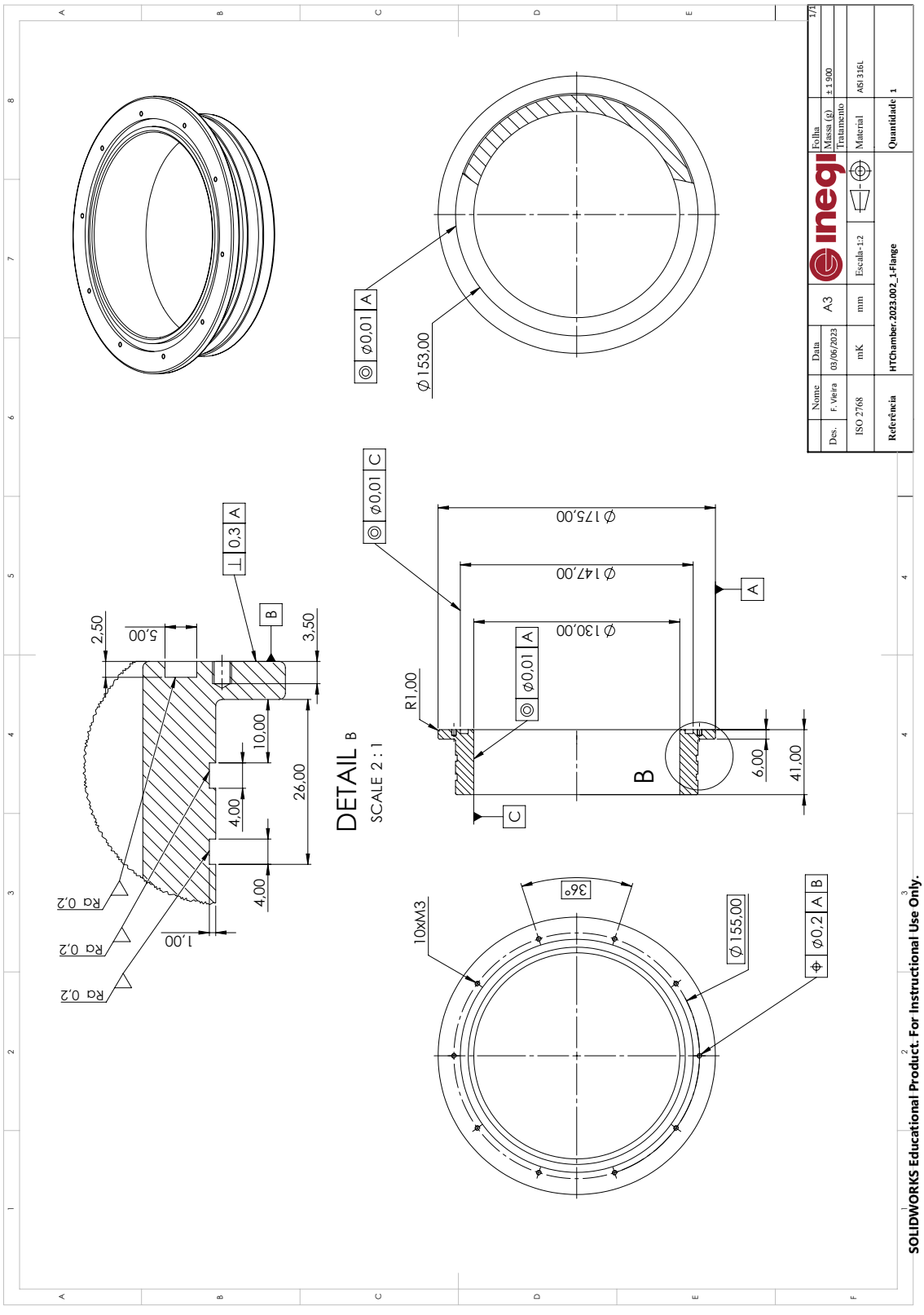
Appendix A

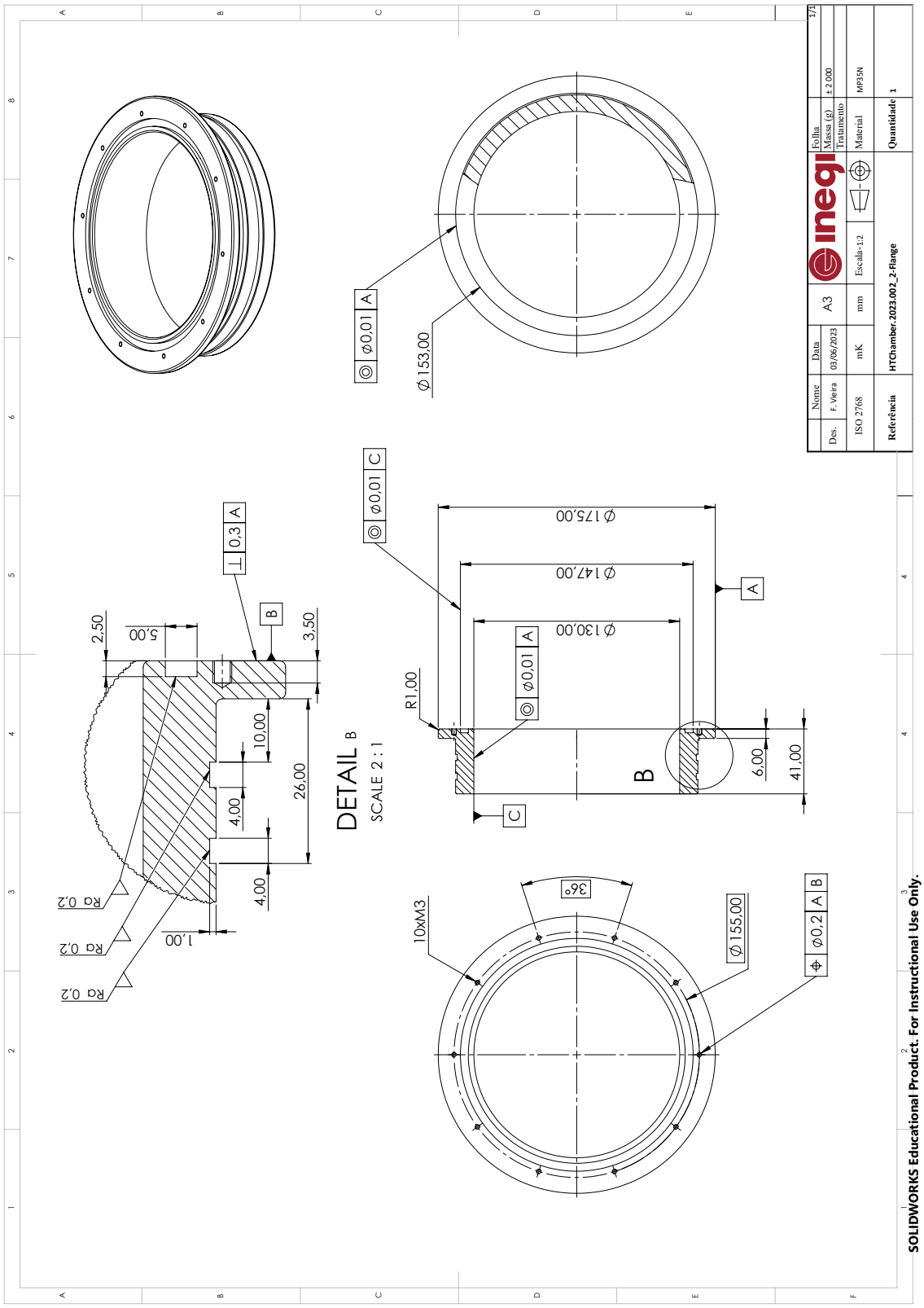
Mechanical Drawing of the solution


SECTION D-D
SCALE 1 : 1
DETAIL B
SCALE 2 : 1
DETAIL A
SCALE 2 : 1
DETAIL C
SCALE 2 : 1
SOLIDWORKS Educational Product. For Instructional Use Only.

Appendix B

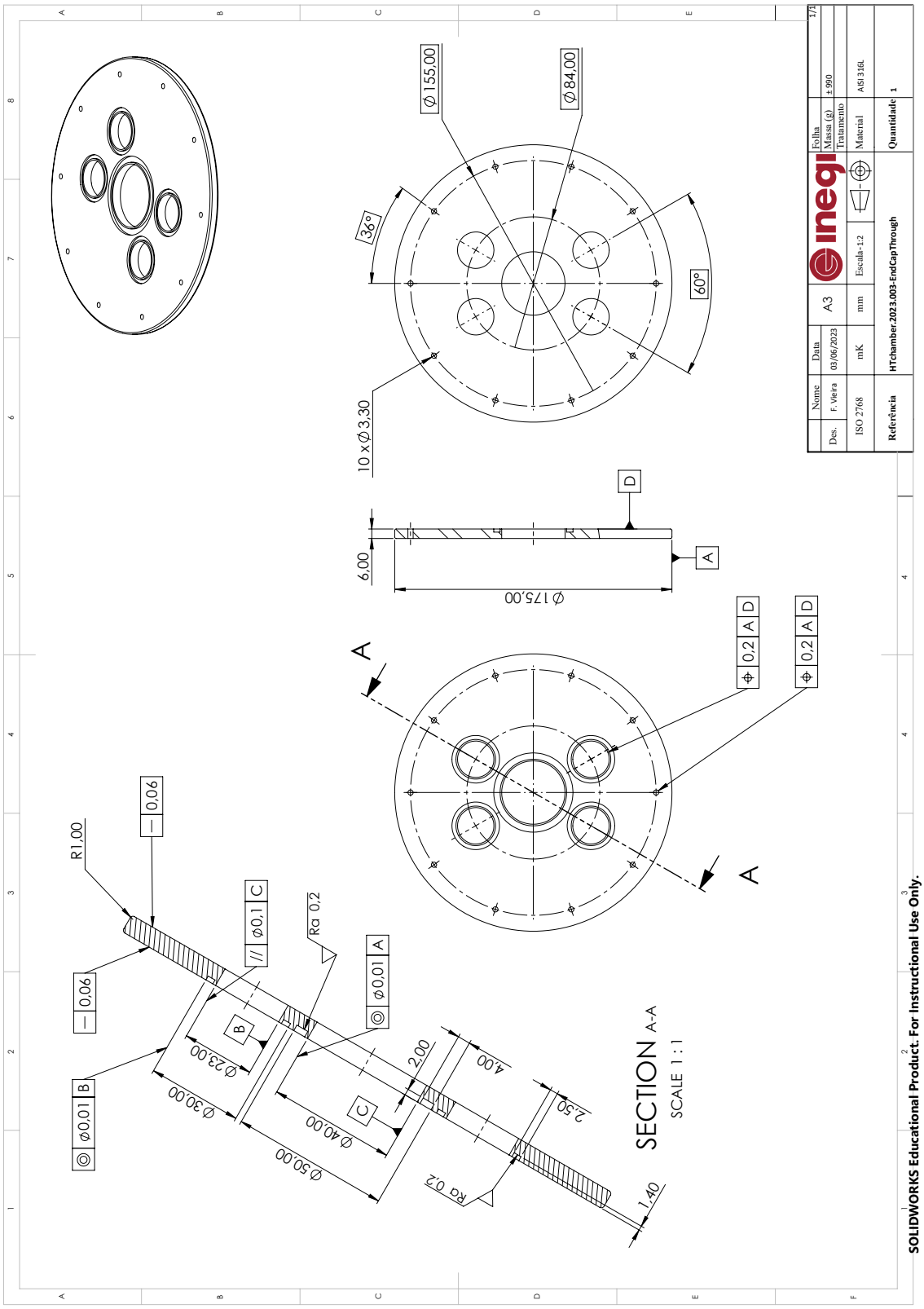
O-ring flanges (2) technical drawings


DETAIL B
SCALE 2 : 1
Ø153,00
Ø155,00
10xM3
36°
Ø175,00
Ø147,00
Ø130,00
R1,00
41,00
6,00
26,00
10,00
4,00
2,50
5,00
3,50
1,00
Ra 0,2
Ra 0,2
Ra 0,2
Folha 1/1
Massa (g) ± 1 900
Tratamento
Material AISI 316L
Escala: 1:2
A3
mm
mK
Data 03/06/2023
F. Vieira
ISO 2768
Referência HTChamber.2023.002_1-Flange
Quantidade 1
SOLIDWORKS Educational Product. For Instructional Use Only.


Ø153,00
⌀0,01 A
Ø175,00
Ø147,00
Ø130,00
⌀0,01 A
⌀0,01 C
R1,00
A
B
C
6,00
41,00
10xM3
36°
Ø155,00
⌖ ⌀0,2 A B
DETAIL B
SCALE 2 : 1
⊥ 0,3 A
B
2,50
5,00
3,50
10,00
4,00
26,00
4,00
1,00
Ra 0,2
Ra 0,2
Ra 0,2
Nome
Data
Des.
F. Vieira
03/06/2023
ISO 2768
mK
A3
mm
Escala: 1:2
Folha
Massa (g)
Tratamento
Material
MP35N
± 2 000
1/1
Referência
HTChamber.2023.002_2-Flange
Quantidade 1
SOLIDWORKS Educational Product. For Instructional Use Only.

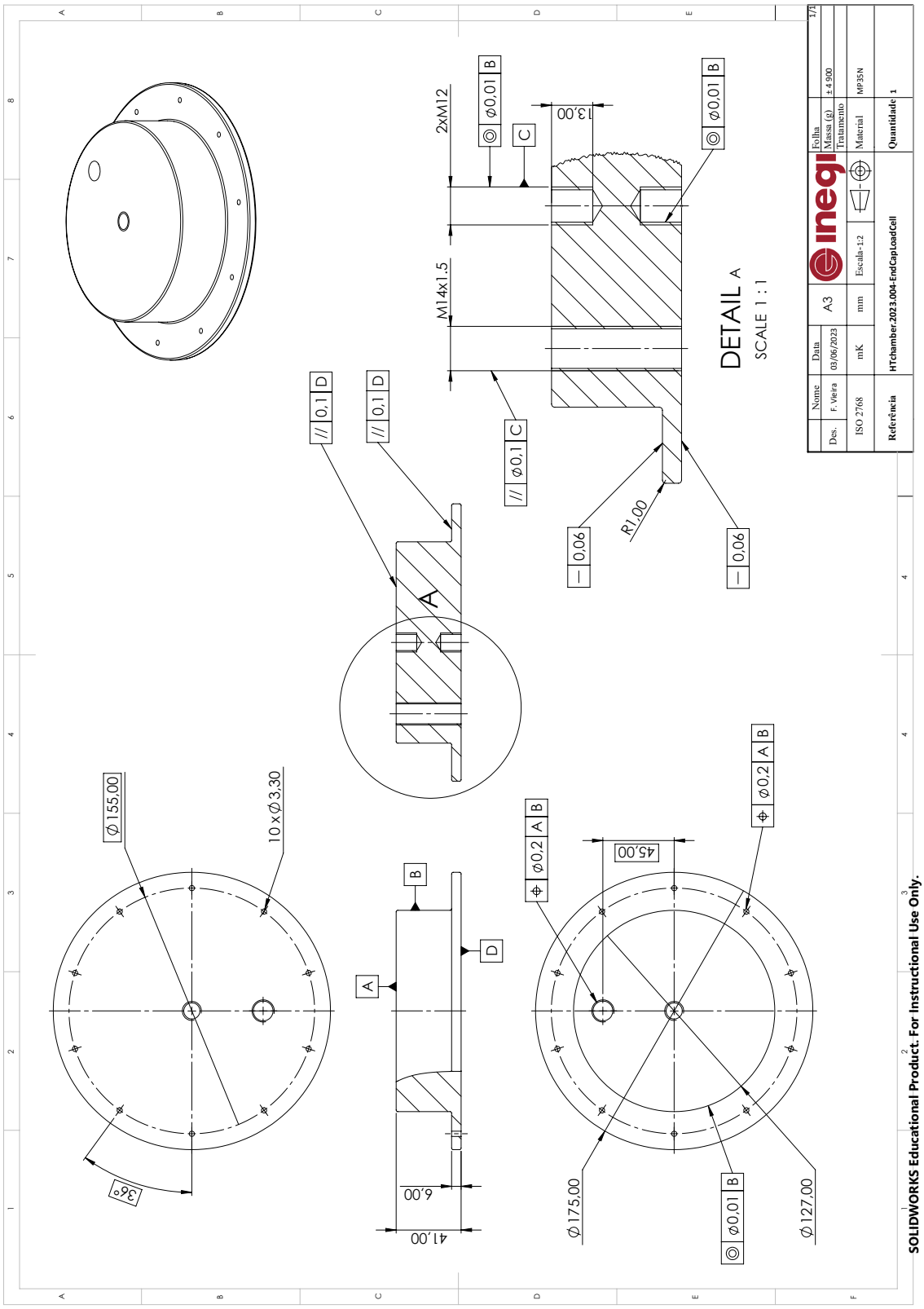
Appendix C

End Cap through (3) technical drawing


Ø155,00
Ø84,00
36°
60°
10 x Ø3,30
6,00
Ø175,00
D
A
SECTION A-A
SCALE 1 : 1
R1,00
0,06
0,06
Ø0,01 B
Ø0,1 C
Ra 0,2
Ø0,01 A
Ø23,00
Ø30,00
Ø40,00
Ø50,00
2,00
4,00
2,50
1,40
Ra 0,2
Ø 0,2 A D
Ø 0,2 A D
Folha 1/1
Massa (g) ± 990
Tratamento
Material ABS 316L
Quantidade 1
Escala: 1:2
Data 03/06/2023
A3
mK
mm
Nome F. Vieira
ISO 2768
Referência HTchamber.2023.003-EndCapThrough
SOLIDWORKS Educational Product. For Instructional Use Only.

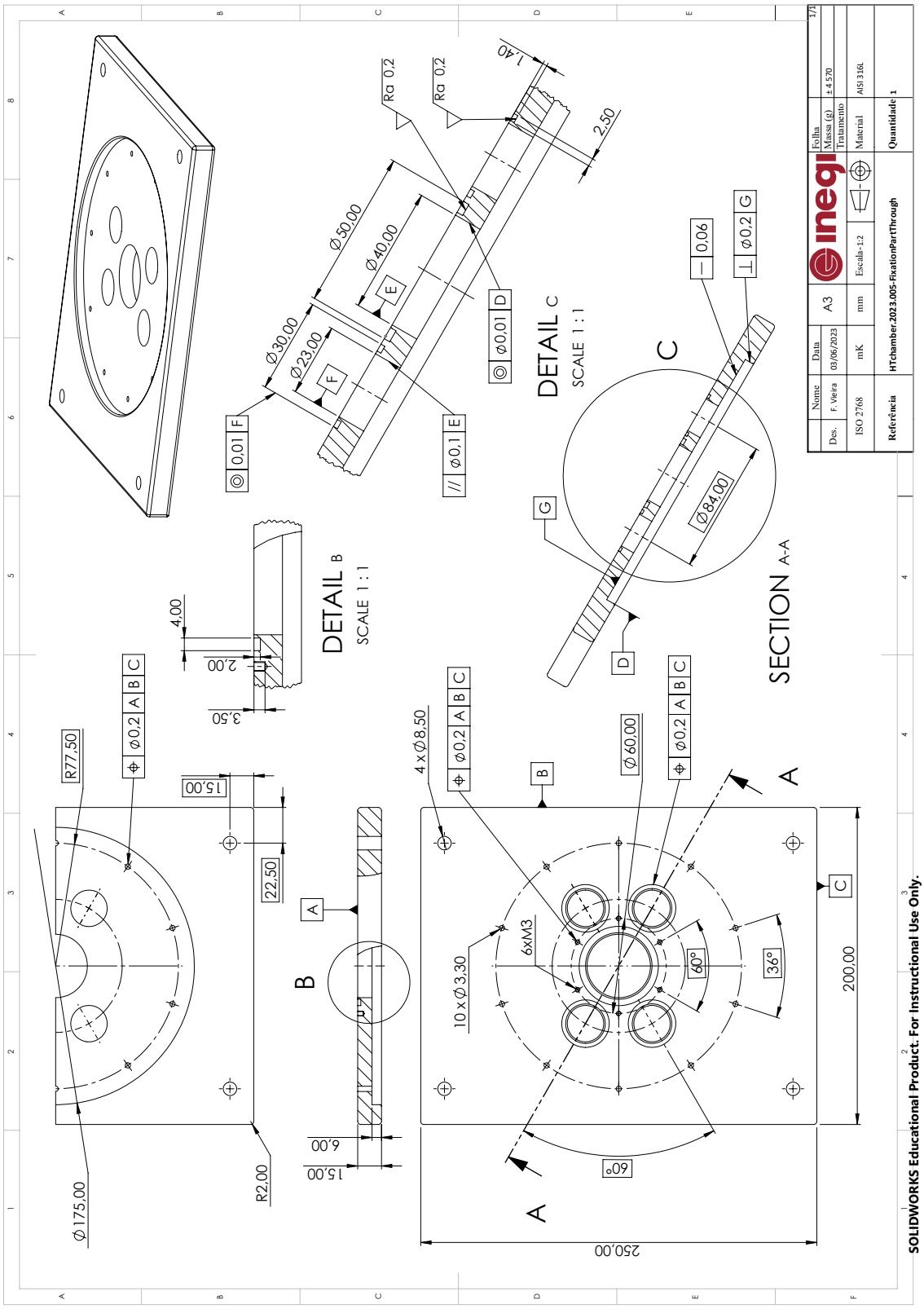
Appendix D

End Cap Load Cell connected (4) technical drawing


DETAIL A
SCALE 1 : 1
2xM12
M14x1.5
13,00
45,00
41,00
6,00
Ø155,00
10 x Ø3,30
Ø175,00
Ø127,00
R1,00
Ø0,01 B
Ø0,1 C
0,1 D
0,06
Ø0,2 A B
36°
Des. F. Vieira 03/06/2023
Nome Data
ISO 2768 mK
A3
mm
Escala: 1:2
Folha
Massa (g) ± 4 900
Tratamento
Material MP35N
Referência HTchamber.2023.004-EndCapLoadCell
Quantidade 1
SOLIDWORKS Educational Product. For Instructional Use Only.

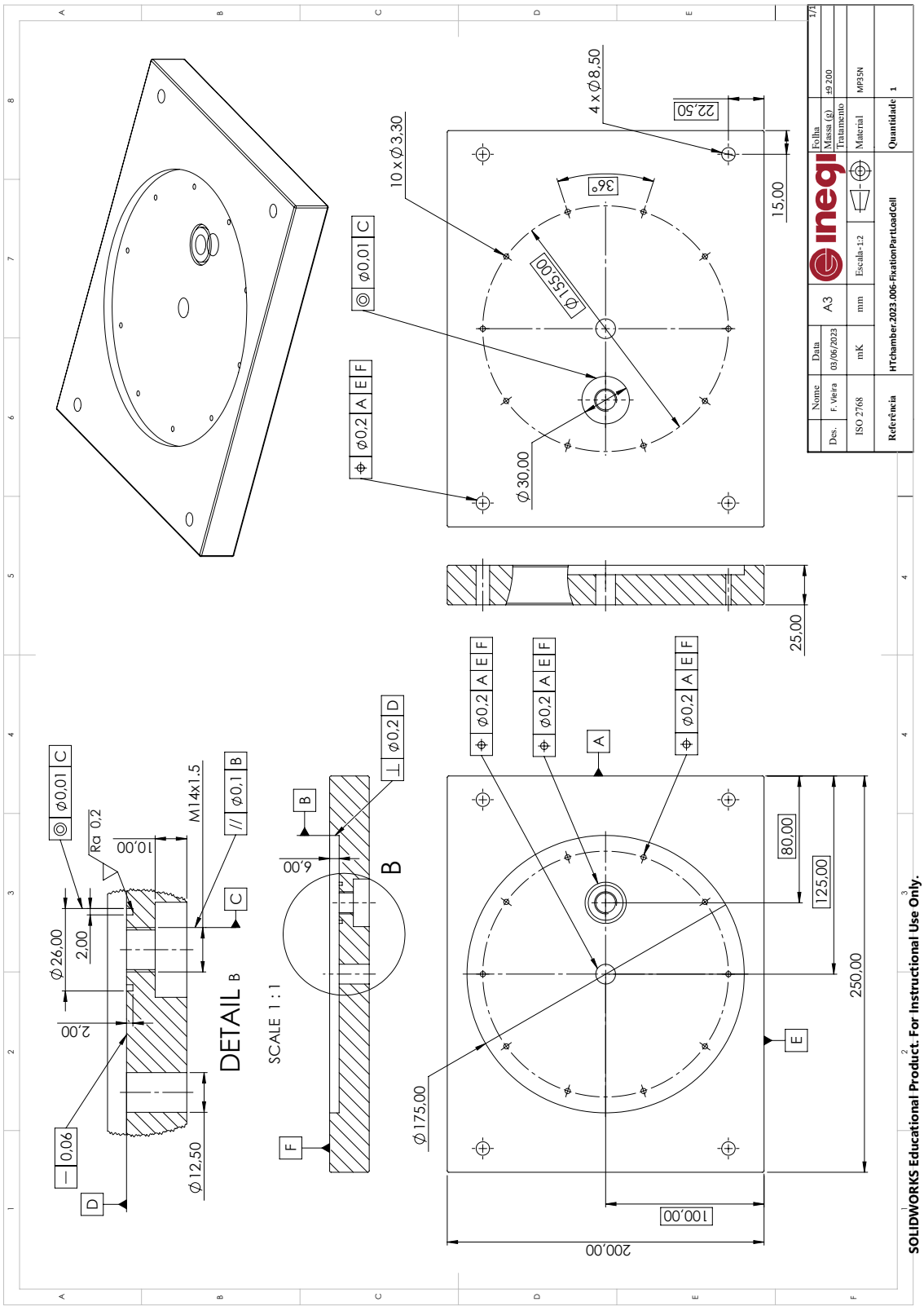
Appendix E

Fixation Part Through (5) technical drawing


DETAIL B
SCALE 1 : 1
DETAIL C
SCALE 1 : 1
SECTION A-A
Ø175,00
R77,50
R2,00
15,00
22,50
4,00
2,00
3,50
6,00
15,00
4 x Ø8,50
10 x Ø3,30
6xM3
Ø60,00
60°
36°
250,00
200,00
Ø50,00
Ø40,00
Ø30,00
Ø23,00
1,40
2,50
Ra 0,2
Ø84,00
0,06
Ø0,2 A B C
Ø0,01 D
Ø0,1 E
0,01 F
Ø0,2 G
Nome
Data
A3
Folha
Massa (g)
Tratamento
Material
AISI 316L
Escala: 1:2
mm
mK
ISO 2768
Des.
F. Vieira
03/06/2023
Referência
HTchamber.2023.005-FixationPartThrough
Quantidade 1
SOLIDWORKS Educational Product. For Instructional Use Only.

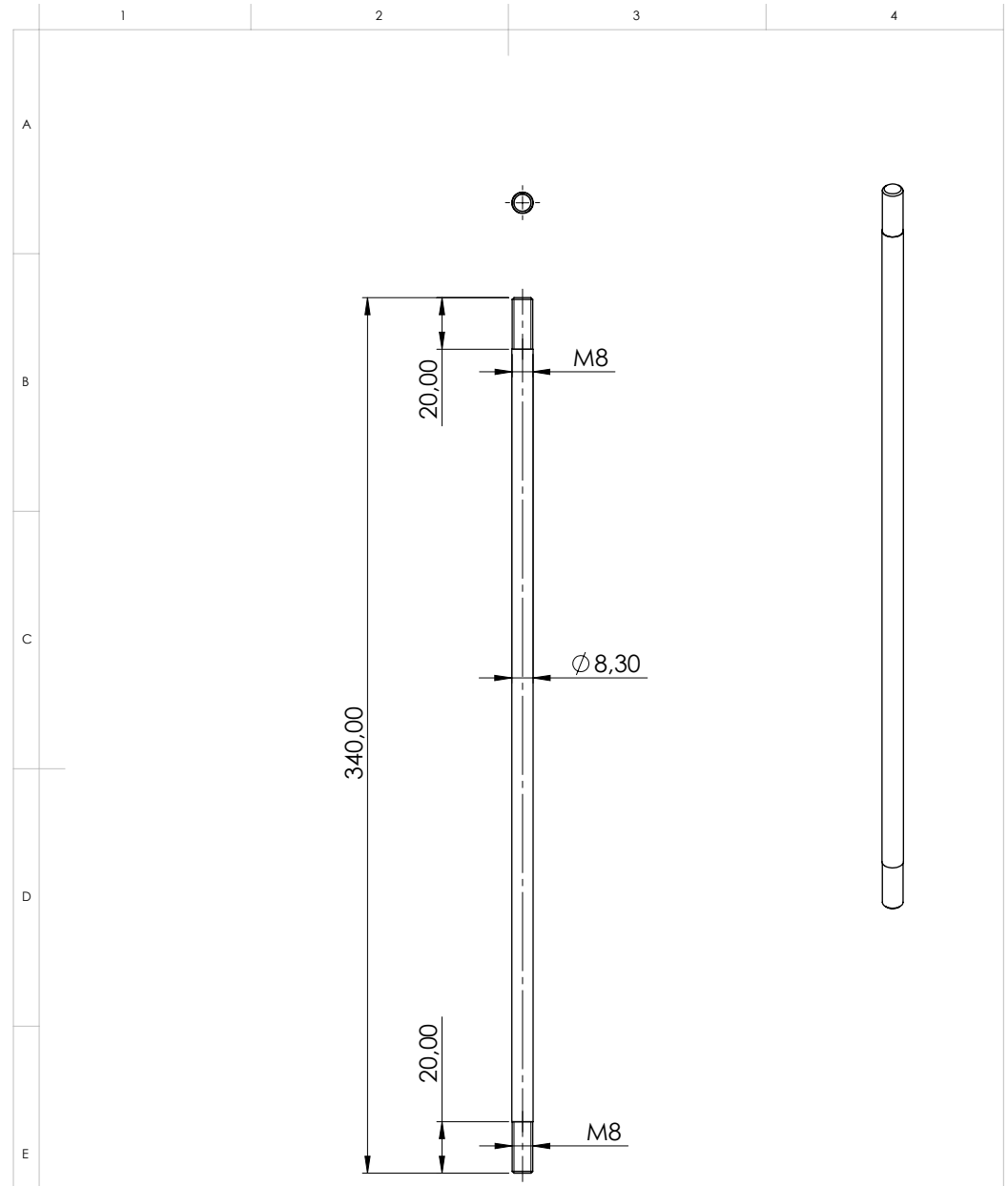
Appendix F

Fixation Part Load Cell connected (6) technical drawing


4 x Ø8,50
22,50
10 x Ø3,30
Ø0,01 C
Ø0,2 A E F
36°
Ø155,00
15,00
Ø30,00
25,00
Ø175,00
100,00
200,00
80,00
125,00
250,00
DETAIL B
SCALE 1 : 1
Ø26,00
2,00
2,00
10,00
M14x1.5
Ø0,1 B
Ra 0,2
Ø12,50
0,06 D
6,00
Ø0,2 D
B
C
E
F
Folha
Massa (g)
Tratamento
Material
MP35N
Escala: 1:2
A3
mm
mK
Data
03/06/2023
Nome
F. Vieira
Des.
ISO 2768
Referência
HTchamber.2023.006-FixationPartLoadCell
Quantidade 1
SOLIDWORKS Educational Product. For Instructional Use Only.

Appendix G

Fixation rod (7) technical drawing

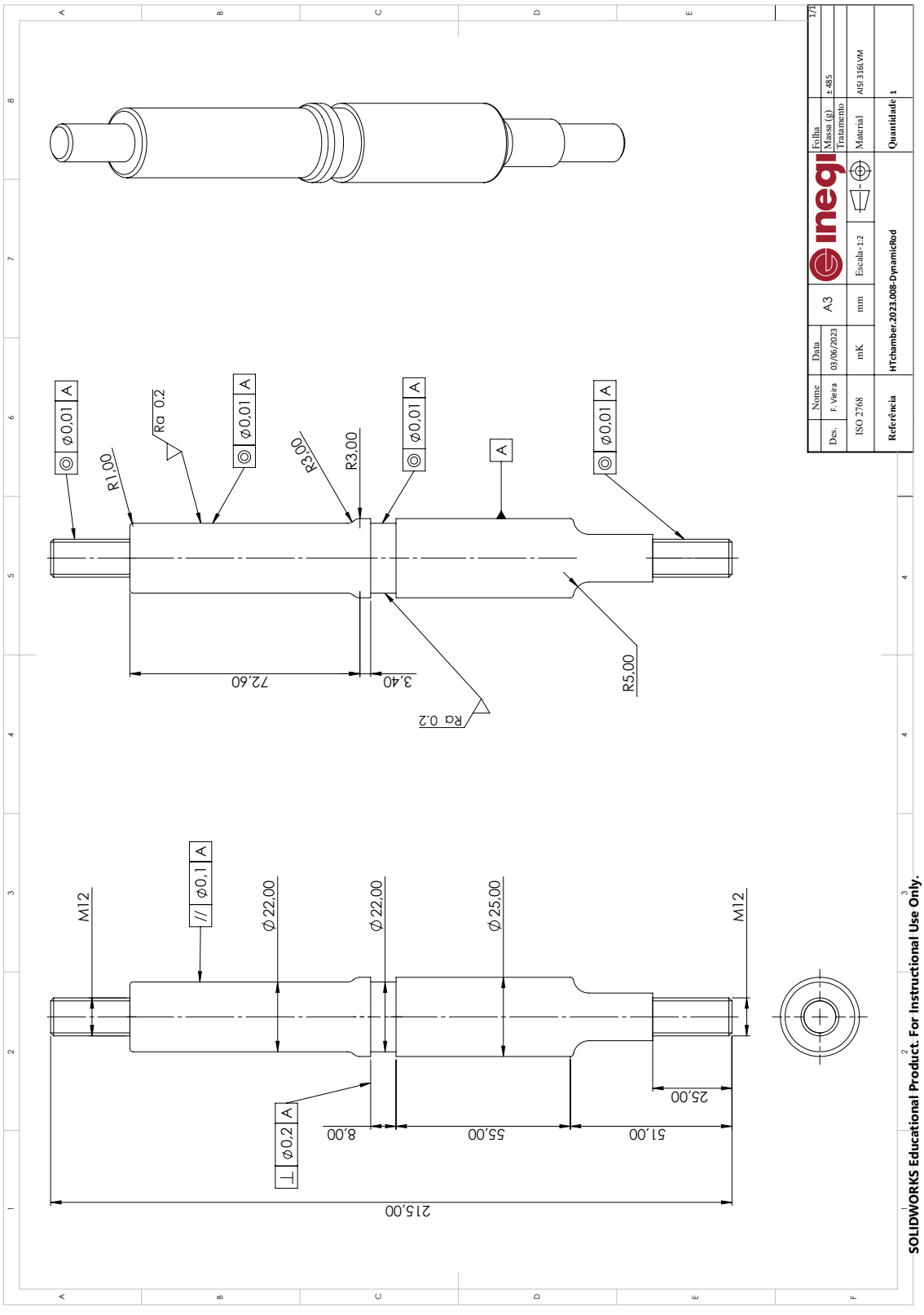


	Nome	Data				Folha	1/1
Des.	F. Vieira	03/06/2023	A4	inegi		Massa (g)	± 125
						Tratamento	
ISO 2768		mK	mm	Escala-1:2		Material	AISI 316L
Referência		**HTchamber.2023.007-RodFixation**				**Quantidade**	4

SOLIDWORKS Educational Product. For Instructional Use Only.

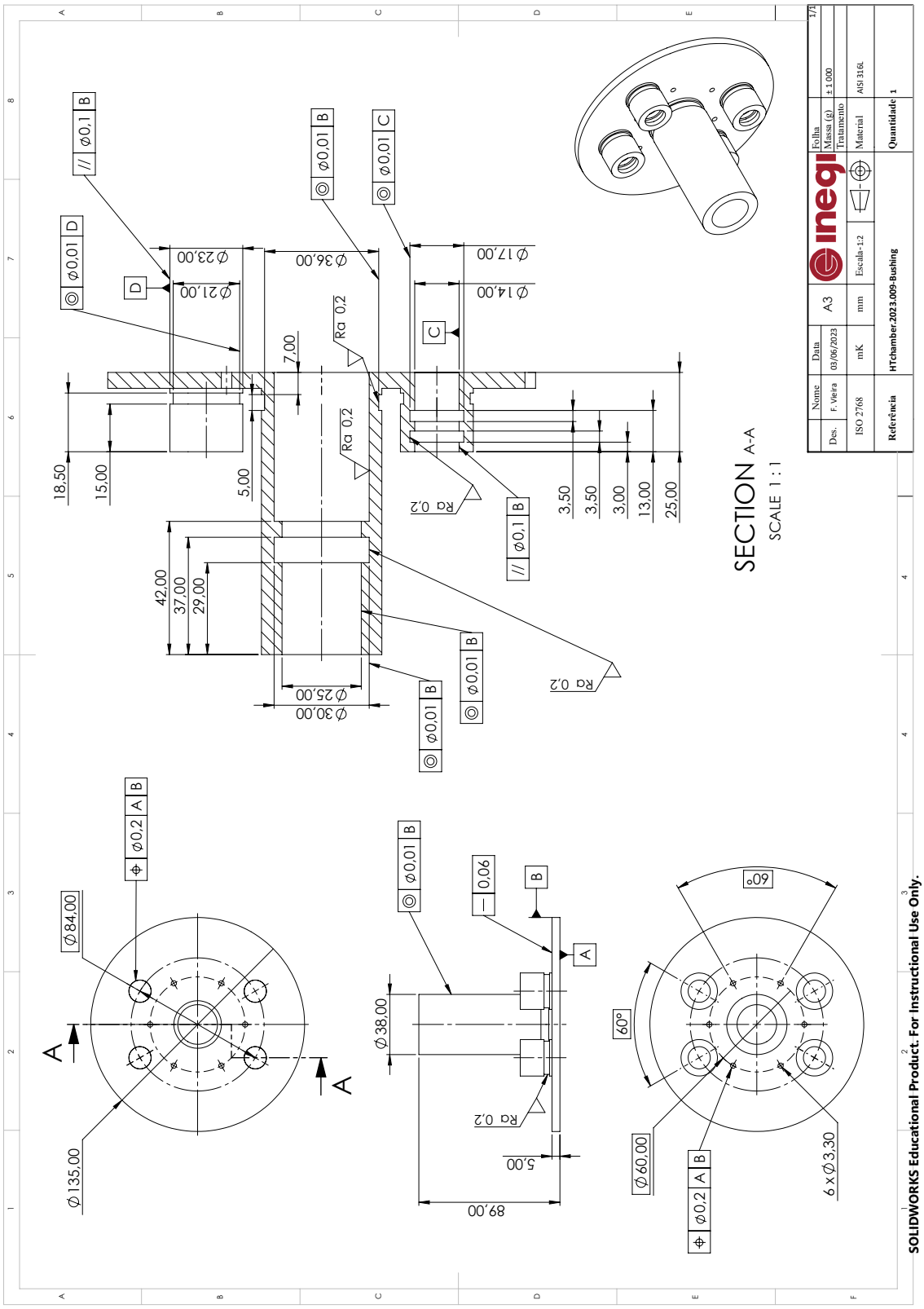
Appendix H

Dynamic Sealing Rod (8) technical drawing


Folha 1/1
Massa (g) ± 485
Tratamento
Material AISI 316LVM
Escala: 1:2 mm
A3
Data 03/06/2023
Nome F. Vieira
Des.
ISO 2768 mK
Referência HTchamber.2023.008-DynamicRod
Quantidade 1
ineqi
SOLIDWORKS Educational Product. For Instructional Use Only.
⌀0,01 A
R1,00
Ra 0.2
R2,00
R3,00
A
R5,00
72,60
3,40
M12
// ⌀0,1 A
⌀22,00
⌀25,00
⊥ ⌀0.2 A
8,00
55,00
51,00
25,00
215,00

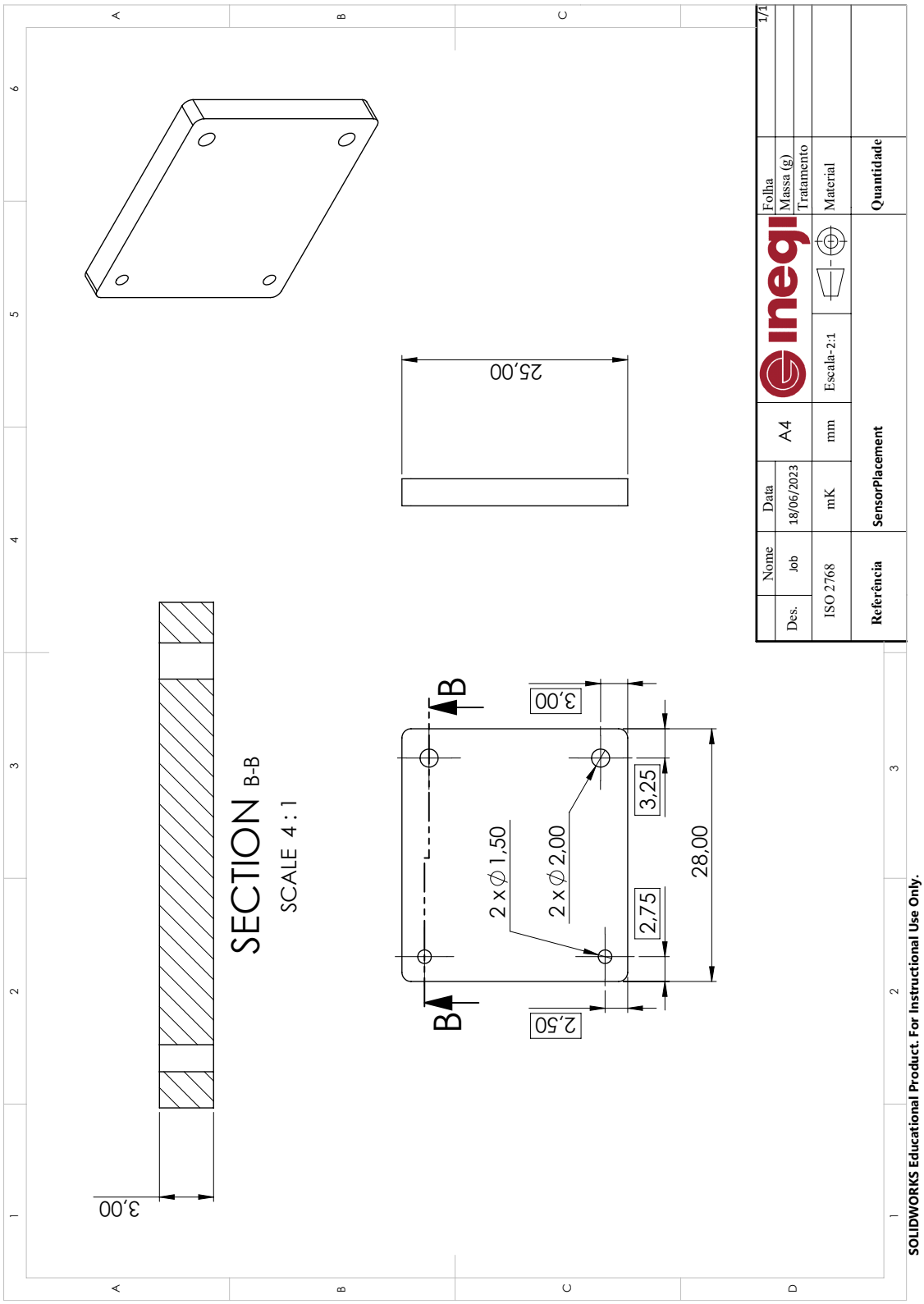
Appendix I

Dynamic Sealing Bushing (9) technical drawing


SECTION A-A
SCALE 1 : 1
Ø84,00
Ø135,00
Ø38,00
89,00
5,00
Ø60,00
6 x Ø3,30
60°
Ø23,00
Ø21,00
Ø36,00
Ø17,00
Ø14,00
Ø30,00
Ø25,00
18,50
15,00
5,00
7,00
42,00
37,00
29,00
3,50
3,50
3,00
13,00
25,00
Ra 0,2
Nome
Data
Des.
F. Vieira
03/06/2023
ISO 2768
mK
A3
mm
Escala: 1:2
Folha
Massa (g)
Tratamento
Material
± 1.000
AISI 316L
Referência
HTchamber.2023.009-Bushing
Quantidade 1
SOLIDWORKS Educational Product. For Instructional Use Only.

Appendix J

Sensor Placement technical drawing


SECTION B-B
SCALE 4 : 1
3,00
25,00
2 x ⌀1,50
2 x ⌀2,00
3,25
2,75
28,00
3,00
2,50
B
B
Des.
Nome
Job
Data
18/06/2023
ISO 2768
mK
A4
mm
Escala-2:1
Folha
1/1
Massa (g)
Tratamento
Material
Referência
SensorPlacement
Quantidade
SOLIDWORKS Educational Product. For Instructional Use Only.

Appendix K

Bill of Materials

Item	Reference	Description	Quantity
1	HTchamber.2023.001 ChamberTube	Fused Quartz Tube 175mm Supplier: Optical Solutions	1
2	HTchamber.2023.002 Flange	O-ring Flanges Manufacture	2
3	HTchamber.2023.003 EndCapThrough	End Cap - Dynamic Section Manufacture	1
4	HTchamber.2023.004 EndCapLoadCell	End Cap - Load Cell connected Manufacture	1
5	HTchamber.2023.005 FixationPartThrough	Fixation part - Dynamic Section Manufacture	1
6	HTchamber.2023.006 FixationPartLoadCell	Fixation part - Load Cell connected Manufacture	1
7	HTchamber.2023.007 RodFixation	Rod - End Threaded M8 - Fixation Manufacture	4
8	HTchamber.2023.008 DynamicRod	Rod for Dynamic Sealing Manufacture	1
9	HTchamber.2023.009 Bushing	Bushing for dynamic rod and hoses Manufacture	1
10	WLP-M14-9.5MM-HC	Power cables penetrator Supplier: BlueRobotics	1
11	Cylinder head screw DIN 912 M3x8 51050_030_008(High)	Cylindrical Head Screw Steel 10.9 M3x8	6
12	Cylinder head screw DIN 912 M3x18 51050_030_018(High)	Cylindrical Head Screw Steel 10.9 M3x18	10
13	Cylinder head screw DIN 912 M3x30 07015_030_030(High)	Cylindrical Head Screw Steel 10.9 M3x30	10
14	Washer DIN 125-1 A 3_2 38130_030_001(High)	Plain Washer DIN 125-1A Steel Zinc plated 140 HV M3	26
15	Washer DIN 125-1 A 8_4 38130_080_001(High)	Plain Washer DIN 125-1A Steel Zinc plated 140 HV M8	8
16	Hexagon nut DIN 934 M8 01300_080_001(High)	Hexagon Nut DIN 934 Steel Zinc plated 8 M12	8
17	O-ring ISO 3601-133	Facial O-ring ISO 3601-133 FKM ID 45.69, CS 2.62	2
18	O-ring ISO 3601-255	Facial O-ring ISO 3601-255 FKM ID 142.47, CS 3.53	1

19	O-ring ISO 3601-162	Radial O-ring ISO 3601-162 NBR ID 145.72, CS 2.62	2
20	O-ring ISO 3601-316	Radial O-ring ISO 3601-316 FKM ID 21.59, CS 5.33	2
21	O-ring ISO 3601-126	Radial O-ring ISO 3601-126 FKM ID 34.59, CS 2.62	1
22	O-ring ISO 3601-118	Facial O-ring ISO 3601-118 FKM ID 21.89, CS 2.62	1
23	O-ring ISO 3601-112	Radial O-ring ISO 3601-112 FKM ID 12.36, CS 2.62	8
24	O-ring ISO 3601-117	Radial O-ring ISO 3601-117 FKM ID 20.29, CS 2.62	4
25	O-ring ISO 3601-024	Facial O-ring ISO 3601-024 FKM ID 28.30, CS 1.78	8
26	Hose 6mm	Hose 6mm type Supplier: SPIR STAR	1 meter
27	Ball Valve H24	H24 - 3/8" Full port Supplier: Habonim	3
28	Check Valves	Check Valve - 3/8" Port - Code 70.03 Supplier: Redfluid	3
29	Pressure Relief Valve	Series 420 Valve - 3/8" Port Supplier: Gotze Armaturen	1
30	Electrolysis Tank	H-Type Tank - 100mL - C2012F1 Supplier: Ossila	1
31	Graphite Electrode	Graphite Electrode - 3mm - C2013L1 Supplier: Ossila	2
32	Pressure and temperature sensor	HT-H2-TPSE Sensor - 60 bar Supplier: Hydrotechnik	1
33	Hydrogen Gas Module	TB600C-H2-1000 - 1000 ppm sensor Supplier: EC sensor	1
34	Hsensor.2023.001 SensorPlacement	H2 Sensor Placement Part Manufacture	1
35	DC Power Supply	Bench Top Power Supply Supplier: Distrelec	1

Appendix L

BlueRobotics Wet Link Penetrator M14

Version 1.2 (Last updated 14-Oct-2022)

WETLINK

WetLink Penetrator (WLP) Technical Specifications

Performance Characteristics[1]

Maximum Tested Depth (seawater)	950 m / 3116 ft
Design Lifetime[2]	3 years or 500 cycles to rated depth

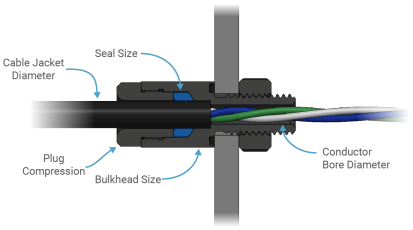
[1] *For reference only, performance may vary depending on application and cable construction, it is the responsibility of the customer to determine suitability for their application*

[2] *Design life was used to inform testing in an accelerated environment, does not reflect warranty period*

Size Index

Seal Size	Bulkhead Sizes	Conductor Bore Diameter [mm]	Plug Compression	Jacket Diameter Range[1] [mm]	Part Number
4.5	M06, M10	3.3 mm	High (HC)	4.0 ± 0.3	**WLP-M06-4.5MM-HC** **WLP-M10-4.5MM-HC**
			Low (LC)	4.5 ± 0.3	**WLP-M06-4.5MM-LC** **WLP-M10-4.5MM-LC**
5.5	M10	4.0 mm	High (HC)	5.0 ± 0.3	**WLP-M10-5.5MM-HC**
			Low (LC)	5.5 ± 0.3	**WLP-M10-5.5MM-LC**
6.5	M10	4.8 mm	High (HC)	6.0 ± 0.3	**WLP-M10-6.5MM-HC**
			Low (LC)	6.5 ± 0.3	**WLP-M10-6.5MM-LC**
7.5	M10	5.7 mm	High (HC)	7.0 ± 0.3	**WLP-M10-7.5MM-HC**
			Low (LC)	7.5 ± 0.3	**WLP-M10-7.5MM-LC**
8.5	M10	6.0 mm	High (HC)	8.0 ± 0.3	**WLP-M10-8.5MM-HC**
			Low (LC)	8.5 ± 0.3	**WLP-M10-8.5MM-LC**
9.5	M14	7.5 mm	High (HC)	9.0 ± 0.3	**WLP-M14-9.5MM-HC**
			Low (LC)	9.5 ± 0.3	**WLP-M14-9.5MM-LC**

[1] *Jacket diameter range varies for foam jacketed cables, see guides for more details*



Tools

Seal Size	Bulkhead Size	Bulkhead Wrench	Bulkhead/Nut Flat Size	Bulkhead Torque	Plug Wrench	Plug Hex Size	Plug Torque
4.5	M06	WL-M06-BULKHEAD-WRENCH	12 mm	1 N·m	WLP-11MM-PLUG-WRENCH	11 mm	14 N·m
4.5	M10	WL-M10-BULKHEAD-WRENCH	16 mm	3.5 N·m	WLP-11MM-PLUG-WRENCH	11 mm	14 N·m
5.5, 6.5, 7.5, 8.5	M10	WL-M10-BULKHEAD-WRENCH	16 mm	3.5 N·m	WLP-14MM-PLUG-WRENCH	14 mm	14 N·m
9.5	M14	WL-M14-BULKHEAD-WRENCH	20 mm	3.5 N·m	WLP-18MM-PLUG-WRENCH	18 mm	20 N·m

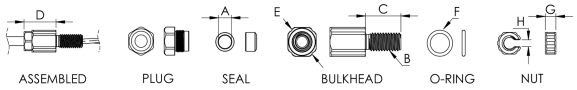
Tested Cables

Part Number	Cable Part Name / Number	Manufacturer	Application	Jacket Diameter [mm]	Jacket Material	Conductors	Tested Current[1]	Nominal Voltage	Max Temp Recommended[1]
WLP-M06-4.5MM-HC **WLP-M10-4.5MM-HC**	Fathom Slim Tether (CAB-NBPUF-1UTP-26AWG-R3)	Blue Robotics	Tether	4.0	PUR Foam	1x UTP 26AWG	-	-	50°C
WLP-M06-4.5MM-LC **WLP-M10-4.5MM-LC**	Lumen/Gripper Cable (CAB-A-3-22AWG-R1)	Blue Robotics	Power / PWM	4.5	PUR	3x 22AWG	-	-	60°C
	Ping Cable (CAB-PUR-4-24AWG-R1)	Blue Robotics	Power / Serial	4.5	PUR	4x 24AWG	-	-	60°C
	Ping 360 Cable (CAB-PUR-3UTP-28AWG-R2)	Blue Robotics	Power / Ethernet	4.7	PUR	3x UTP 28AWG	-	-	50°C
WLP-M10-5.5MM-HC	chainflex® control cable CF9 (CF9-02-06)	IGUS	Power / Signal	5.0	TPE	6x 24AWG	-	300V	60°C
WLP-M10-5.5MM-LC	Etherline® (2170283)	LAPP	Cat5e	5.6	PUR	2x SFTP 26AWG	-	125V	60°C
WLP-M10-6.5MM-HC	Unitronic® (302206)	LAPP	Power / Signal	5.8	PVC	6x 22AWG	-	300V	60°C
WLP-M10-6.5MM-LC	T200 Thruster Cable (CAB-PUR-3-16AWG-R2)	Blue Robotics	Power	6.4	PUR	3x 16AWG	48A	-	60°C
	Etherline® (2170300)	LAPP	Cat5e	6.3	PUR	4x SFTP 26AWG	-	1000V	60°C
WLP-M10-7.5MM-HC	Fathom ROV Tether (CAB-NBPUF-4UTP-26AWG-R3)	Blue Robotics	Cat5 / Tether	7.6	PUR Foam	4x UTP 26AWG	-	-	50°C
WLP-M10-7.5MM-LC	Ethernet and Power Cable (CAB-PUR-2-22AWG-4UTP-26AWG-R1)	Blue Robotics	Cat5 + Power	7.5	PUR	4x UTP 26AWG + 2x 22AWG	-	-	60°C
WLP-M10-8.5MM-HC	chainflex® control cable CF9 (CF9-02-12)	IGUS	Power / Signal	7.7	TPE	12x 24AWG	-	300V	60°C
WLP-M10-8.5MM-LC	Power Cable, 2-conductor (CAB-A-2-12AWG)	Blue Robotics	Power	8.3	PUR	2x 12AWG	60A	-	60°C
WLP-M14-9.5MM-HC	T500 Thruster Cable (CAB-PUR-3-12AWG-R1)	Blue Robotics	Power	9.0	PUR	3x 12AWG	100A	-	60°C

[1] *Current ratings evaluated at ambient temperatures in water* [2] *Sustained high temperatures can lead to performance loss over long periods of time*

Physical Properties

Bulkhead Size	M06	M10	M14
Seal Sizes (A)	4.5	4.5 , 5.5, 6.5, 7.5, 8.5	9.5
Bulkhead Thread (B)	M6 x 1	M10 x 1.5	M14 x 1.5
Bulkhead Thread Length (C)	10 mm	20 mm	25 mm
Recommended Bulkhead Through Hole Size	6.2	10.2	14.2
Assembled Height from Endcap (D)	23.5 mm	18 - 26 mm	23 mm
Overall Outer Diameter (E)	13 mm	18 mm	22 mm
O-ring Size (F)	1.5x7 Buna-N 70A	-013 Buna-N 70A	1.5x15 Buna-N 70A
Nut Height (G)	4 mm	8 mm	8 mm
Nut Slot Width (H)	3.5 mm	5 mm	9 mm
Assembled air weight (no cable)	7.6 g	13.9 - 15.6 g	24.9 g
Assembled water weight (no cable)	5.1 g	10.2 - 10.7 g	16.4 g
Seal Material	FKM		
Seal Material Temperature Range	-25°C to 200°C		
Bulkhead & Plug Material	7075-T6 Aluminum, Anodized		



Test Procedure[1]

Minimum Number of Test Samples	36
Test Pressure	950 msw
Number of Cycles	500 cycles
Water Temperatures at Pressure	2°C to 40°C
Tested Current at Pressure *(if applicable)*	✓
Temperature Shock Cycling in Air	-30°C to 70°C
Cable Axial Strain *(10 cycles)*	3.5 to 7.5 kg
Cable Radial & Torsional Straining	✓
1000V Hipot Test & Continuity Test	✓
Accelerated Age Test	✓

[1] *Test values shown for reference only, it is the responsibility of the customer to determine suitability for their application*

Appendix M

SPIR STAR 6mm Hose

Hose Type 6mmHydrogen

640061

ID6 - Series: W

SPIR STAR



Applications

Oil and Gas: Connecting hose from dispenser to fuelling nozzle for gaseous compressed hydrogen

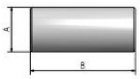
Technical Information

Inner Core: Polyoxymethylene (POM) with low permeation rate
Pressure Support: 4 layers of high-tensile steel wire
Outer Cover: Polyamide (PA)
Color: purple
Temperature: -40°C to +85°C [-40°F to 185°F]

Ø ID	Ø OD	Working Pressure –	Working Pressure (SF 4,0:1)	Burst Pressure	Bend Radius	Weight	Insert ID
6,3 mm	12,6 mm	--	962,5 bar	3.850 bar	180 mm	0,295 kg/m	4,5 mm
0,25 inch	0,50 inch	--	13.956 psi	55.825 psi	7,09 inch	0,198 lbs/ft	0,18 inch

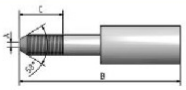
Sleeve

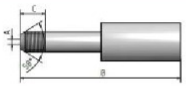
Part no.	Thread	Material		Dimensions (mm) A	B	C	
Sleeve							
10640125	-	AISI 316	-	16,4	49	-	-

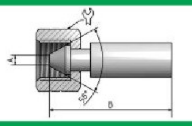


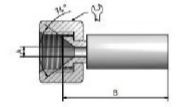
Insert

Part no.	Thread	Material	Nut	Dimensions (mm) A	B	C	
HP fitting							
40640207W	3/8"x24UNF LH	Stainless steel	-	4,5	89	19,1	-
MP fitting							
40640307W	3/8"x24UNF LH	Stainless steel	-	4,5	87	11,1	-
40640317W	9/16"x18UNF LH	Stainless steel	-	4,5	99	12,7	-
Type M female swivel							
20640607W	9/16"x18UNF	Stainless steel	50540605	4,5	62	20	19
JIC female swivel							
20640617W	9/16"x18UNF	Stainless steel	50540605	4,5	57	-	19









© Copyright by SPIR STAR® | Revision 10.11.2020

Hose Type 6mmHydrogen

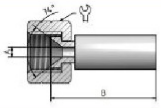
640061

ID6 - Series: W

SPIR STAR®

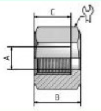
Insert

Part no.	Thread	Material	Nut	Dimensions (mm) A	B	C	⌀
STAR-Crimp							
60640609W	7/16"x20UNF	Stainless steel	incl.	4,5	61	-	17



Swivel nut

Part no.	Thread	Material	Relief bores	Dimensions (mm) A	B	C	⌀
Swivel nut							
50540605	9/16"x18UNF	AISI 316	1 radial	9,2	18	14	19



Bend restrictor

Part no.	Material	Crimp ring	Dimensions (mm) ⌀	Length
PU bend restrictor				
1.9518306A	PU	1003035	34	250



Hose securing grip

Part no.	Mesh length (mm)	Overall length (mm)	Breaking strength (kN)	Suitable for SPIR STAR® hose outer diameter (mm)
Hose securing grip				
9056400-ES	600,00	800,00	10,20	10-15



Hose securing grip long version				
905640L-ES	600,00	990,00	10,20	10-15



Important Information!

This hose must not be used in vehicles.

The outer cover is non conductive. The electrical resistance from end fitting to end fitting is < 0,3 Ohm/m.
The outer cover of the hose has to be pin pricked.
The hose assembly has to be exchanged every 2 years in service or after a pull out event.
Each hose assembly will be tested with water and helium according ISO 19880-5 before shipping.

Production related variations of the burst pressure of up to 5 % are possible. Other colors upon request.
The safety factors between the burst pressure and the working pressure as well as the test pressure depend on the operating conditions. For gaseous media the outer cover is to be pinpricked.
Regarding the safety factor for gaseous media please contact your local SPIR STAR® assembling center.
The indicated working pressure refers to the hose only. Depending on the used fitting the permitted working pressure of a hose assembly may be less.
**) Blast-Pro® fittings may only be used for tube cleaning operations inside the tube. They have not been designed for the use outside of tubes.*
We reserve our rights for technical changes without notice. Subject to printing errors.

© Copyright by SPIR STAR® | Revision 10.11.2020

Appendix N

Habonim H24 Valve

H24 ¼"-½" | DN8-DN15 | PN500 (7,250PSI)
¾"-1½" | DN20-DN40 | CLASS 2500 PN420 (6,000PSI)

Hydrogen Service High Pressure Floating Ball 3 Piece Threaded-Body

Technical Information

Operation

Maximum Working Pressure:
Size ¼"-½" - 500bar (7,250psi)
Size ¾"-1½" - Class2500 414bar (6,000psi)

Working temperature: -60°C up to +260°C (-76°F up to +500°F).

Design

- Threaded body
- Automation-ready with standard ISO 5211 connecting plate
- Total HermetiX Integrity package with:
  ISO15848-1 and API 641 emission standard certificated design
  ISO10497 and API607 fire-safe standard certificated design
  Double body sealing

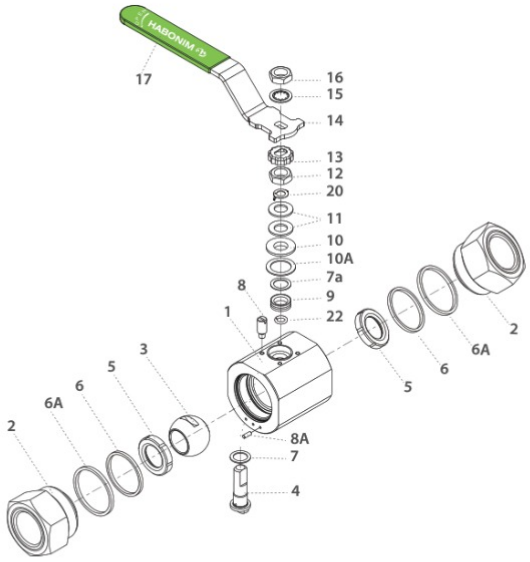
Testing & Certifications

- TPED Certified, up to 414bar (6,000psi) MWP
- 100% shell & inline leak tested
- Marine classification (on demand): DNV GL, LR, BV, ABS, KR,
- RINA, others

Materials

- Stainless steel body & ends
- All materials compatible for Hydrogen use

Components & materials



Item	Description	Material specification	Qty.
1	Body	Acc. Ordering Code	1
2	End	Acc. Ordering Code	2
3	Ball	Acc. Ordering Code	1
4	Stem	Acc. Ordering Code	1
5*	Seat	Acc. Ordering Code	2
6*	Inner seal	Acc. Ordering Code	2
6A*	Outer seal	Acc. Ordering Code	2
7*	Stem thrust seal	PEEK, CF PEEK, PCTFE	1
7a*	Anti-abrasion ring	PEEK, CF PEEK, PCTFE	1
8	Stop pin	S. Steel	1
8A	Dowel Pin	S. Steel	1
9*	Stem seal	CF PTFE, TFM	1
10	Follower	S. Steel	1
10A*	Slide bearing	S. Steel	1
11	Disc spring	S. Steel	2
12	Stem nut	S. Steel	1
13	Locking clip	S. Steel	1
14	Handle	S. Steel	1
15	Serrated washer	S. Steel	1
16	Handle nut	S. Steel	1
17	Sleeve	PVC	1
20	Anti static device	S. Steel	1
22	O-ring	Acc. Ordering Code	1
23	Tag (not shown)	S. Steel	1

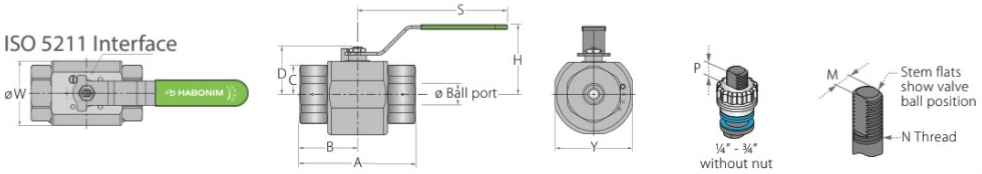
* Repair kit components

H24 ¼"-½" | DN8-DN15 | PN500 (7,250PSI)
¾"-1½" | DN20-DN40 | CLASS 2500 PN420 (6,000PSI)

Hydrogen Service High Pressure Floating Ball 3 Piece Threaded-Body

Valve dimensions

ISO 5211 Interface



Std. port	Full port	Unit	Ball port	A	B	C	D	H	M	N	P	W	S	Y	weight kg/lb	kv / cv
	DN8	mm	11.15	91	45.5	21.50	37.90	42.1	5.54	⅜" UNF	11.1	54	179	45	0.8	4.3
	¼"	inch	0.44	3.58	1.79	0.84	1.49	1.66	0.22		0.43	2.12	7.05	1.77	1.76	5.00
DN15	DN10	mm	11.15	91	45.5	24.50	37.90	42.1	5.54	⅜" UNF	11.1	54	179	45	0.8	6.9
½"	⅜"	inch	0.44	3.58	1.79	0.84	1.49	1.66	0.22		0.43	2.12	7.05	1.77	1.76	8.00
DN20	DN15	mm	14.3	104.25	52.12	23.90	40.30	45	5.54	⅜" UNF	11.1	62	179	60	1.27	10
¾"	½"	inch	0.56	4.10	2.05	0.94	1.59	1.77	0.22		0.43	2.44	7.05	2.36	2.79	12.00
DN25	DN20	mm	20.6	126.6	63.3	37.90	55.60	60.3	7.54	7/16" UNF	15.4	84.5	193	77	2.1	28
1"	¾"	inch	0.81	4.98	2.49	1.49	2.19	2.37	0.29		0.60	3.32	7.60	3.03	4.63	32.00
DN32	DN25	mm	25.4	137.25	68.62	42.50	60.2	68.7	7.54	7/16" UNF	15.4	93	193	85	2.9	49
1¼"	1"	inch	1.00	5.40	2.70	1.67	2.37	2.70	0.29		0.90	3.66	7.60	3.34	6.39	57.00
DN40	DN32	mm	31.8	161.94	80.97	43.55	73.00	81.1	8.7	9/16" UNF	19.6	99	287	95	4.8	69
1½"	1¼"	inch	1.50	6.37	3.18	1.71	2.87	3.19	3.19		0.77	3.89	11.30	3.74	10.58	80.00

Ordering Code System

"Mandatory option" options are marked with green background | "Standard offer" options are marked with light green background

1 2	3 4 5 6	7 8	9	10	11 12	13	14	15	16	17	18	19 20 21 22	23	24 25 26 27 28 30
0 5	F H	2 4	W	-	6 6	M	M	L	H	G	/	N P T	-	
Size	Features	Series	Design		Body/Ends material	Ball material	Stem material	Seat material	Inner Seal	Outer Seal		End Connection		Special features

Size (1-2)			MWP bar (psi)	
Code	inch	mm	414 (6,000)	500 (7,250)
02	¼"	8	+	+
03	⅜"	10	+	+
05	½"	15	Full port	Std. port only
07	¾"	20	+	n/a
10	1"	25	+	n/a
12	1¼"	32	+	n/a
15	1½"	40	Std. port only	n/a

Features (3-6)	
H	Hydrogen Service
F	Fire safe
B	Full port
O	Clean assembly for O2 service

Series (7-8)	
24	HP Float 3 piece

Design (9)	
W	Total HermetiX Integrity package

Body/Ends material (11-12)	
6	S. Steel 316L

Ball material (13)	
M	High Strength S. Steel

Stem material (14)	
M	High Strength S. Steel

Seat material (15)	
L	Virgin PEEK

Inner Seal Material (16)	
H	HNBR
V	Viton
T	PTEF
G	Expanded graphite

Outer Seal Material (17)	
G	Expanded graphite
T	PTFE
H	HNBR
V	Viton

End connections (19-22)	
Threaded Ends	
NPT	ASME B1.20.1 - National Pipe Taper thread
BSPP	ISO228-1 - Pipe Parallel thread
DIN3852	DIN3852 - Pipe Parallel thread
BSPT EN 10226	10226 - Pipe Taper thread
AS5202	AS 5202 on-face gasket sealing threaded connection
MNPT	Male NPT
SAE J1926-A	SAE J1926-A
Welded	
XBW80	Extended buttweld ends (sch80)

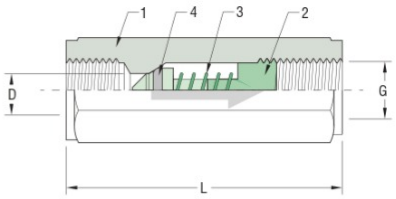
Appendix O

Redfluid Check Valve

SERIE VERTIC / VERTIC SERIE / *SERIE VERTIC*

VÁLVULAS Y ACCESORIOS / **VALVES & ACCESSORIES**/ *VÀLVULES I ACCESSORIS*





VALVULAS DE RETENCIÓN SERE VERTIC **VERTIC CHECK VALVES**

Válvulas de retención con flujo libre en un sentido y bloqueo en otro para eliminiar el efecto de la presión de retorno en los circuitos neumáticos e hidráulicos. Interiormente estas válvulas están formadas por un sistema de cierre automático por pistón con resorte.

Chick valves with free flow in one way and blockead in the oteher way for preventing revese flow and stopping back pressure in hydraulic and pnematic circuits. In the valve, there is an automatic lock system with a piston and a spring.

CONNECTIONS: BSP (UNI/ISO 228) NPT(ANSI.B.1.20.1)

Code	PN	G	L	D	Orifice mm2	HEX
70.01	350	1/8	42	4	12	14
70.02	350	1/4	50	7	22	19
70.03	350	3/8	60	10	42	24
70.04	350	1/2	65	11	75	27
70.05	300	3/4	75	17	125	37
70.06	250	1	93	21	230	41
70.07	250	1 1/4	110	29	340	50
70.08	210	1 1/2	112	34	509	55
70.09	150	2	120	48	1640	75

TECHNICAL FEATURES

	Description	Material
1	Body	AISI 316
2	Lock screw	AISI 316
3	Spring	AISI 316
4	Poppet	AISI 316

STANDARD FEATURES

+	Safety factor: K=2,5	
+	Cracking Pressure : 0,5 Bar	Optional Alterantive Cracking Pressure Spring
+	FKM Seals (-25 ºC +230 ºC)	

OPTIONAL

Description	Material	Temperature
Seals (optional)	FKM-VITON	-25 ºC / +230 ºC
	P.T.F.E.	-60 ºC / +180 ºC
	EPDM	-40 ºC / +175 ºC
	NBR	-30 ºC / +120 ºC
	SILICONE	-100 ºC / +200 ºC

SERIE VERTIC ACERO CARBONO / **VERTIC SERIES CARBON STEEL**
SERIE VERTIC ACER CARBONI

CONNECTIONS: BSP (UNI/ISO 228) NPT(ANSI.B.1.20.1)

Code	A	PN (bar/PSI)	Max Flow (l/min)	L	HEX
70.01.1/8 F	BSPP 1/8	400 (5800)	5 (1.3)	47 (1.85	14 (0.55)
70.02.1/4 F	BSPP 1/4	350 (5000)	15 (4)	55 (2.16)	19 (0.75)
70.03.3/8 F	BSPP 3/8		30 (8)	65 (2.56)	24 (0.94)
70.04.1/2 F	BSPP 1/2	320 (4600)	50 (13)	75 (2.95)	27 (1.06)
70.05.3/4 F	BSPP 3/4	300 (4350)	90 (23)	86,5 (3.41)	35 (1.38)
70.06. 1F	BSPP 1	250 (3600)	150 (40)	110 (4.33)	41 (1.61)
70.07.1 1/4F	BSPP 1 1/4		200 (50)	123 (4.84)	55 (2.16)
70.08.1 1/2F	BSPP 1 1/2	210 (3000)	300 (80)	138 (5.43)	60 (2.36)
70.09. 2F	BSPP 2	150 (2100)	430 (110)	160 (6.30)	70 (2.76)

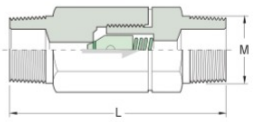
EQUIPAMIENTO DE SERIE
- Presión de apertura = 1 Bar
- Sellado: de asiento con NBR (-20 º C + 80 º C)

STANDARD FEATURES
- Spring cracking = 1 Bar
- Sealing: Poppet with NBR seal (-20 ºC + 80 ºC)

EQUIPAMENT DE SÈRIE
- Pressió d'obertura = 1 Bar
- Segellat: Punxó amb NBR (-20 º C + 80 º C)

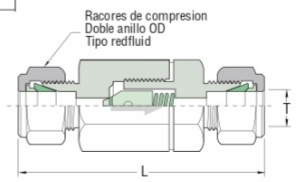
SS316 OTRAS OPCIONES / **OTHER OPTIONS** SS316
ALTRES OPCIONS ACER INOXIDABLE SS316

ROSCA M-M / **MALE-MALE**



M	L
1/8	58
1/4	60
3/8	62
1/2	79

RACORES DE COMPRESIÓN / TWIN FERRULE FITTINGS



T	L
1/8	60
1/4	60
5/16	75
3/8	75
1/2	85

Appendix P

Gotze Armaturen pressure relief valve

Type test approved safety valves angle-type for industrial applications

→ Series 420

3.5

420

Safety valves made of stainless steel, angle-type with threaded connections



■ SUITABLE FOR

Liquids	neutral and non-neutral	
Air, gases and vapours	neutral and non-neutral	
Steam		

■ EXAMPLES OF USE

For the protection of:
- pressure tanks and -systems for neutral / non-neutral vapours, gases and liquids
- steam boilers and steam plants

Please observe plant-specific regulations and use of appropriate valve version and sealing material.

- chemical plants, biogas plants
- process technology
- desalination plants
- process equipment construction and medical technology
- shipbuilding industry and marine equipment
- secondary areas in the food-, beverage-, pharmaceutical- and cosmetics-industries
- offshore-applications
- general applications with screwed pipe connections

Safety valves are set and sealed at the factory.

■ MATERIAL

■ SPECIFICATION

1/4" – 3/8"	– 40°C to + 260°C depending on version	0,5 – 50 bar depending on version

■ APPROVALS

TÜV-Type test approval 2069	**D/G, F, F/K/S[1]**
EU type examination	**S/G, L, F/K/S[1]**
TR ZU 032/2013 - TR ZU 010/2011	**D/G (S/G), F (L), F/K/S[1]**

Requirements

AD 2000 Data sheet A2	DIN EN ISO 4126-1
TRD 421	PED 2014/68/EU
TRB 801 No. 22 and No. 23[1]	

Classification society

DNV	DNV
Lloyd's Register EMEA	LR EMEA
American Bureau of Shipping	ABS
Bureau Veritas	BV
Russian Maritime Register of Shipping	RS
Registro Italiano Navale	RINA

■ MATERIALS

Component	Material	DIN EN	ASME
Inlet body	Stainless steel	1.4404	316 L
Outlet body	Stainless steel	1.4404	316 L
Internal parts	Stainless steel	1.4404	316 L
Spring	Stainless steel	1.4310	302
Metallic bellows (optional)	Stainless steel	1.4571	316 Ti
PTFE-bellows (optional)	PTFE	PTFE	PTFE

[1]only for versions with bellows

Series 420 ■ VALVE VERSION

t	gastight version of spring housing	for neutral and non-neutral media without counter pressure. The environment is protected from being affected by the medium. 0,5 to 1,5 bar gastight version (without bellows).
tb	gastight version with bellows	for neutral and non-neutral media. spring and moving parts as the environment are protected from being affected by the medium. Version of bellows depending on set pressure: **DN8:** 1,6 to 12 bar PTFE bellows; 12,1 to 50 bar stainless steel bellows **DN10:** 1,6 to 12 bar PTFE bellows; 12,1 to 50 bar stainless steel bellows

■ MEDIUM

GF	gaseous and liquid	Air, vapours, gases, liquids and - depending on seal - also for steam Only for steam boilers <10l

■ TYPE OF LIFTING MECHANISM

L	Lifting lever
0	without lifting device

■ AVAILABLE NOMINAL DIAMETERS AND CONNECTION SIZES

Nominal diameter DN		**8**			**10**		
Inlet		1/4" (8)	KV (8mm)	KV (10mm)	3/8" (10)	KV (10mm)	KV (12mm)
Outlet	3/8" (10)	■	■	■	■	■	■
	KV (12mm)	■	■	■	■	■	■

■ TYPE OF CONNECTION INLET / OUTLET THREADED CONNECTIONS

m / f	Standard	Male thread BSP-P / Female thread BSP-P	DIN EN ISO 228-1 / DIN EN ISO 228-1
SV / f		Cutting ring threaded connection / female thread BSP-P	EN ISO 8434-1 / DIN EN ISO 228-1
KV / KV		Screw compression fitting / Screw compression fitting	EN ISO 8434-1 / EN ISO 8434-1

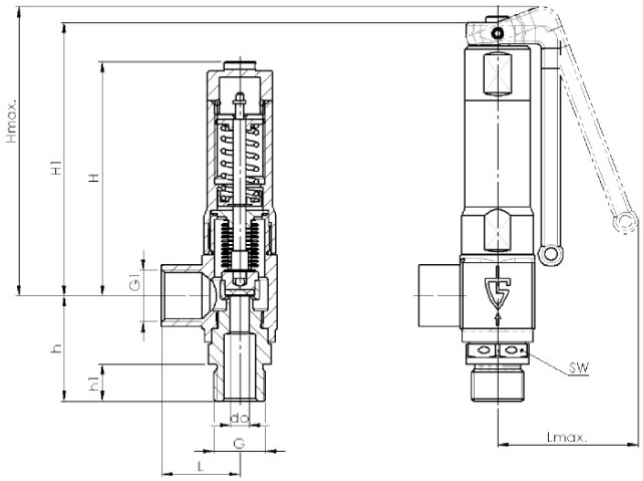
■ SEALS

EPDM	Ethylene propylene diene	Elastomere moulded seal (0,5 – 30 bar)	–40°C to +170°C
FKM	Fluorcarbon	Elastomere moulded seal (0,5 – 30 bar)	–20°C to +200°C
FFKM	Perfluorinated rubber	Elastomere moulded seal (0,5 – 30 bar)	–10°C to +260°C
PTFE	Polytetrafluoroethylene	Flat seal (0,5 – 50 bar)	–40°C to +225°C

■ NOMINAL DIAMETERS, CONNECTIONS, INSTALLATION DIMENSIONS

Series 420: Connection, installation dimensions, ranges of adjustment			
Nominal diameter	DN	8	10
Connection DIN EN ISO 228	G	1/4" (8)	3/8" (10)
Outlet DIN EN ISO 228	G1	3/8" (10)	3/8" (10)
Installation dimensions in mm	L	25	25
	Lmax	45	45
	H	75	75
	H1	87	87
	Hmax	93	93
	h	34	34
	h1	12	12
	SW	20	20
	do	6	6
Weight	kg	0,3 / 0,4	0,25 / 0,35
Range of adjustment	bar	0,5-50	0,5-50

■ MAIN DIMENSIONS, INSTALLATION DIMENSIONS



Appendix Q

Assembly and User Guide



Assembly and User Guide

Atmospheric chamber for in-situ mechanical testing in H_2 rich environment

U.PORTO

1. Before using the equipment

⚠ Before using the mechanical chamber, please read carefully all this information.

⚠ The designed mechanical chamber allows a maximum load of 20 000 N. It is not recommended to use this equipment with higher loads, regarding the leakage risks.

⚠ In the equipment usage, guarantee a safety distance to the chamber and ensure that emergency measures are applied and followed.

⚠ This equipment might be used by anyone who has read and understood the information in this user guide, that has training to perform the mechanical testing and understand the hazards when working with hydrogen gas.

⚠ Before the equipment usage, verify if all the elements of the system, presented in chapter X, are present and correctly assembled, and ensure that these elements do not look damaged of present deformation that that might jeopardise the well-functioning of the chamber.

⚠ This mechanical chamber must only be used according to the equipment and components described in section 2.2. The replacement of components is responsibility of the user as well as any consequential events that might arise from this.

© INEGI all rights reserved

2. Equipment description

The equipment described in this manual, the rich atmosphere testing system, was designed to perform hydrogen embrittlement testing with axial force, in hydrogen gas rich environment. It should be used in machine with linear movement, to perform hydrogen induced crack mechanical testing.

This chamber is specifically designed for vertical assembly and is not intended for horizontal assembly. In the vertical direction, it can be assembled in both directions, having a predefined part to fix the load cell and the machine moving part. These components should only be assembled in their designated location and should not be assembled elsewhere. Allowable assembly orientations and the location to fix the load cell and the dynamic part are presented in figure 1.

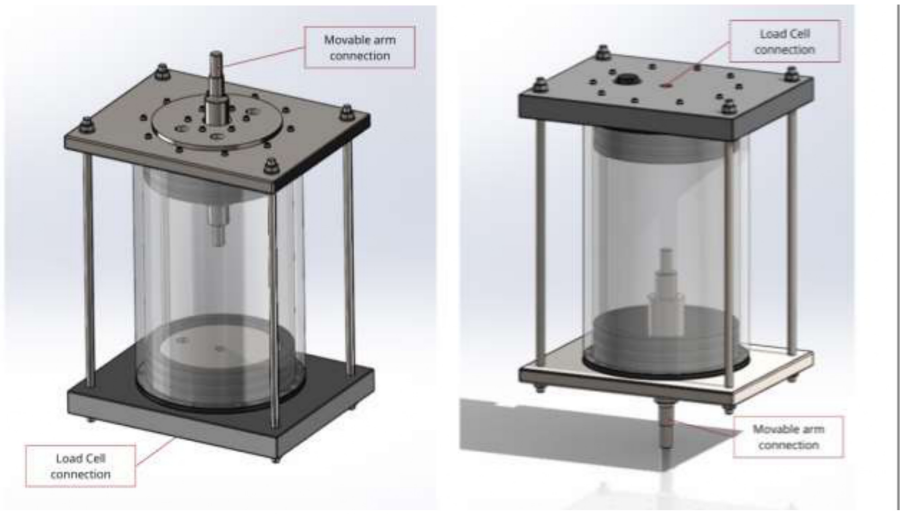


Figure 1 - Chamber assembly orientations

© INEGI all rights reserved

2.1. Exploded view of the chamber solution equipment

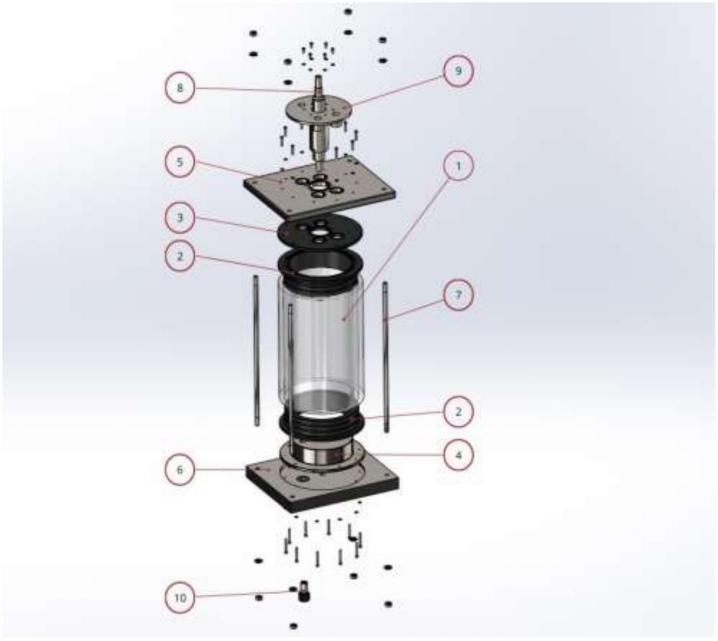


Figure 2 - Exploded view of the chamber components

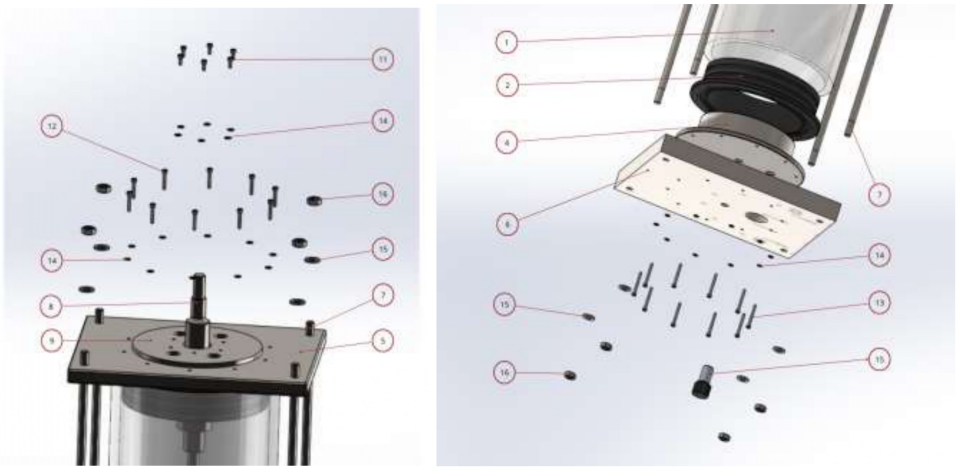


Figure 3 - Detailed view of the screws' sections

© INEGI all rights reserved

2.2. Bill of materials

Table 1 - Bill of materials

Item	Reference	Description	Quantity
1	HTchamber.2023.001 ChamberTube	Fused Quartz Tube φ175mm Supplier: Optical Solutions	1
2	HTchamber.2023.002 Flange	O-ring Flanges Manufacture	2
3	HTchamber.2023.003 EndCapThrough	End Cap - Dynamic Section Manufacture	1
4	HTchamber.2023.004 EndCapLoadCell	End Cap - Load Cell connected Manufacture	1
5	HTchamber.2023.005 FixationPartThrough	Fixation part - Dynamic Section Manufacture	1
6	HTchamber.2023.006 FixationPartLoadCell	Fixation part - Load Cell connected Manufacture	1
7	HTchamber.2023.007 RodFixation	Rod - End Threaded M8 - Fixation Manufacture	4
8	HTchamber.2023.008 DynamicRod	Rod for Dynamic Sealing Manufacture	1
9	HTchamber.2023.009 Bushing	Bushing for dynamic rod and hoses Manufacture	1
10	WLP-M14-9.5MM-HC	Power cables penetrator Supplier: BlueRobotics	1
11	Cylinder head screw DIN 912 M3x8 51050_030_008(High)	Cylindrical Head Screw Steel 10.9 M3x8	6
12	Cylinder head screw DIN 912 M3x18 51050_030_018(High)	Cylindrical Head Screw Steel 10.9 M3x18	10
13	Cylinder head screw DIN 912 M3x30 07015_030_030(High)	Cylindrical Head Screw Steel 10.9 M3x30	10
14	Washer DIN 125-1 A 3_2 38130_030_001(High)	Plain Washer DIN 125-1A Steel Zinc plated 140 HV M3	26
15	Washer DIN 125-1 A 8_4 38130_080_001(High)	Plain Washer DIN 125-1A Steel Zinc plated 140 HV M8	8
16	Hexagon nut DIN 934 M8 01300_080_001(High)	Hexagon Nut DIN 934 Steel Zinc plated 8 M12	8
17	O-ring ISO 3601-133	Facial O-ring ISO 3601-133 FKM ID 45.69, CS 2.62	2
18	O-ring ISO 3601-255	Facial O-ring ISO 3601-255 FKM ID 142.47, CS 3.53	1

© INEGI all rights reserved

19	O-ring ISO 3601-162	Radial O-ring ISO 3601-162 NBR ID 145.72, CS 2.62	2
20	O-ring ISO 3601-316	Radial O-ring ISO 3601-316 FKM ID 21.59, CS 5.33	2
21	O-ring ISO 3601-126	Radial O-ring ISO 3601-126 FKM ID 34.59, CS 2.62	1
22	O-ring ISO 3601-118	Facial O-ring ISO 3601-118 FKM ID 21.89, CS 2.62	1
23	O-ring ISO 3601-112	Radial O-ring ISO 3601-112 FKM ID 12.36, CS 2.62	8
24	O-ring ISO 3601-117	Radial O-ring ISO 3601-117 FKM ID 20.29, CS 2.62	4
25	O-ring ISO 3601-024	Facial O-ring ISO 3601-024 FKM ID 28.30, CS 1.78	8
26	Hose 6mm	Hose 6mm type Supplier: SPIR STAR	1 meter
27	Ball Valve H24	H24 - 3/8" Full port Supplier: Habonim	3
28	Check Valves	Check Valve - 3/8" Port - Code 70.03 Supplier: Redfluid	3
29	Pressure Relief Valve	Series 420 Valve - 3/8" Port Supplier: Gotze Armaturen	1
30	Electrolysis Tank	H-Type Tank - 100mL - C2012F1 Supplier: Ossila	1
31	Graphite Electrodes	Graphite Electrode - 3mm - C2013L1 Supplier: Ossila	2
32	Pressure and temperature sensor	HT-H2-TPSE Sensor - 60 bar Supplier: Hydrotechnik	1
33	Hydrogen Gas Module	TB600C-H2-1000 - 1000 ppm sensor Supplier: EC sensor	1
34	Hsensor.2023.001 SensorPlacement	H2 Sensor Placement Part Manufacture	1
35	DC Power Supply	Bench Top Power Supply Supplier: Distrelec	1

© INEGI all rights reserved

3. Equipment assembly

Before the assembly, ensure that all the parts stated in table 1 are present and in proper conditions.

3.1. Movable section assembly

In this step, it will be assembled one O-ring flange (AISI 316L), nº2, the through hole end cap, nº3, the through hole fixation part, nº5, and the O-rings nº 17, 18, 19 and 25. The O-rings will be applied in first place, in the locations specified in figure 4.

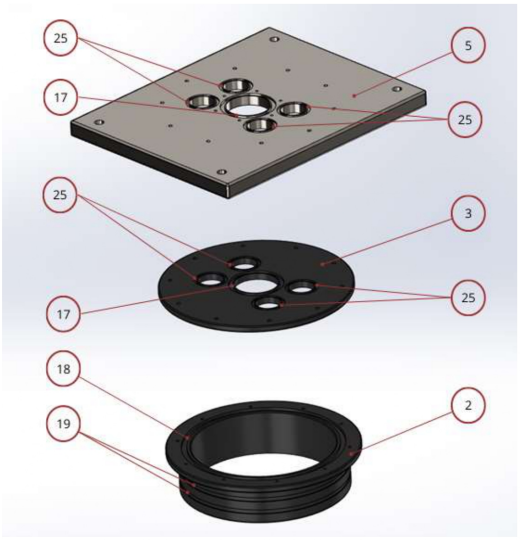


Figure 2 - Dynamic section O-rings placement

The washers (14) and screws (12) will be assembled as shown in figure 3, and the final assembly of this section is presented in figure 5.



Figure 3 - Dynamic section final assembly

© INEGI all rights reserved

3.2. Load Cell connected section

Next, it will be assembled one O-ring flange (MP35N), nº2, the end cap load cell, nº4, the fixation part load cell, nº6, and the O-rings nº 18, 19 and 22. The O-rings will be applied in first place, in the locations specified in figure 6.



Figure 4 - Load cell connected section O-rings placements

The washer(14), screws (13) and penetrator (10) will be assembled as shown in figure 3, and the final assembly of this section is presented in figure 7.

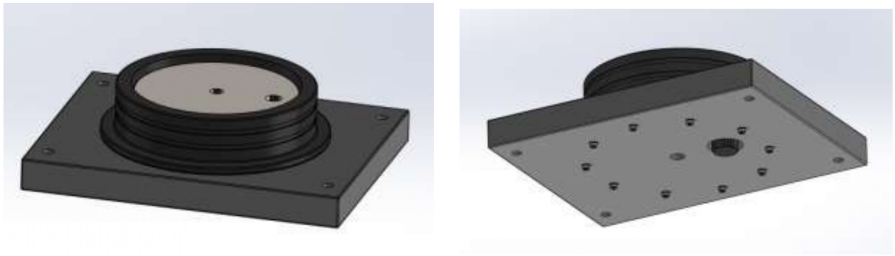


Figure 5 - Load cell section final assembly

© INEGI all rights reserved

3.3. Dynamic Sealing

The dynamic sealing is assembled next, with the Dynamic Rod, nº8, the bushing, nº9, the hoses, nº26, and the O-rings nº 20, 21,23, 24 and 25. The O-rings will be applied in first place, in the locations specified in figure 8.



Figure 6 - Dynamic sealing O-rings placement

© INEGI all rights reserved

The washer(14) and screws (11) will be assembled as shown in figure 3, and the final assembly of this section is presented in figure 9.

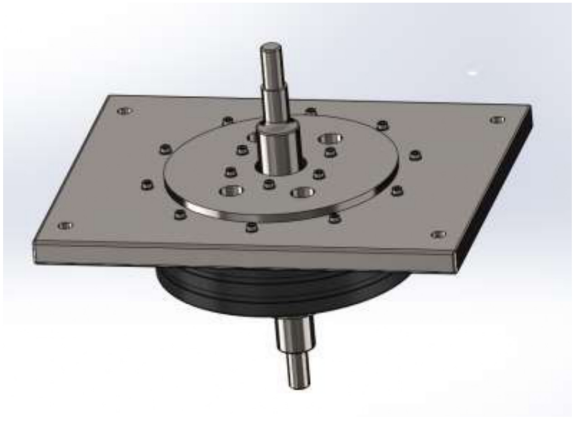


Figure 7 - Dynamix Sealing final assembly

3.4. Chamber Assembly

After assembling these components, they are assembled to the quartz tube, n°1. This assembly can be seen in figure 10.

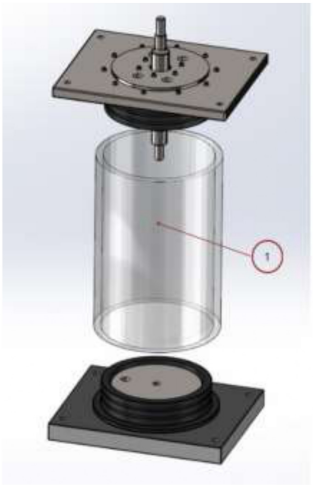


Figure 8 - Chamber assembly

© INEGI all rights reserved

To fix this system are applied the four rods, nº7, the nuts, nº16. and the washers, nº15. This assemble is shown in figure 11.



Figure 9 - Final Solution Assembly

The hoses, nº 26, and valves, nº 27, 28 and 29 are then inserted in the intended places, as seen in figure 12.

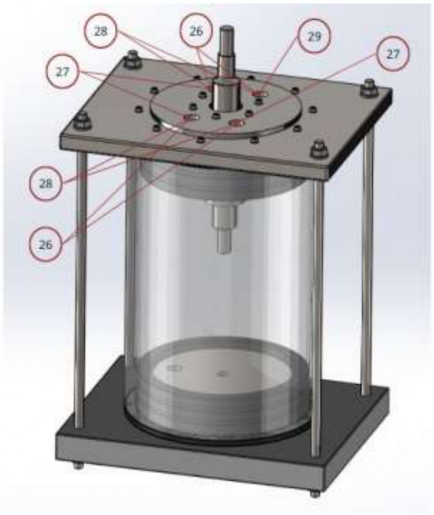


Figure 10 - Remaining components assembly

© INEGI all rights reserved

4. Equipment use

Before the equipment use, the verification of the components conditions is required, as all of them must be in good conditions.

To use the system the connection is firstly required to ensure the machine connection and the correct chamber sealing.

The figure shows one placements of the chamber, assembled in one machine, with clamps already positioned.

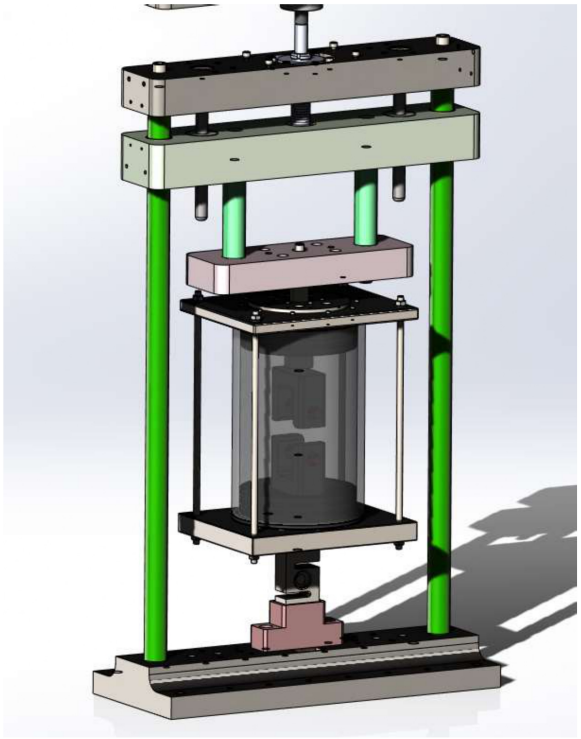


Figure 11 - Testing chamber assembled in one machine, with clamps connected

© INEGI all rights reserved

5. Equipment Maintenance

This equipment's parts must be inspectorate regularly to ensure that:

1. The O-rings do not possess any damages that can compromise the sealing;
2. The end caps, O-rings flanges and fixation parts are in proper state not presenting any fail;
3. All the bolted connections are properly assembled, and the screws and nuts tightened;
4. The components do not possess any corrosion signs. If this happens, the components must be replaced, and possible measures should be applied;
5. There are no components deformations. If that is noted, the components must be replaced before the system use;
6. The Cl_2 containment is properly applied, and no leaks are expected.

© INEGI all rights reserved



INEGI - Institute of Science and Innovation in
Mechanical and Industrial Engineering

Campus da FEUP | Rua Dr. Roberto Frias, 400 | 4200-465 Porto | Portugal
T. +351 22 957 87 10 | inegi@inegi.up.pt

www.inegi.pt



U.PORTO